Mesophase Formation in Discotic Liquid Crystalline polymers

P.H.J. Kouwer

Mesophase Formation in Discotic Liquid Crystalline polymers

PROEFSCHRIFT

ter verkrijging van de graad van doctor
aan de Technische Universiteit Delft,
op gezag van de Rector Magnificus prof. dr. ir. J.T. Fokkema
in het openbaar te verdedigen op maandag 27 mei 2002 om 13.30 uur

door Paul Herco Jaroslav KOUWER

doctorandus in de scheikunde
geboren te Nijmegen

Dit proefschrift is goedgekeurd door de promotor:

Prof. dr. S.J. Picken

Samenstelling promotiecommissie:

Rector Magnificus,	Voorzitter
Prof. dr. S.J. Picken,	Technische Universiteit Delft, promotor
Prof. dr. W.J. Mijs,	Technische Universiteit Delft
Prof. dr. J.W. Goodby	University of Hull, United Kingdom
Prof. dr. E.J.R. Sudhölter	Wageningen Universiteit
Prof. dr. T. Rasing	Katholieke Universiteit Nijmegen
Dr. W.F. Jager,	Technische Universiteit Delft
Dr. P. van der Schoot	Technische Universiteit Eindhoven

Published and distributed by: DUP Science

DUP Science is an imprint of
Delft University Press
P.O. Box 98
2600 MG Delft
The Netherlands
Telephone: +31 15 27 85 678
Telefax: + 31 15 27 85 706
E-mail: Info@Library.TUDelft.NL

ISBN 90-407-2302-8

Keywords: liquid crystals, polymers, specific interactions.

Printed in The Netherlands

Contents

1 Introduction

1.1 Liquid Crystals

Definition. Liquid crystals constitute a class of materials that combines solid state properties with properties of liquids. Usually, matter is considered either fully ordered (crystalline) or fully disordered (liquid, gas, glass). In crystalline phases, molecules possess orientational order and three-dimensional positional order, while in amorphous or isotropic phases the molecules lack (long-range) order. In the various liquid crystalline phases or mesophases (meso is intermediate), the molecules are in between the two extremes, i.e. they possess orientational order and possibly partial positional order, but the latter only in one or two dimensions.

When molecules show liquid crystalline behavior in their molten state, their anisotropic properties are often directly related to the strongly anisometric molecular shape, i.e. one of the molecular axes strongly deviates from the other two. This leads to two major subclasses: rod-shaped and disk-shaped liquid crystals. From the first, predominantly nematic phases (only orientational order) and layered or smectic phases (orientational and one-dimensional positional order) are obtained. Discotic liquid crystals mainly form nematic and columnar phases (with orientational and two-dimensional positional order).

History.[1] Thermotropic liquid crystals (or mesogens) were discovered and first investigated in the late 19th century.[2] The early work focussed on a structural characterization and classification of liquid crystals,[3] in which X-ray diffraction and optical (polarizing) microscopy played a significant role. To investigate the anisotropic materials, a large number of homologous series of mesogens was prepared.[4] Despite the absence of applications, the field retained a substantial scientific interest. This resulted in a steadily growing number of mesogens as well as an increased understanding of the various (smectic) mesophases. Experimental investigations resulted in the basic understanding that is important in today's applications, such as alignment techniques, responses to external fields, birefringence and the formation of chiral phases. Meanwhile, theoreticians contributed to the field of liquid crystals as well, i.e. equations for mean-field theories,[5] viscosities[6] and elastic constants[7] were derived, and these were supported by experimental data, accumulated for a wide range of materials.

However, the major break-through for liquid crystals was the discovery of practical applications (display technology) in the 1960s.[8] The subsequent explosion in research efforts yielded various interesting developments, greatly expanding the field of research. For example, studies of liquid crystalline side-chain and main-chain polymers,[9] starting in the 1970s, showed that the properties of liquid crystals and polymers could be combined successfully. Also, mesophases were observed in non-rod-shaped liquid crystals, such as disk-shaped mesogens[10] and, more recently, bent-core (banana-shaped) mesogens.[11]

Nowadays, research on liquid crystals is still expanding. In order to optimize the performance of current applications (like displays, LEDs and photovoltaic cells) extended knowledge on the structure property relationships of liquid crystals is required. Apart from a continuing development of the field of liquid crystals in science and for applications, liquid crystal theories have proven to be a solid basis for other fields of interest. For example, liquid crystals can be used as model compounds to study molecular interactions and their effects on self-organization in, supramolecular chemistry and block-copolymers.

Classification of mesophases.[12] The short history described above discusses *thermotropic* liquid crystals, showing liquid crystalline behavior in their molten state. In contrast, *lyotropic* liquid crystals exhibit mesophases in solution. Thermotropic mesogens, are generally subdivided into two main classes: *rod-shaped* (calamitic) and *disk-shaped* (discotic) mesogens, although mesogens with other shapes have been reported as well.[13] Regardless of their molecular structure, liquid crystals are classified according to their symmetries and degree of long range order. In the nematic phase only orientational order is maintained, while any long-range positional order is absent. For discotic liquid crystals, multiple nematic phases have been reported, see Figure 1.1. In the nematic discotic (N_D) phase,[14] single molecules exhibit a nematic organization. In the nematic columnar (N_{Col}) phase,[15] the molecules stack into (short) columns and these molecular assemblies are responsible for the nematic arrangement. Recently, we have reported a new nematic phase, referred to as the nematic lateral (N_L) phase. In this phase, large disk-shaped assemblies – built up from disk-shaped molecules – show a nematic arrangement.[16a,b] Interestingly, also transitions between the various nematic phases have been reported.[16b-d] The existence of multiple nematic phases, clearly indicates that the observed phases are not necessarily confined to the local organization of the molecules, but can be determined by supramolecular assemblies at much larger length scales.

Figure 1.1. Nematic phases of: (a) rod-shaped molecules (N); (b) disk-shaped molecules (N_D) and of molecular aggregates: (c) nematic columnar (N_{Col}) phase and (d) nematic lateral (N_L) phase. Note that the extent of order in the N_L and N_{Col} phase can be much larger.

The most important mesophases with long-range positional order are smectic (Sm), columnar (Col) and cubic (Cub) phases. In smectic phases, often seen for rod-shaped mesogens, the molecules are ordered into layers, showing (quasi-) long-range positional order in one direction. Different types of organization within the layers give rise to the large number of smectic phases known today.[12] In Figure 1.2 three common smectic phases are depicted. In the SmA phase (a) the mean orientation of the rods is orthogonal to the layer direction and no positional order within the layers is found. Subclasses distinguish between the local arrangement of the tails or the mesogens. The SmC phase (b) is analogous to the SmA phase, but the mesogens are tilted at a temperature-dependent angle with respect to the layer normal. The hexatic B phase (c) shows a short-range positional order within the layers, although the hexagonal organization can extend over long distances. Note that no correlation between the layers is observed. In the SmB, or better plastic or soft crystal B phase, the molecules do have long-range positional order in the layers and also (weakly) between the layers. Because of the three-dimensional order, the molecules lack mobility and hence, the SmB phase is not liquid crystalline phase in the true sense of the word. Only fast rotation around the mesogens long axis distinguishes the SmB phase from a crystalline phase. Other smectic phases (up to SmO, from which B,E,G,H,J,K are plastic crystals) differ in the organization within the layers.

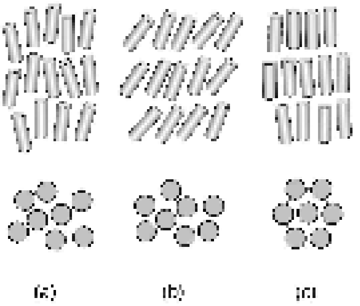

Figure 1.2. Smectic mesophases (from rod-shaped molecules). Side-view (top) and top-view (bottom): (a) smectic A (SmA); (b) smectic C (SmC); (c) hexatic B.

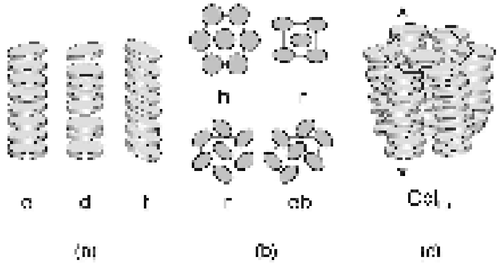

Figure 1.3. Columnar mesophases (from disk-shaped molecules): (a) side-view: ordered (o); disordered (d) and tilted (t); (b) top-view: hexagonal (h), rectangular (r) and oblique (ob); (c) example: Columnar hexagonal ordered (Col_{ho}).

Disk-shaped molecules commonly prefer a columnar organization showing two-dimensional positional order. The several columnar phases are distinguished by the order within the columns and the order between the columns (Figure 1.3). Both are indicated in a subscripted suffix. The most common phases are columnar hexagonal (Col_h) and rectangular (Col_r) phases. Often the order in the column (disordered (d) or ordered (o)) is not indicated. Unlike the smectics, the classification of columnar liquid crystals is still in progress. It proves to be difficult to determine the type of columnar phase exactly, because the optical textures are often ambiguous and X-ray diffraction frequently offers insufficient structural details.

1.2 Disk-shaped liquid crystals

Although anticipated in the 1920s,[17] the observation of the first disk-shaped liquid crystals was not reported before 1977.[10] This relatively new class of liquid crystals has gained an increasing interest, both from a scientific and an application point of view. Despite the growing effort, the field remains small compared to the traditional rod-shaped liquid crystals.

Usually, discotic liquid crystals are built up from a rigid aromatic core that is laterally substituted by multiple flexible tails. Some examples are shown in Figure 1.4. The size of the core can range from as small as benzene (a) or cyclohexane to large aromatic systems, such as benzocoronenes (c), phtalocyanines or porphyrines (d).[18a] The flexible tails (often alkyl) are substituted to the rigid core directly, or via an ether, thioether or ester linkage. Substituted triphenylenes (b) are by far the most investigated mesogens. In Chapter 2, a concise introduction into disk-shaped liquid crystals is presented. A more comprehensive review on the various discotic mesogens known to date as well as their liquid crystalline properties has been published recently.[18a,b]

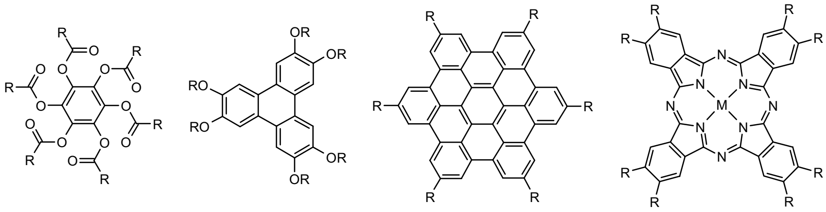

(a) R = Alkyl (b) R = Alkyl (c) R = $C_{12}H_{25}$ (d) M = 2H, Ni, Zn, Cu, Pd, Co, $-(SiO)_n-$ R = Alkyl, OAlkyl, ...

Figure 1.4. Structures of some well-known DLCs (a) benzene hexa-*n*-alkanoate; (b) hexaalkoxy triphenylene; (c) hexa-peri-hexabenzocoronene (d) phtalocyanines.

Some general properties and corresponding applications can be considered for disk-shaped liquid crystals.[18b,c] In contrast to their rod-shaped counterparts, the short axis of the disk-shaped mesogens orients along the director (**ñ**) of a nematic or columnar phase. Hence, the disks align perpendicular to the director (note that the columns align parallel to the director). Consequently, most discotics have a negative birefringence ($\Delta n \equiv n_{//} - n_{\perp}$). Although twisted nematic (TN) cells have been prepared from discotic liquid crystals,[19] they are generally not suitable for switching applications due to their long response times and negative dielectric anisotropy (Δ < 0). Currently, films of discotic mesogens in a tilted or homeotropic alignment are successfully applied as (static) compensation layers in display technology.[20]

A general difficulty for the structural characterization and application of discotic liquid crystals arises from negative diamagnetic of most N_D and columnar phases. This implies that the application of a magnetic field to such samples does not result in a uniaxial orientation, as is the case with rod-shaped mesogens. In contrast, the director is oriented in a plane, perpendicular to the field direction. To obtain single domain textures other techniques have to be applied, like spinning or drawing the sample.[21] In addition, many surface alignment techniques can be used to obtain homeotropically phases (**ñ** ⊥ surface).[19] Much more difficult are surface alignment techniques that produce uniform planar aligned phases (**ñ** // surface). The difficulties of reliably controlling the director alignment in discotic LC's hinders the introduction of discotic liquid crystals in display applications.

Several studies on conduction in various columnar phases have been reported.[18c,22] Since generally the columns are surrounded by multiple insulating alkyl chains, the conduction along the column is much better than perpendicular to the column and hence quasi one-dimensional conduction is accomplished. The interest in this phenomenon is not purely scientific, but it is also stimulated by possible applications, e.g. for light emitting diodes and photovoltaic cells.

1.3 Polymer liquid crystals

Already since the 1970s, liquid crystalline polymers have been synthesized. Traditionally, the field is classified in main chain and side chain liquid crystalline polymers, according to the position of the mesogen along the polymer backbone. An alternative classification distinguishes rigid-rod polymers and semi-flexible liquid crystalline polymers. Rigid-rod polymers are characterized by a stiff rod-shaped (or board-shaped) backbone, see Figure 1.5. Since no separate mesogenic moieties can be distinguished, the length of the mesogen is variable, and is determined by the degree of polymerization and the persistence length. These stiff polymers can show both thermotropic and lyotropic liquid crystalline behavior. They can be processed to reach a high degree of orientation,[23] which results in ultra high strength and high modulus materials that are suitable for mechanical applications. Some commercial examples of rigid-rod polymers are shown in Figure 1.5.

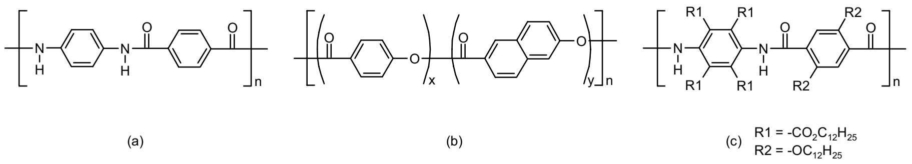

Figure 1.5. Examples of rigid-rod polymer liquid crystals: (a) Twaron® or Kevlar® poly(*p*-phenylene-terephtalamide)[24a] (lyotropic); (b) Vectra® copolymer of 4-hydroxybenzoic acid and 2-hydroxy-6-naphtoic acid[24b] (thermotropic); (c) rigid-board polymer liquid crystals, a substituted polyaramide.[24c]

The class of semi-flexible liquid crystalline polymers (SFLCPs) comprises all polymers with the mesogens separated by flexible spacers, irrespective of the position of the mesogen with respect to the polymer backbone. In this class, the size of the mesogenic moiety well defined and a rational comparison can be drawn between the properties of the SFLCP and the corresponding low molar mass mesogen. An important difference between the SFLCP and the low molar mass mesogen is that the latter usually crystallizes, while the polymer vitrifies at low temperatures. When the mesophase is frozen in, the phase can be denoted as G_M, where M describes the structure of the vitrified mesophase.[25]

A further classification distinguishes the SFLCPs by their precise chemical structure, e.g. (*i*) side-chain SFLCPs (Figure 1.6a),[9c-d,26] where the mesogens are grafted on the polymer backbone via a flexible spacer; (*ii*) main-chain SFLCPs (Figure 1.6b),[9b] where the mesogens are positioned in the backbone between two flexible spacers; and (*iii*) combined SFLCPs (Figure 1.6c),[9e] a combination of (*i*) and (*ii*) with mesogens in the main chain as well as in the side chains. When multifunctional monomers are applied in a polymerization reaction, networks are obtained (Figure 1.6d). Depending on the curing temperature (which determines the mesophase), the properties of this phase can be fixed permanently.[9f]

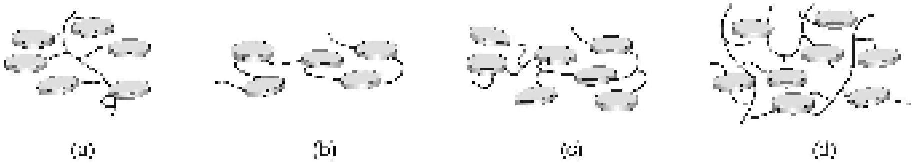

Figure 1.6. Schematic representation of SFLCPs with disk-shaped mesogens: (a) side chain SFLCP; (b) main chain SFLCP; (c) combined (main chain/side chain) SFLCP and (d) semi-flexible liquid crystalline network.

1.4 Specific interactions in discotic liquid crystals

Supramolecular chemistry – the chemistry beyond the molecule – has a large number of non-covalent interactions at its disposal.[27] These secondary interactions include forces like (*i*) electrostatic interactions (ion-dipole, dipole-dipole), (*ii*) hydrogen bonding, (*iii*) π-π stacking, (*iv*) Van der Waals forces (dispersion and induction forces) and (*v*) hydrofobic or, more general, solvofobic effects. The interplay of the non-covalent interactions results in a net attractive or repulsive force between molecules.[28]

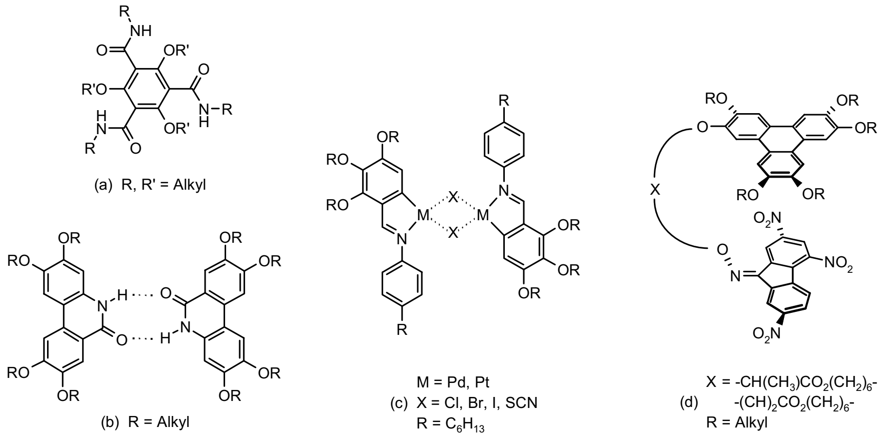

(a) R, R' = Alkyl

(b) R = Alkyl

M = Pd, Pt
(c) X = Cl, Br, I, SCN
R = C_6H_{13}

X = $-CH(CH_3)CO_2(CH_2)_6-$
(d) $-(CH)_2CO_2(CH_2)_6-$
R = Alkyl

Figure 1.7. Examples of specific interactions in discotic liquid crystals: (a,b) Hydrogen bonding and (c) ion-dipole interaction and (d) charge transfer interaction (stacks of alternating donor and acceptor groups). Note that in (a) the H-bonds are directed perpendicular to the plane of the disk and in (b) directed in the plane of the disk.

By using directional forces, specific interactions may be constructed, such as hydrogen bonding, metal-ligand interactions, charge transfer interactions and solvofobic effects. These interactions may be utilized to construct mesogens (see b and c for discotic mesogens) or to stabilize (or destabilize) a particular phase (see a and d for stabilization of columnar mesophases). Especially stabilization and induction of mesophases have been reported for ion-π and ion-dipole interactions,[29a] hydrogen bonding[29b] and charge transfer interactions.[29c] Some examples of liquid crystals, wherein specific interactions play a major role, are displayed in Figure 1.7.

Charge transfer interactions. A charge transfer (CT) complex is formed when an electron is (partially) transferred from the highest occupied molecular orbital (HOMO) of a donor (D) to the lowest unoccupied molecular orbital (LUMO) of an acceptor (A). The CT effect, responsible for the covalent bonding character ($D^+–A^-$) is additional to other attractive forces, like π-π interactions which are a combination of electrostatic and Van der Waals interactions between aromatic molecules.[30]

$$\mathrm{D} + \mathrm{A} \rightarrow \mathrm{D}^{+}\text{—}\mathrm{A}^{-} \qquad \text{with} \qquad K_{\mathrm{C}} = \frac{[\mathrm{D}^{+}\text{—}\mathrm{A}^{-}]}{[\mathrm{D}][\mathrm{A}]} \tag{1.1}$$

For weak complexes, like those discussed in this thesis, the concept of charge transfer complexation can be described well by the theory of Mulliken,[31] which will be discussed qualitatively using the energy diagram, shown in Figure 1.8. The ground state of the complex, represented by wave function ψ_N, can be considered as the sum of two terms:

$$\psi_{N} = a\,\psi_{0}(\mathrm{D}\ ?\ \mathrm{A}) + b\,\psi_{1}(\mathrm{D}^{+}\text{—}\mathrm{A}^{-}) \tag{1.2}$$

in which function ψ_0 relates to the hypothetical 'non-bonding' state. This state has a lower energy compared to the separate constituents, due to an overall attractive interaction, constructed from all kinds of relevant interactions, for example dipole-dipole, solvofobic and/or Van der Waals interactions. Function ψ_1 relates to the state in which the electron is transferred from the donor to the acceptor, with the formation of a covalent bond. Coefficients *a* and *b* characterize the fractions 'no-bond' and CT structures. In the ground state of π-π systems usually a 2 b. The transition $\psi_N \rightarrow \psi_E$ of the complex, referred to as the CT band has no analogy to either the donor or the acceptor, but is a transition of the DA complex. Note that besides this transition of the complex to its excited state (with energy $h\nu_{CT}$) also the donor and the acceptor show transitions to their excited states (with related energies $h\nu_D$ and $h\nu_A$, respectively), both not shown in the energy diagram of Figure 1.8. Since in the ground state applies that a 2 b, the intensities in the UV-Vis spectrum of the transitions of the pure D and A are not expected to decrease much. The exited state ψ_E can be described similarly as the ground state:

$$\psi_E = a^*\psi_1(D^+\text{—}A^-) - b^*\psi_0(D ? A) \tag{1.3}$$

However, now the larger part of the molecules is in the CT state: $a^* 2 b^*$. Starting from these equations, quantitative results can be obtained regarding the heat of formation ΔH and the charge transfer energy $h\nu_{CT}$, see also Figure 1.8.

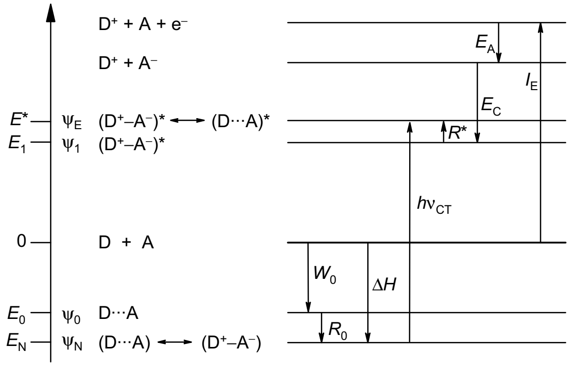

Figure 1.8. Schematic energy diagram of an intermolecular CT complex with energy levels E and corresponding wave functions ψ: D: donor; A: acceptor; E_A: electron affinity (acceptor); I_E: ionization potential (donor); E_C: Coulomb energy; R: Resonance energy; $h\nu_{CT}$: charge transfer energy; ΔH: complexation enthalpy; W: Van der Waals binding energies; suffixes 0 and * denote ground and exited state, respectively.

Because of the clearly visible charge transfer band (of energy $h\nu_{CT}$), the complexes are often referred to as charge transfer (CT) complexes. However, electron donor acceptor (EDA) complexes would be a more appropriate name, since with the CT interactions, contributions of other mechanisms may be present, such as electrostatic, inductive and dispersive forces.[30,32] In this thesis the term CT interactions is used to describe the ensemble of attractive interactions between electron rich (donor) mesogens and electron deficient (acceptor) molecules.

1.5 Characterization of liquid crystals.

The properties of liquid crystalline materials can be studied with a wide range of techniques. To investigate phase transitions, usually differential scanning calorimetry (DSC) experiments are performed. By measuring the energy flow at a constant heating or cooling rate, phase transitions are easily detected. Often the actual mesophases can be identified by optical polarizing microscopy (OPM) experiments. The defects of a phase give rise to the characteristic textures that are visible between two crossed polarizers. It must be stressed that phase characterization by OPM only is not always sufficient, since sometimes textures of different phases are similar (various columnar phases) or are undistinguishable (e.g. the three nematic phases for disk-shaped mesogens). In these cases X-ray diffraction (XRD) measurements can give detailed information on the *local* environment of the molecules. A comprehensive discussion of XRD is given in Appendix A of Chapter 3. The optical microscope can also be used for quantitative retardation experiments (on aligned samples only), where the optical retardation ($\propto$ birefringence) is measured as a function of temperature.

Rheology gives insight in the (macroscopic) flow mechanisms of the materials. Analysis of the moduli as function of temperature and frequency can give detailed information on microscopic structure formation. Some examples of rheological experiments are given in this thesis, but a more detailed overview will be published later.[33] Dielectric relaxation spectroscopy (DRS) measures the relaxation of (molecular) dipoles as a function of frequency and temperature. This makes DRS a good probe for the motions of dipoles on local (molecular) scales in the materials. From a dielectric relaxation spectrum, phase transitions as well as the properties of the various phases can be determined. An introduction into the basics of the technique and the applied analysis methods are discussed in Appendix B of Chapter 3. Other experimental techniques such as nuclear magnetic resonance (NMR) spectroscopy, and neutron and light scattering, were not applied and will not be discussed in this thesis.

1.6 Scope of the thesis

In this thesis, the synthesis and characterization of novel disk-shaped mesogens, the corresponding side chain polymers and the charge transfer complexes of both with appropriate acceptors, are described. The synthesis of all materials, mesogens, acceptors and polymers, is compiled in Chapter 2. Subsequent chapters describe the liquid crystalline properties of the materials, obtained by investigation with various techniques. The chapters are arranged according to the type of compound(s). The effect of attaching the mesogen to a polymer backbone is a theme that is discussed throughout the work, but it is highlighted in Chapter 3. The induction and manipulation of a wide range of liquid crystalline phases by means of charge transfer interactions of disk-shaped mesogens and non-mesogens with various disk-shaped electron acceptors is demonstrated in Chapters 4 and 5. In addition, Chapter 5 discusses the discovery of the new nematic lateral phase. In Chapter 6, the pronounced role of the substituent, linking the tails to mesogen is discussed. The thesis ends with a small chapter containing general thoughts and conclusions, with respect to preceding chapters.

References and notes

(1) Historical reviews are written by: (a) Gray, G.W. In Handbook of Liquid Crystals; Demus, D., Goodby, J.W., Gray, G.W., Spiess, H.W., Vill, V., Eds.; Wiley VCH: New York, 1998; Vol. 1, pp 1-16. (b) Kelker, H.; Knoll, P.M. *Liq. Cryst.* **1989**, *5*, 19

(2) (a) Reinitzer, F. *Monatsh. Chem.* **1888**, *9*, 421. For an English translation read: *Liq. Cryst.* **1989**, *5*, 7. (b) Lehman, O. *Z. Phys. Chem.* **1889**, *4*, 462.

(3) Friedel, G. *Ann. Phys.* **1922**, *18*, 273.

(4) Vorländer, D. *Kristallographie der Flüssigkeiten*; Akadem. Verlaganstalt: Leipzig, 1924.

(5) (a) Maier, W.; Saupe, A. *Z. Naturforsch.* **1958**, *13a*, 564. (b) Maier, W.; Saupe, A. *Z. Naturforsch.* **1959**, *14a*, 882. (c) Maier, W.; Saupe, A. *Z. Naturforsch.* **1960**, *15a*, 287.

(6) (a) Leslie, F.M. *Quart. J. Mech. Appl. Math.* **1966**, *19*, 357-370. (b) Ericksen, J.L. *Arch. Ratl. Mech. Anal.* **1966**, *23*, 266-275. (c) Leslie, F.M. *Arch. Ratl. Mech. Anal.* **1968**, *28*, 265-283. (d) Ericksen, J.L. *Mol. Cryst. Liq. Cryst.* **1969**, *7*, 153-164.

(7) (a) Zocher, H. *Trans. Faraday Soc.* **1933**, *29*, 945. (b) Frank, F.C. *Disc. Faraday Soc.* **1958**, *25*, 19.

(8) Schadt, M. *Appl. Phys. Lett.* **1971**, *18*, 127-128.

(9) For reviews on liquid crystalline polymers and networks read: (a) In *Liquid Crystalline Polymers*; Carfagna, C., Ed.; Pergamon: Oxford, 1994. (b) Chiellini, E.; Laus, M. In *Handbook of Liquid Crystals*; Demus, D., Goodby, J.W., Gray, G.W., Spiess, H.W., Vill, V., Eds.; Wiley VCH: New York, 1998; Vol. 3, pp 26-51. (c) In *Side Chain Liquid Crystal Polymers*; McArdle, C.B., Ed.; Blackie: Glasgow, 1989. (d) Pugh, C.; Kiste, A.L. In *Handbook of Liquid Crystals*; Demus, D., Goodby, J.W., Gray, G.W., Spiess, H.W., Vill, V., Eds.; Wiley VCH: New York, 1998; Vol. 3, pp 123-206. (e) Zentel, R. In *Handbook of Liquid Crystals*; Demus, D., Goodby, J.W., Gray, G.W., Spiess, H.W., Vill, V., Eds.; Wiley VCH: New York, 1998; Vol. 3, pp 52-65. (f) Brandt, H.; Finkelmann, H. In *Handbook of Liquid Crystals*; Demus, D., Goodby, J.W., Gray, G.W., Spiess, H.W., Vill, V., Eds.; Wiley VCH: New York, 1998; Vol. 3, pp 277-302.

(10) Chandrasekhar, S.; Sadashiva, B.K.; Suresh, K.A. *Pramana* **1977**, *9*, 471.

(11) Akutagawa, T.; Matsunaga, Y.; Yasuhara, K. *Liq. Cryst.* **1994**, *17*, 659-666.

(12) Recent information on nomenclature and classification of liquid crystals can be found in: Goodby, J.W.; Gray, G.W. In Handbook of Liquid Crystals; Demus, D., Goodby, J.W., Gray, G.W., Spiess, H.W., Vill, V., Eds.; Wiley VCH: New York, 1998; Vol. 1, pp 17-23.

(13) Demus, D. In *Handbook of Liquid Crystals*; Demus, D., Goodby, J.W., Gray, G.W., Spiess, H.W., Vill, V., Eds.; Wiley VCH: New York, 1998; Vol. 1, Chapter VI.3, pp 153-171.

(14) Tinh, N.H.; Destrade, C.; Gasparoux, H. *Phys. Lett.* **1979**, *72A*, 25.

(15) (a) Ringsdorf, H.; Wüstefeld, R.; Zerta, E.; Ebert, M.; Wendorff, J.H. *Angew. Chem. Int. ed. Engl.* **1989**, *28*, 914-918. (b) Praefcke, K.; Singer, D.; Kohne, B.; Ebert, M.; Liebmann, A.; Wendorff, J.H. *Liq. Cryst.* **1991**, *10*, 147-159.

(16) (a) The novel N_L phase will be discussed in Chapters 4 and 5. Note that the actual proof of the identification of the N_L phase is discussed comprehensively in paragraph 5.3. (b) Kouwer, P.H.J.; Jager, W.F.; Mijs, W.J.; Picken, S.J. *Macromolecules* **2001**, *34*, 7582-7584. (c) Kouwer, P.H.J.; Mijs, W.J.; Jager, W.F.; Picken, S.J. *Macromolecules* **2000**, *33*, 4336-4342. (d) Kouwer, P.H.J.; Gast, J.; Jager, W.F.; Mijs, W.J.; Picken, S.J. *Mol. Cryst. Liq. Cryst.* **2001**, *364*, 225-234.

(17) Vorländer, D. *Z. Phys. Chem.* **1923**, *105*, 211.

(18) (a) Cammidge, A.N.; Bushby, R.J. In *Handbook of Liquid Crystals*; Demus, D., Goodby, J.W., Gray, G.W., Spiess, H.W., Vill, V., Eds.; Wiley VCH: New York, 1998; Vol. 2B, pp 693-748. (b) Chandrasekhar, S. In *Handbook of Liquid Crystals*; Demus, D., Goodby, J.W., Gray, G.W., Spiess, H.W., Vill, V., Eds.; Wiley VCH: New York, 1998; Vol. 2B, pp 749-780. (c) Boden, N.; Movaghar, B. In *Handbook of Liquid Crystals*; Demus, D., Goodby, J.W., Gray, G.W., Spiess, H.W., Vill, V., Eds.; Wiley VCH: New York, 1998; Vol. 2B, pp 781-798.

(19) Vauchier, C.; Zann, A.; Le Barny, P.; Dubios, J.C.; Billard, J. *Mol. Cryst. Liq. Cryst.* **1981**, *66*, 103-114.

(20) (a) Kamada, K.; Watanabe, J.; Arakawa, K.; Kozono, H. In *Eur. Pat. Appl. EP 646829 A1*; Fuji Photo Film Co., 1995. (b) Mori, H.; Itoh, Y.; Nishiura, Y.; Nakamura, T.; Y., S. *Jap. J. Appl. Phys.* **1997**, *36*, 143-147.

(21) (a) Goldfarb, D.; Luz, Z.; Zimmerman, H. *Journal de Physique (France)* **1981**, *42*, 1303-1311. (b) Fontes, E.; Heiney, P.A.; Ohba, M.; Haseltine, J.N.; Smith, A.B. *Phys. Rev. A* **1988**, *37*, 1329-1334.

(22) Adam, D.; Schuhmacher, P.; Simmerer, J.; Haussling, L.; Siemensmeyer, K.; Etzbach, K.H.; Ringsdorf, H.; Haarer, D. *Nature* **1994**, *371*, 141-143.

(23) Because of the variable lengths of the mesogens, only nematic phases are expected. Hence, only orientational order and no positional order (like in smectic phases) is observed for rigid-rod polymers.

(24) (a) Cottis, S.G.; Economy, J.; Nowak, B.E. *US Pat. Appl. USP 3637595*; Carborandum: USA, 1972. (b) Calundann, G.W. *US Pat. Appl. USP 4161470*; Celanese: USA, 1979. (c) Ebert, M.; Herrmann-Schönherr, O.; Wendorff, J.H.; Ringsdorf, H.; Tschirner, P. *Makrom. Chem., Rapid Commun.* **1988**, *9*, 445-451.

(25) The polymer backbone does not always prevent crystallization. Since $T_m > T_g$, the liquid crystalline polymer may exhibit (semi)crystalline phase before the amorphous material vitrifies.

(26) Finkelmann, H.; Ringsdorf, H.; Wendorff, J.H. *Makromol. Chem.* **1978**, *179*, 273.

(27) Lehn, J.M. *Supramolecular Chemistry*; VCH: Weinheim, New York, 1995.

(28) (a) Lawrence, D.S.; Jiang, T.; Levett, M. *Chem. Rev.* **1995**, *95*, 2229-2260. (b) Philip, D.; Stoddart, J.F. *Angew. Chem. Int. ed. Engl.* **1996**, *35*, 1154-1196.

(29) (a) Giroud-Godquin, A.M. In *Handbook of Liquid Crystals*; Demus, D., Goodby, J.W., Gray, G.W., Spiess, H.W., Vill, V., Eds.; Wiley VCH: New York, 1998; Vol. 2B, pp 901-932. (b) Kato, T. In *Handbook of Liquid Crystals*; Demus, D., Goodby, J.W., Gray, G.W., Spiess, H.W., Vill, V., Eds.; Wiley VCH: New York, 1998; Vol. 2B, pp 969-979. (c) Praefcke, K.; Singer, D. In *Handbook of Liquid Crystals*; Demus, D., Goodby, J.W., Gray, G.W., Spiess, H.W., Vill, V., Eds.; Wiley VCH: New York, 1998; Vol. 2B, pp 945 - 967.

(30) (a) Hunter, C.A.; Sanders, J.K.M. *J. Am. Chem. Soc.* **1990**, *112*, 5525-5534. (b) Hunter, C.A.; Lawson, K.R.; Perkins, J.; Urch, C.J. *J. Chem. Soc., Perkin Trans. 2* **2001**, 651-669.

(31) (a) Mulliken, R.S. *J. Am. Chem. Soc.* **1952**, *74*, 811. (b) Mulliken, R.S.; Rerson, W.B. *Molecular Complexes*; Wiley: New York, 1969. (c) Mulliken, R.S. *J. Phys. Chem.* **1952**, *56*, 801.

(32) (a) Heaton, N.J.; Bello, P.; Herradon, B.; Campo, A.d.; Jiménez-Barbero, J. *J. Am. Chem. Soc.* **1998**, *120*, 9632-9645. (b) In some cases the complex formation is almost entirely attributed to quadrupolar forces, for example in benzene-hexafluorobenzene complexes. Note that in such complexes no charge transfer is observed.

(33) Franse, M.W.C.P. Te Nijenhuis, K., Picken, S.J., Manuscript in preparation.

2 Materials

Abstract

The research described in this thesis is based on mesogens with a pentakis(phenylethynyl)-benzene core and electron acceptors based on trinitrofluorenone. The synthesis of the donors with various substituents is described; they include alkyl, alkoxy, thioalkyl and amide groups. The low molecular weight mesogens were synthesized via a palladium catalyzed cross-coupling reaction of a terminal acetylene with a pentabromophenol derivative in moderate to good yields. Although the reaction proceeded usually well, it proved to be very difficult to separate the mesogens from side-products, like the four-fold substituted materials. Acceptor molecules, used to investigate CT complexes of the mesogens were prepared by functionalization of trinitrofluorenone. Donors and acceptors were coupled to form symmetric and asymmetric twins. A polymer analogous substitution reaction of the donors or acceptors with poly(acryloyl chloride) yielded the corresponding side chain polymers. Using this versatile method a wide range of copolymers, including donor-acceptor copolymers was synthesized.

2.1 Literature survey of disk-shaped electron donors and acceptors

This first paragraph discusses some of the well-known discotic liquid crystalline systems, and these are compared with the disk-shaped materials discussed in this thesis. The overview includes low molar mass materials, polymers and charge transfer complexes. A more comprehensive review on discotic liquid crystals has been published recently.[1] Paragraph 2.2 gives the preparation of the materials used in this thesis. The experimental details on the preparation and characterization of the materials are described in section 2.3.

2.1.1 Electron donating mesogens

Most of the (organic) disk-shaped liquid crystals, described in literature are built up from an aromatic core, substituted with alkyl or alkoxy tails.[1] Hence, they can be classified as electron-rich liquid crystals. A few examples are shown in Figure 2.1. Mesogens with a triphenylene core (a) have been studied most extensively. Alkoxy substituted triphenylenes[2] show columnar mesophases, while the benzoate esters also show nematic phases at high temperatures.[3] Their relatively easy preparation combined with their colorless appearance gave rise to a large number of studies to possible applications, such as optical films and for one-dimensional conduction.[4] Asymmetric substitution of the core, using clever synthesis[5] and/or elaborate purification procedures[6] opened routes to side-chain and main-chain polymers. In addition, the asymmetrically substituted mesogens frequently showed liquid crystalline properties that strongly deviated from their symmetric counterparts.[7] Derivatives of truxene,[8a,b] oxatruxene[8c] and thiatruxene[8d] (b) show a rich, but complicated phase behavior, including multiple re-entrant phases. The exact details of these fascinating materials are not well understood. Members of the five and six-fold phenyl ethynyl substituted benzenes (c) regularly show nematic phases that, in general, are not very common for disk-shaped mesogens. This class of mesogens is introduced in Chapter 2.1.3 more in detail.

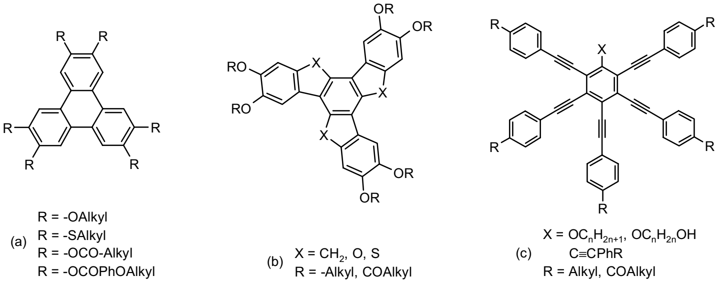

Figure 2.1. Examples of well-studied electron rich DLCs, based on (a) triphenylenes, (b) truxenes, oxatruxenes and thiatruxens; and (c) five- or six-fold (phenylethynyl) substituted benzenes.

2.1.2 Discotic liquid crystalline polymers

In the mid 1980s, the first liquid crystalline polymers built from disk-shaped mesogens were reported.[6] The polymers were prepared from asymmetrically substituted triphenylenes. Today, after the discovery of better routes to mono- and difunctionalized triphenylenes,[5] a wider range of polymers based on triphenylene can be prepared and studied more effectively. A number of triphenylene based SFLCPs[9] are shown in Figure 2.2.

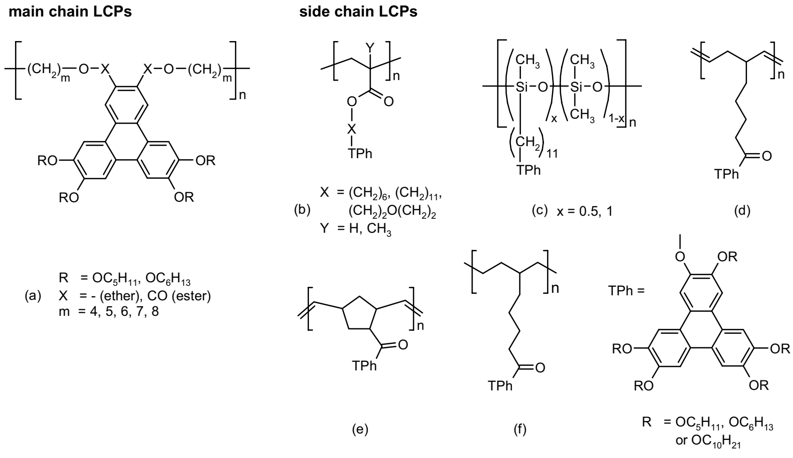

Figure 2.2. (a) Triphenylene based main-chain LCPs and (b-f) side-chain LCPs with backbones based on (b) poly(meth)acrylate; (c) polysiloxanes; (d) polybutadiene; (e) poly(vinylene-cyclopentylene); (f) polybutylene.

Nearly all polymers with discotic mesogens incorporated show columnar phases (Col_X or in rare cases N_{Col}). Interestingly, some cases have been reported, where after polymerization of the liquid crystalline monomers amorphous materials were found. When the liquid crystalline phase is retained, small changes of the spacer (and the backbone) induce a wide variety in phase behavior, which verifies their role in the process of (meso)phase formation.

Various contributions on triphenylene-based SFLCPs have led to an increasing knowledge on phase behavior of these complex materials. For example, the liquid crystalline properties of the main chain polymers (a)[5b,10] show a strong dependence on the spacer length.[10a] The side chain polymers (b),[11] (c)[6] and (d-f)[12] show low glass transition temperatures, ranging from –40 °C to +10°C, depending on the backbone and spacer. Unexpectedly, for the clearing temperatures a much wider temperature range was observed (from 35°C for a pentyl-substituted triphenylene to 120°C for a hexyl-substituted triphenylene).

Also, other discotic LCPs have been reported, e.g. based on phtalocyanines,[13] and triphenylene hexabenzoyl esters.[14a] The latter is the only example of a nematic mesophase found in a discotic LCP, so far. In addition to discotic LCPs with a linear backbone, also discotic LC elastomeric networks have been prepared.[14] Crosslinking of the multifunctional disk-shaped mesogens was carried out in the (possibly macroscopically oriented) mesophase.

2.1.3 Five and six-fold (phenylethynyl) substituted benzenes

By multiple coupling a terminal acetylene with a polybromobenzene, a new class of disk-shaped (or star-shaped) molecules was established.[15,16] Early reports describe the synthesis of the symmetrically substituted benzenes but no mesophases were found in these materials, due to the absence of the long flexible tails.[17] Nevertheless, the reaction of hexabromobenzene with a terminal acetylene proved to be an interesting route towards rigid star-shaped materials, bearing a variety of groups at the core, including porphyrins,[18a] derivatives of aminoacids[18b,c] and platinum complexes.[18b]

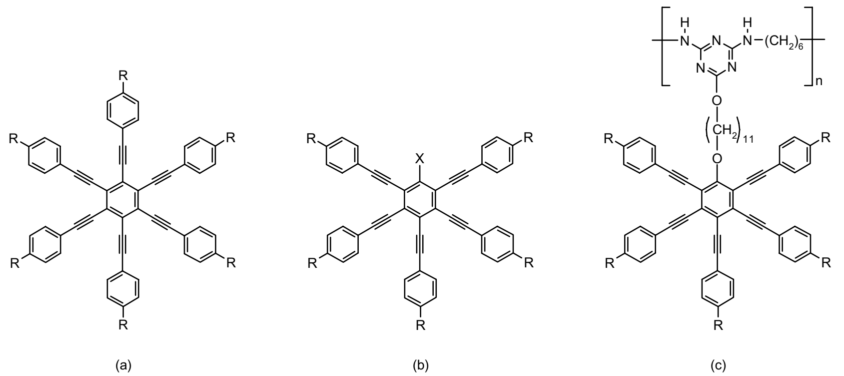

(a) (b) (c)

Figure 2.3. Examples of multi ethynyl substituted benzenes: (a) symmetrically substituted derivatives; (b) derivatives with one single functional group and (c) macromolecular derivative with triazine-based backbone.

In the late eighties the first (symmetrical) liquid crystalline derivatives were reported, bearing multiple alkyl tails at the central core (Figure 3a).[16] Shortly after, asymmetric materials were reported (Figure 3b). In these materials, the sixth position of the central core was substituted by a single aliphatic side chain, which in its turn, could be functionalized as well. A short overview of the liquid crystalline properties is presented in Table 2.1.

As is clear from the table, many members of this class form a nematic phase, which was rather uncommon in the late 1980s, since most disc-shaped mesogens only formed columnar phases. Symmetrically substituted members show (narrow) mesophases when the tail length exceeds C_4. A (racemic mixture of) branched tails shows a much wider mesophase window due to a strong suppression of the crystallization process. With the five-fold substituted discotics, only the nonsubstituted core does not form any mesophase. Tails as short as methyl groups induce N_D phases. Obviously, by using chiral substituents cholesteric (N_D*) phases can be established. The only reported polymers bearing these mesogen are shown in Figure 2.3c. The remarkable SmA phase found in the polymer, is believed to originate from the strong H-bond interactions, due to the triazine moieties of the polymer backbone.[19]

Table 2.1. Thermal behavior of multi ethynyl substituted benzenes (see Figure 2.3 for structures).

	R	**X**	**phase behavior (temperatures in °C)**	**reference**
(a)	C_5H_{11}	–	K 170 N_D 185 I/d	20
symmetrically substituted	C_6H_{13}	–	K 124 N_D 142 I	20
	C_7H_{15}	–	K 98 N_D 131 I	20
	C_8H_{17}	–	K 80 N_D 96 I	16
	rac-$C_3H_6CH(CH_3)C_5H_{11}$	–	K 8 N_D 69 I	21
	OC_7H_{15}	–	K 109 N_D 193 I	22
	$C_6H_4C_5H_{11}$	–	K 170 Col >240 d	23
(b)	H	$OC_{11}H_{22}OH$	K 123 I	24
a-symmetrically substituted	CH_3	$OC_{11}H_{22}OH$	K 174 N_D 246 I	25
	C_5H_{11}	$OC_{11}H_{22}OH$	K 67 N_D 94 I	26
	C_5H_{11}	$OC_{10}H_{20}CO_2H$	K 84 N_D 91 I	26
	C_6H_5	$OC_{16}H_{33}$	K 171 Col ~230 N_D 250 I/d	23
	$C_6H_4C_5H_{11}$	$OC_{16}H_{33}$	K 106 N_D 285 I/d	23
	$OC^*H(CH_3)C_2H_5$	$OC_{16}H_{33}$	K 88 N_D* 100 I	27
(c)	H	–	G_I 112 I	19
	C_5H_{11}	–	? SmA 158 I	19

2.1.4 Electron Acceptors

In the literature only a limited number of suitable electron acceptors for the formation of charge transfer complexes are described (Figure 2.4). To effectively manipulate the phase behavior of a donor, a planar and relatively large structure is required. Although hexacyanohexaazatriphenylene (a) have been complexed successfully with triphenylenes,[28a] the material and its corresponding hexaesters showed macroscopic phase separation with the pentakis(phenyletyhnyl) benzene donors.[28b] It is questionable whether charge transfer interactions play an important role in complexes of perfluorotriphenylene (b) with (substituted) triphenylenes, since no CT band is observed in the adsorption spectrum. The stabilization of the columnar mesophase has been attributed to attractive quadrupolar interactions.[29]

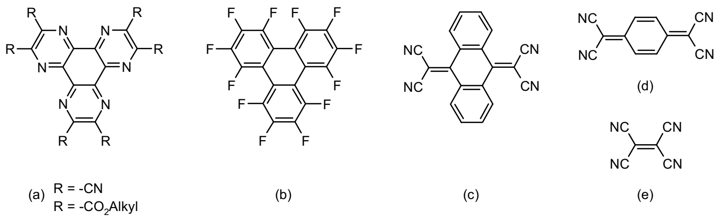

Figure 2.4. Examples of electron acceptors based on (a) 1,4,5,9,10,12-hexaazatriphenylene; (b) perfluorotriphenylene; (c); 11,11,12,12-tetracyananthraoquinodimethane (TCAQ); (d) 7,7,8,8-tetracyanoquinodimethane (TCNQ) and (e) tetracyanoethylene.

The most widely exploited acceptors are based on 2,4,7-trinitro-9-fluorenone[30] (TNF, **A2**). TNF offers the advantages of a high electron affinity with an easy preparation. In addition it offers a single functionalization site, which is a prerequisite to prepare side chain polymers. Acceptors based on TNF are shown in Figure 2.5. Nonfunctionalized TNF-based acceptors (Figure 2.5a-d) are well known in the literature. Compounds (a-c) are commercially available, or can be prepared easily by a nitration reaction of 9-fluorenone, followed by a condensation reaction with malonitril for **A3**,[31] or diethyl malonic acid for the diester (d). Introduction of a single functional group can take place at the keto position by an oxim exchange reaction, resulting in the carboxylic acid derivatives (e,f).[32] Alternatively, a carboxylic acid group can be introduced prior to nitration (e.g. 2.4g).[33]

The effective acceptor strengths for CT complexation of the TNF derivatives depend strongly on the substituent at the 9-position and much less on the presence of three or four nitro substituents. In order of increasing acceptor strength: (e) ≈ (f) 0 (a)< (d) (b) 0 (c).[34]

Functionalized TNF derivatives have been incorporated in the backbone and on the sidechain of macromolecules. Main chain polymers (h) were prepared by transesterification of (d) with the appropriate diols,[35] and proved to be successful macromolecular CT complexing agents. Dependent on the spacer length columnar or N_{Col} mesophases were observed. Copolymers (i) were obtained by a polymer analogous esterification reaction of (f) with a hydroxyl functionalized polysiloxane.[36] Polyacrylates (j) were synthesized by free-radical (co)polymerization of the ethylacryl derivative of (g) with methyl acrylate. The copolymers with a low TNF content were readily obtained, while the preparation of copolymers with a high TNF fraction or homopolymers of the acceptor resulted in the formation of oligomers in low yields.[37] Interestingly, no macromolecular TNF derivatives have been reported in which the TNF moiety is completely "uncoupled" from the polymer backbone with a sufficiently long spacer.

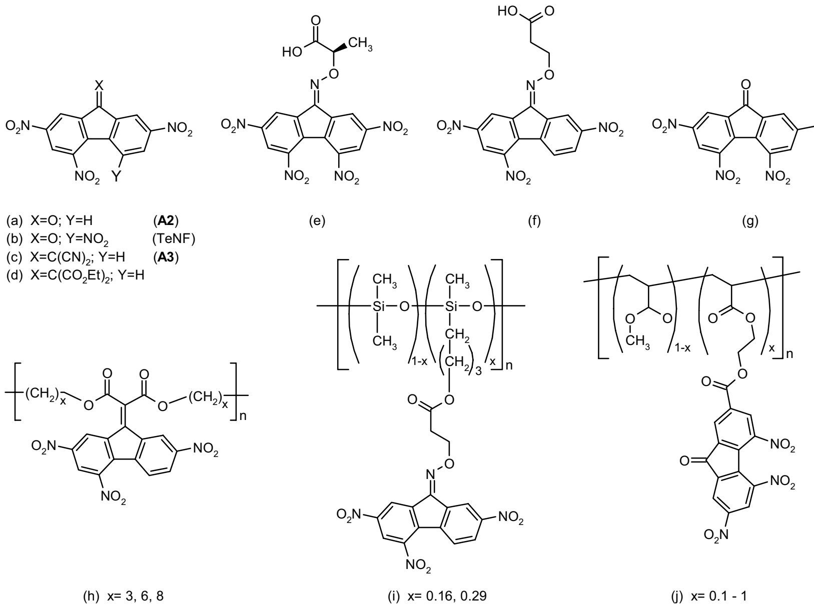

(a) X=O; Y=H (**A2**)
(b) X=O; Y=NO_2 (TeNF)
(c) X=$C(CN)_2$; Y=H (**A3**)
(d) X=$C(CO_2Et)_2$; Y=H

(e)

(f)

(g)

(h) x= 3, 6, 8

(i) x= 0.16, 0.29

(j) x= 0.1 - 1

Figure 2.5. Some low and high molar mass TNF-based acceptors: (a) TNF (**A2**); (b) 2,4,5,7-tetranitro-9-fluorenone (TeNF); (c) 2,4,7-trinitro-9-fluorenylidenemalonitril (**A3**); (d) the chiral *S*-2-(2,4,5,7-tetranitro-9-fluorenylideneaminooxy)propionic acid (+TAPA); (e) 3-(2,4,7-trinitro-9-fluorenylideneaminooxy)propionic acid; (f) 2,5,7-trinitro-9-fluorenone-2-carboxylic acid; (g-i) semi-flexible acceptor polymers.

2.2 Preparation of electron donors, acceptors and corresponding polymers

This thesis is based on donors based on the five-fold phenyl ethynyl substituted benzene core and acceptors based on TNF. The donors have been modified chemically by introduction of various tails at the lateral phenyl groups. The mesogens are intrinsically monofunctional, which is a prerequisite to synthesize side chain polymers. To uncouple the thermal properties of the mesogen and the backbone as effectively as possible, a long spacer (C_{11}) was used. In general, the length of the spacer has been kept constant. Although the effect of the spacer on the phase behavior should not be neglected, the spacer length was not a variable in this study. The same C_{11} spacer was used for the oxim-functionalized acceptors. The preparation of donors, acceptors, their symmetric and asymmetric dimers as well as their corresponding (co)polymers is discussed in the following paragraphs.

2.2.1 Preparation of the terminal acetylenes

The donors are prepared by a cross-coupling reaction of a terminal acetylene with a pentabromophenol derivative.[16,38] Being not available commercially, three routes were employed to synthesize the proper terminal acetylenes. The first two routes comprise an overall dehydration reaction of acetophenones.

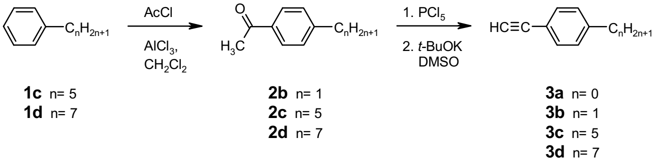

Scheme 2.1. Method 1: Acetylene synthesis via dehydration of acetophenone with PCl_5.

Alkylaryl substituted acetylenes were prepared from the corresponding alkylacetophenones, using PCl_5 and *t*-BuOK (Scheme 2.1). We found that the application of DMSO as a solvent (instead of *t*-BuOH) in the second step reduces the reaction time from 72 hours to only 2 hours. By this change in solvents, the yields remained unaffected.

For alkoxy or thioalkyl substituted acetophenones a milder route was used (Scheme 2.2), involving a Vilsmeier-Haack reaction on the enol tautomer of the acetophenone.[39] In our laboratories, the route was readily scaled-up to larger quantities, starting with 25 grams of the appropriate acetophenone. Chlorocinnamaldehyde **7** was treated with an aqueous NaOH solution in dioxane. Application of a phase transfer catalyst (e.g. *n*-Bu_4NHSO_4) allowed a much more concentrated (phase separated) reaction mixture.

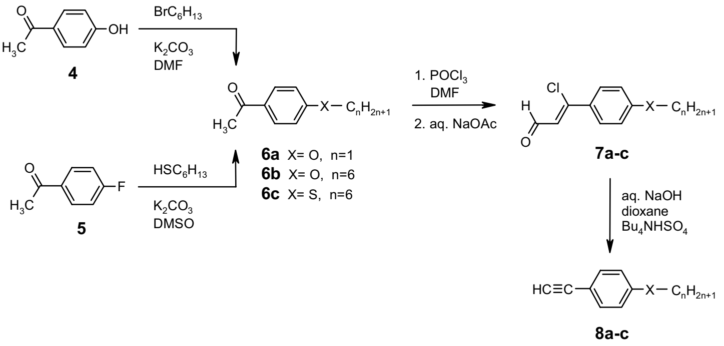

Scheme 2.2. Method 2: Acetylene synthesis via dehydration of acetophenone with Vilsmeier-Haack reaction, followed by an elimination reaction.

A third route to prepare terminal acetylenes employs the Sonogashira reaction.[15] Starting from an arylhalide, a protected acetylenic moiety was attached and the protective group was removed (Scheme 2.3). Protection is required, since the mono-substituted arylacetylene is much more reactive than the acetylene itself. Good protective groups are trimethylsilyl (removal by KOH in methanol or milder with *n*-$Bu_4N^+F^-$) and 2-hydroxyisopropyl (removal by a base-catalyzed retro-Favorsky elimination). Both routes were used, but the trimethylsilyl protective group proved to be easier to handle. It is important to stress that aryl bromides are much less reactive than their corresponding aryl iodides.[40]

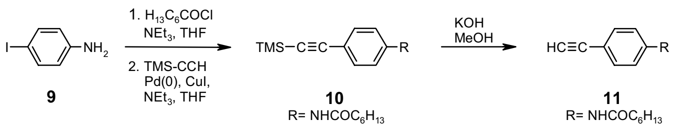

Scheme 2.3. Method 3: Acetylene synthesis via palladium catalyzed cross-coupling reaction, followed by a removal of the trimethylsilyl (TMS) protective group.

Some other routes to prepare terminal acetylenes have been subjected to preliminary investigations. Although they were not employed to prepare the here discussed mesogens, the routes are mentioned below. A direct method to obtain terminal acetylenes includes substitution of an arylhalide with HC≡CZnBr or HC≡CMgBr under Sonogashira conditions.[41] Another route to terminal acetylenes starts from the corresponding benzaldehyde. Reaction with $Ph_3P{=}CBr_2$, subsequent HBr elemination and a hydrogen-bromo exchange at the acetylenic position yields the acetylene in moderate to good yields.[42]

2.2.2 Preparation of the mesogens

A five-fold Sonogashira cross-coupling reaction was used to attach the acetylenes to a central benzene core.[15,16,38] The reaction involves choices of the type and amount of catalyst (Pd(0) complex), co-catalyst (Cu^+) and solvents and a wide range of procedures has been published.[40] Once the details of the coupling reactions had been worked out carefully, the coupling itself usually was straightforward. However, the purification of most materials was difficult, i.e. separation of the four-fold substituted isomers from the product, often reduced the yields of the reaction considerably, see the experimental section 2.3.

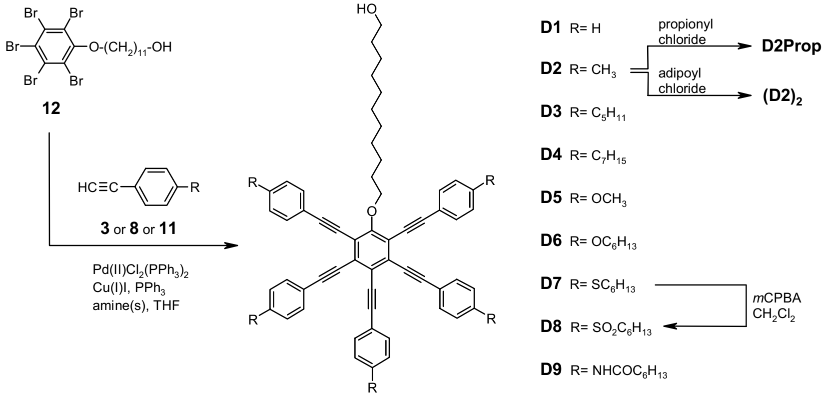

Scheme 2.4. Synthesis of the mesogens **D1-D9.**

It should be noted that only acetylenes with electron donating substituents have been prepared. Attempts to synthesize materials with slightly electron withdrawing substituents failed due to fast dimerization or decomposition of the acetylene. To prepare **D8** with (weak) electron withdrawing sulfone groups attached, the corresponding thioether was oxidized under mild conditions (to preserve the triple bonds and the terminal hydroxyl functionality).[43] The propionate derivative (**D2Prop**) and a adipoyl derivative **(D2)₂** of the methyl-substituted mesogen **D2** were prepared to allow fair comparison between polymers and monomer/dimer.

A range of terminal acetylenes has been prepared in order to make an even wider variety of mesogens, see Figure 2.6. However, the intended discotic materials were not obtained for various reasons. Firstly, there is the competition between the Sonogashira reaction (Pd and Cu catalyzed) and side reactions that consume the acetylene, e.g. oxidative dimerization of the acetylene (Cu catalyzed). Acetylenes with electron withdrawing groups (**13c**,**d**,**e**) were quickly consumed during the reaction, while the desired products were not obtained. Socondly, ferrocenyl acetylene **13f** did not fully couple due to steric reasons. The substitution reaction stopped at an average substitution of only 3 ferrocene groups per central core, although ferrocenyl acetylene was still present in the reaction mixture. Finally, acetylenes **13a**,**b**,**g**,**h** seemed to couple well, but the products were difficult to purify, due to their inability to crystallize in all four cases. The main impurities included (isomers of) less substituted products.

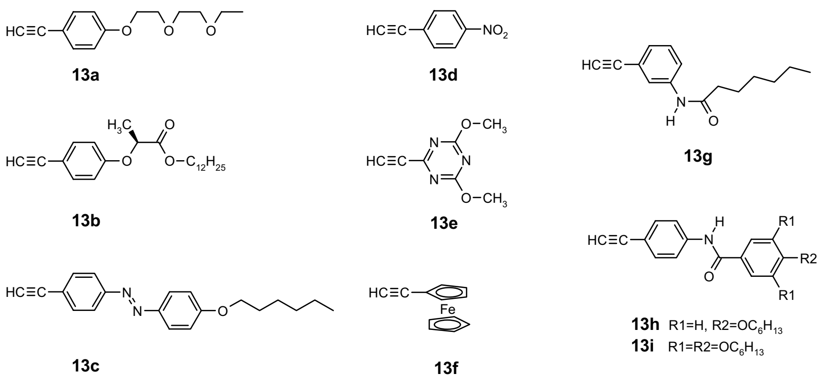
13a **13d** **13g** **13b** **13e** **13c** **13f**

13h R1=H, R2=OC_6H_{13}

13i R1=R2=OC_6H_{13}

Figure 2.6. Synthesized terminal acetylenes from which the corresponding mesogen could not be obtained at all or not with a desired level of purity.

2.2.3 Preparation of electron acceptors

The electron acceptors, we used in our studies are based on multi-nitrated fluorenone.[44] TNF (**A2**) and **A3** are commercially available, but can also be prepared without much effort, see Chapter 2.1.4. To functionalize TNF with a sufficiently long spacer, acetoxim was coupled to an 11-hydroxyundecyl spacer. By a transoximation reaction of **15** with **A2** in acetic acid, catalyzed with *p*-toluenesulfonic acid (*p*TSA),[32b] the terminally acetylated product was obtained. The acetyl group was removed by saponification under acidic conditions, yielding **A1**.

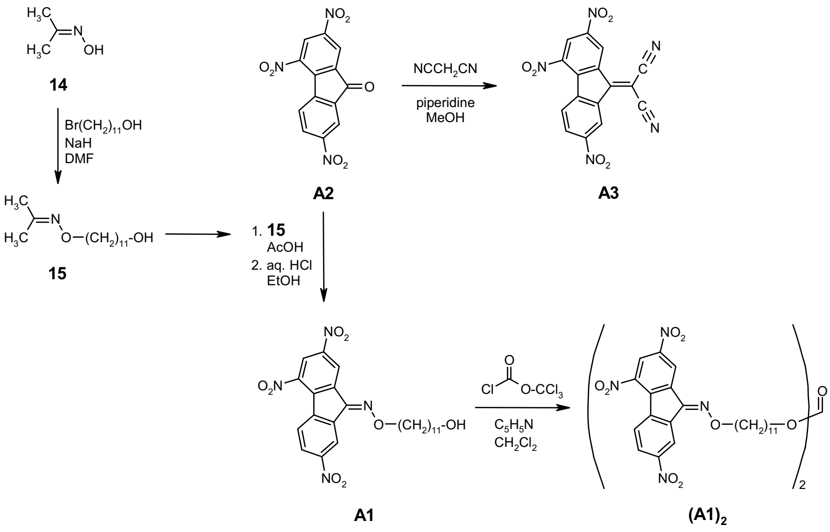

Scheme 2.5. Synthesis of electron acceptors **A1** and dimer **(A1)$_2$**.

A bifunctional acceptor was prepared by coupling of **A1** with diphosgene. It should be noted that both **A1** and its dimer **(A1)$_2$** show broad melting trajectories. We believe this can be attributed to the presence of two isomers in **A1** (see Figure 2.7) and hence three isomers in **(A1)$_2$** (*EE*, *EZ* and *ZZ*). A strong argument for the presence of stable, nonexchanging isomers is the double set of signals observed in the ^{1}H NMR spectra of **A1**. From integration of the NMR data, it is deduced that a nearly 1:1 ratio of both isomers is present.

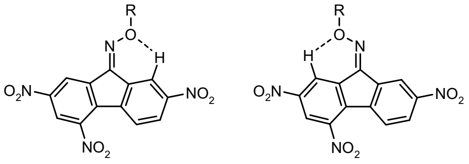

trans or entgegen (*E*) cis or zusammen (*Z*)

Figure 2.7. Stable *E*,*Z*-isomers of functionalized TNF derivatives.

2.2.4 Preparation of intramolecular charge transfer complexes

To investigate a charge transfer complex at equimolar ratios while preventing phase separation, the donor and the acceptor moieties have been linked covalently. Only a few examples are known in literature, that use the TNF derivative shown in Figure 2.5f as the acceptor moiety and triphenylene or pentakis(phenylethynyl)benzene based systems as donors.[45,46]

The linked CT complexes **D1A1** and **D2A1** (Scheme 2.6) were synthesized to study as model compounds of the nonlinked complexes as well as the copolymers. Both intramolecular charge transfer complexes have spacer lengths corresponding to those of the non-linked complexes as well as to those of the (co)polymers. This is in contrast to the materials known from literature, which have much shorter spacers. The coupling reaction was performed in two steps to prevent dimerization of one of the constituents. While the carboxylic acid functionalized acceptor (**A1-CO₂H**) was obtained in high yields, the donor-acceptor coupling reactions resulted in low yields (30-50%).

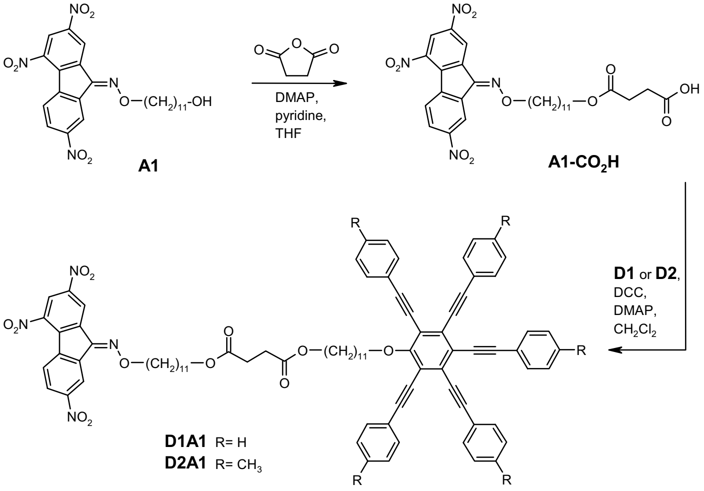

Scheme 2.6. Synthesis of intramolecular CT complexes **D1A1** and **D2A1**.

2.2.5 Preparation of the polymers

Polymerization of the acrylate derivatives of **D1** or **A1** under standard free-radical conditions did not yield any products. After all initiator had been consumed, mainly starting product was recovered.[47] Plausible reasons are the consumption of radicals by the triple bonds and nitro groups (both are present in a much higher concentration that the actual acrylic moiety) and the low concentration of the monomers in the polymerization medium, due to solubility problems. Therefore, another approach was made, attaching the desired substituents to a reactive polymer backbone, a procedure commonly known as a polymer analogous reaction (Scheme 2.7).[48] Poly(acryloyl chloride) **18** was prepared from acryloyl chloride under standard free radical conditions.[49] By a nucleophilic substitution of the reactive chlorine by the mesogenic alcohol, polyacrylates in moderate to high yields were obtained. Since a complete substitution of the polymer backbone cannot be achieved, unreacted acyl groups remain in the polymer. At later stages, they might crosslink or hydrolyze to form carboxylic acid groups, which are expected to have a large impact on the thermal behavior the polymer. To prevent this, the remaining acyl groups were converted to methyl esters with an excess of methanol. Note that this method produces (random) copolymers.

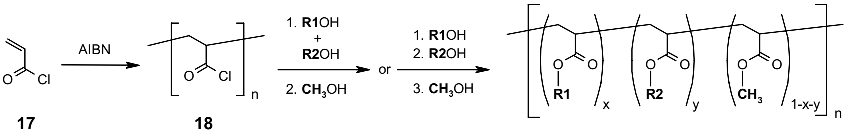

Scheme 2.7. Polymerization of and the polymer analogous reaction.

Applying the polymer analogous reaction offers more advantages. Either by using a mixture of alcohols or by adding them subsequently to the reaction mixture, (random) copolymers with a wide range of chemical compositions can be obtained. (see Scheme 2.8 and Table 2.2).

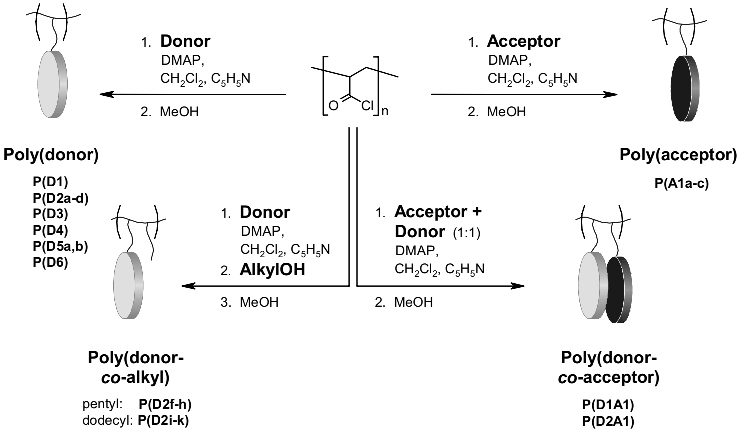

Scheme 2.8. Schematic representation of the synthesis of polymers bearing donor and/or acceptor groups.

The reaction described above has been used to synthesize a number of donor and/or acceptor substituted polymers. Studies of the preparation of **P(A1)** showed that **A1** can be substituted up to 95% to the polymer backbone. Further investigations on the degree of substitution have been performed with **D2**. A series of polymers with a varying degree of mesogen substitution (30% - 90%) has been synthesized. In addition, a series of copolymers with pentyl and dodecyl ester groups have been prepared to investigate the thermal behavior of materials with a lower mesogen density.[50] Furthermore, two intramolecular CT copolymers have been prepared.[51] It is marked that with an equal amount of donor and the acceptor in the feed, an equal degree of substitution was found in the polymer. This implies that the terminal hydroxyl groups in the donor and acceptor have similar reactivities.

Table 2.2. Prepared polymers. Yields based on mesogen conversion. The weight fraction 'rigid mesogen' was calculated as the fraction of purely rigid material, the fraction 'flexible' as the rest (i.e. dangling side groups, spacer and polymer backbone). The fractions were calculated from ^1H NMR spectra. Sample **P(D2e)** was prepared by mixing **P(D2c)** and **P(D2d)** via dissolving them in a common solvent and evaporation of the solvent.

Polymer	**Substituents**		**Degree of substitution [%-mol]**			**Weight content [%-wt]**		**Yield [%]**
	R1	**R2**	**R1**	**R2**	**CH_3**	**rigid mesogen**	**flexible tails, spacer**	
P(D1)	**D1**	–	78	–	22	70.3	29.7	98
P(D3)	**D3**	–	~50	–	~50	~47	~53	59
P(D4)	**D4**	–	~50	–	~50	~42	~58	38
P(D2a)	**D2**	–	90	–	10	73.8	26.2	46
P(D2b)	**D2**	–	64	–	36	70.8	29.2	70
P(D2c)	**D2**	–	48	–	52	67.5	32.5	35
P(D2d)	**D2**	–	31	–	69	61.5	38.5	43
P(D2e)[c]	**D2**	–	–	–	–	64.5	35.5	–
P(D2f)	**D2**	n-C_5H_{11}	69	31	–	69.7	30.3	33
P(D2g)	**D2**	n-C_5H_{11}	41	43	16	62.0	38.0	43
P(D2h)	**D2**	n-C_5H_{11}	42	50	8	61.7	38.3	30
P(D2i)	**D2**	n-$C_{12}H_{25}$	61	11	28	68.3	31.7	37
P(D2j)	**D2**	n-$C_{12}H_{25}$	45	45	10	57.8	42.2	36
P(D2k)	**D2**	n-$C_{12}H_{25}$	33	42	25	52.9	47.1	65
P(D5a)	**D5**	–	64	–	36	65.7	34.3	62
P(D5b)	**D5**	–	71	–	29	66.5	33.5	75
P(D5c)	**D5**	–	83	–	17	67.7	32.3	53
P(D6a)	**D6**	–	60	–	40	48.5	51.5	81
P(D6b)	**D6**	–	63	–	37	48.8	51.2	68
P(A1a)	**A1**	–	77	–	23	56.7	43.3	70
P(A1b)	**A1**	–	91	–	9	58.4	41.6	
P(A1c)	**A1**	–	95	–	5	58.8	41.2	58
P(D1A1)	**D1**	**A1**	36	36	28	–	–	94
P(D2A1)	**D2**	**A1**	43	43	14	–	–	61

2.3 Experimental procedures

General. All materials were used as purchased unless mentioned otherwise. Phenylacetylene (**3a**) and 2,4,7-trinitro-9-fluorylidenemalonitril (**A3**) are commercial available. Compounds $Pd(II)Cl_2(PPh_3)_2$ and 2,4,7-trinitro-9-fluorenone (**A2**) were prepared according to literature procedures.[30,52] Tetrahydrofurane (THF) was distilled from $LiAlH_4$, CH_2Cl_2 from P_2O_5, dixoane from sodium and pyridine from CaH_2. Acryloyl chloride and propionyl chloride were distilled prior to use. The alcohols 1-pentanol and 1-dodecanol were dried on molecular sieves prior to use.

Instrumental. Nuclear magnetic resonance (NMR) spectra were taken on a Varian VXR 300 or VXR 400 MHz spectrometer. Chemical shifts are reported in ppm relative to TMS. NMR data of the various donors refer to

Figure 2.8. Infrared spectra were recorded between NaCl plates on a Mattson Polaris infrared Fourier transform spectrometer. Molecular weights were determined by gel-permeation chromatography (GPC) in THF against narrow polystyrene standards. The thermal properties of the materials were investigated by a Perkin-Elmer DSC 7 differential scanning calorimeter (in a nitrogen atmosphere). A standard heating and cooling rate of $10°C\cdot min^{-1}$ was used. Transition temperatures were determined as the maximum or minimum of the exotherm or endotherm. The mesophases were identified on a Jenapol optical polarizing microscope, equipped with a Mettler FP82 HT hot stage and a Mettler FP80 central processor. For birefringence studies, the microscope was equipped with an adjustable quarter wave plate. Further mesophases analysis was performed by X-ray diffraction measurements, using a Bruker HISTAR area detector equipped with a Siemens Kristalloflex 710D X-ray generator with graphite-monochromated CuαK radiation ($\lambda = 1.54$ Å). The samples were oriented in a magnetic field using a Supper SmCo permanent magnet with a field of about 1.5 T and could be heated using a custom build capillary heating element. The maximum diffraction angle was 30°. For the dielectric experiments disk-shape samples were prepared consisting of gold plated circular brass electrodes, between which the sample material was put together with quartz spacers (diameter ~ 50 μm). Preparation took place under flowing gaseous nitrogen. Dielectric experiments were performed using a combination of three dielectric measurement systems, covering a total frequency range from 10^{-2} to 10^{9} Hz: (*i*) a frequency response analyzer (Schlumberger 1260) equipped with a custom made dielectric interface (developed by TNO) for frequencies between 10^{-2} and 10^{3} Hz; (*ii*) a Hewlett-Packard 4284A precision LCR-meter for frequencies between 10^{3} and 10^{6} Hz; and (*iii*) a Hewlett-Packard 4291A Rf-analyzer for the frequency range from 10^{6} and $1.8\cdot10^{9}$ Hz. The sample was placed in a nitrogen cryostat (Novocontrol), the temperature of which was controlled with a stability of better than ± 50 mK.

4'-Pentylacetophenone (2c). Acetyl chloride (170 mmol) was added in 15 minutes to a vigorously stirred, cooled (0°C) mixture of $AlCl_3$ (170 mmol) in CH_2Cl_2 (150 mL). In 30 minutes **1c** (135 mmol) was added, the clear solution was stirred at 0°C (2 hrs) and allowed to warm to room temperature. The reaction mixture was poured into ice and extracted with ether (3×), the combined organic layers were washed with 1N HCl (2×) and water (2×), dried with $MgSO_4$ and the solvent was evaporated. The product was pure enough to be used directly in the next step. Yield: 95%. ^{1}H-NMR ($CDCl_3$): δ 7.80, 7.18 (2×dd, 4H, CH aromatic); 2.68 (t, 2H, CH_2Ph); 2.62 (s, 3H, $COCH_3$); 1.7-1.2 (m, 6H, CH_2 aliphatic); 0.89 (t, 3H, CH_3).

4'-Heptylacetophenone (2d). The procedure as described for **2c** was used. No extra purification was performed. Yield: 89%. ^{1}H-NMR ($CDCl_3$): δ 7.88, 7.22 (2×dd, 4H, CH aromatic); 2.70 (t, 2H, CH_2Ph); 2.62 (s, 3H, $COCH_3$); 1.7-1.2 (m, 10H, CH_2 aliphatic); 0.89 (t, 3H, CH_3).

4-Ethynyltoluene (3b). In 15 minutes **2b** (100 mmol) was added to PCl_5 (110 mmol). The clear solution was stirred overnight at room temperature. Formed $POCl_3$ was removed under reduced pressure and carefully DMSO (80 mL) was added while the mixture was cooled at room temperature in a water bath. Potassium *tert*-butoxide (200 mmol) was added in small portions in 60 minutes. After the addition was completed, the water bath was removed and the mixture was heated at 70°C for 1 hour. The reaction mixture was poured into water and extracted with diethyl ether (3×). The combined organic layers were washed with water and brine, dried over $MgSO_4$ and the solvent was evaporated. Distillation under reduced pressure, T_b = 99-100°C at 80 mmHg, lit. 168-170°C,[53] yielded 55% of a colorless oil. ^{1}H-NMR ($CDCl_3$): δ 7.38, 7.05 (2×dd, 4H, CH aromatic); 3.00 (t, 2H, HC≡C); 2.33 (s, 3H, CH_3).

4-Pentyl-1-ethynylbenzene (3c). The procedure as described for **3b** was used. Distillation, T_b = 65°C at 0.35 mbar yielded 41% of a colorless oil. ^{1}H-NMR ($CDCl_3$): δ 7.39, 7.12 (2×dd, 4H, CH aromatic); 3.01 (s, 1H, HC≡C); 2.58 (t, 2H, CH_2Ph); 1.60, 1.31, 1.29 (m, 6H, CH_2 aliphatic); 0.88 (t, 3H, CH_3). ^{13}C-NMR ($CDCl_3$) δ 143.97, 132.05, 128.42, 119.26 (aromatic); 83.90, 76.44 (acetylene); 35.87, 31.43, 30.90, 22.52, 14.00 (aliphatic).

4-Heptyl-1-ethynylbenzene (3d). The procedure as described for **3b** was used. Distillation, T_b = 98°C at 0.40 mbar yielded 60% of a colorless oil. ^{1}H-NMR ($CDCl_3$): δ 7.39, 7.09 (2×dd, 4H, CH aromatic); 3.00 (s, 1H, HC≡C); 2.57 (t, 2H, CH_2Ph); 1.63-1.21 (m, 10H, CH_2 aliphatic); 0.89 (t, 3H, CH_3). ^{13}C-NMR ($CDCl_3$) δ 143.94, 132.06, 128.41, 119.30 (aromatic); 83.90, 76.47 (acetylene); 36.92, 31.83, 31.26, 29.24, 29.19, 22.69, 14.11 (aliphatic).

4'-Hexyloxyacetophenone (6b). A mixture of **4** (100 mmol), 1-bromohexane (133 mmol), K_2CO_3 (200 mmol), KI (5 mmol) and DMF (150 mL) was stirred at 100°C for 1 hour. After TLC indicated full conversion, the reaction mixture was cooled, poured into water (500 mL) and extracted with ether (2×). The combined organic layers were washed with a diluted HCl solution (2×) and a $NaHCO_3$ solution (2×), dried over $MgSO_4$ and the solvent was evaporated. Distillation (T_b = 137-138°C at 0.1 mbar), yielded the product as a colorless oil in 81%. ^{1}H-NMR ($CDCl_3$): δ 7.8, 6.8 (2×dd, 2×2H, CH aromatic); 4.0 (t, 2H, CH_2O); 2.5 (s, 3H, CH_3 acetyl); 2.0-1.2 (m, 8H, CH_2); 0.9 (t, 3H, CH_3 tail).

4'-Hexylsulfanylacetophenone (6c). A mixture of **5** (50 mmol), 1-hexylthiol (50 mmol) and K_2CO_3 (100 mmol) in DMSO (25 mL) was stirred at 80 ºC for 3 hours. The reaction mixture was precipitated in water, extracted with ether (3×) . The combined organic layers were washed with water (3×) , dried over $MgSO_4$ and the solvent was evaporated. The product crystallized upon standing and was used without purification in the next step, assuming a nearly quantitative yield. ^{1}H-NMR ($CDCl_3$): δ 7.96, 7.39 (2×dd, 4H, CH aromatic); 3.03 (t, 2H, CH_2S); 2.60 (s, 3H, $COCH_3$); 1.8-1.2 (m, 8H, CH_2 aliphatic); 0.89 (t, 3H, CH_3).

4-Ethynylanisole (8a). Phosphorousoxychloride (50 mL) was added dropwise to DMF (200 mL) at 0°C. The mixture was allowed to warm to room temperature, stirred for 30 minutes, cooled again to 0°C and a solution of **2** (167 mmol) in DMF (50 mL) was added in 15 minutes. After addition the mixture was heated at 50°C until TLC indicated complete consumption of the starting material. The reaction mixture was poured into a 20% sodium acetate solution (1 L), allowing the mixture to warm to 60°C. After cooling over night, the crude intermediate product **7a** was filtered from the solution in a ~90 % yield. The yellow solid was used for the next reaction without further purification. A small sample was crystallized for NMR analysis: ^{1}H-NMR ($CDCl_3$): δ 10.12 (d, 1H, CHO); 7.12, 7.88 (2×dd, 4H, CH aromatic); 6.77 (d, 1H, C=CH); 3.92 (s, 3H, CH_3O). A solution of **7a** (all from the previous step) and phase transfer catalyst $(n\text{-Bu})_4N^+HSO_4^-$ (0.5 g, 1.5 mmol) in dioxane (200 mL) was refluxed and a 2N NaOH solution (250 mL) was added at once. The dark solution was refluxed for 30 minutes, cooled, neutralized and the dioxane was evaporated under reduced pressure. The aqueous layer was extracted with diethyl ether (3×) and the combined organic layers were washed with diluted HCl solution (2×), water (2×) and brine (1×), dried on $MgSO_4$ and the solvent was evaporated. Pure **8a** was obtained by separation over a column. The crude product was diluted with 40 mL eluent (CH_2Cl_2:hexane 1:2) and applied to a 300 mL column of SiO_2. Extraction with the eluent until all product was regained, yielded a colorless oil in 70 % (overall yield). ^{1}H-NMR ($CDCl_3$): δ 6.82, 7.41 (2×dd, 4H, CH aromatic); 3.77 (s, 3H, CH_3O); 2.98 (s, 1H, C≡CH).

4-Ethynyl-1-hexyloxybenzene (8b). The procedure as described for **8a** was used. Purification was performed by application of the product, diluted with pet. ether (40 mL) to a SiO_2-column and extraction with pet. ether until all the product was obtained (overall yield: 48%) or distillation, T_b = 120 ºC at 0.50 mbar (overall yield 35%). ^{1}H-NMR ($CDCl_3$): δ 7.41, 6.82 (2×dd, 4H, CH aromatic); 3.94 (t, 2H, CH_2O); 2.98 (s, 1H, HC≡C); 1.78-1.25 (m, 8H, CH_2 aliphatic), 0.91 (t, 3H, CH_3). ^{13}C-NMR ($CDCl_3$) δ 159.56, 133.56, 114.47, 113.89 (aromatic); 83.79, 75.64 (acetylene); 68.09 (CH_2O); 31.57, 29.14, 25.70, 22.59, 14.02 (aliphatic).

4-Ethynyl-1-hexylsulfanylbenzene (8c). The procedure as described for **8a** was used. Purification was done by applying the product, diluted with pet.ether (40 mL) to a column and extraction with pet.ether until the product was obtained. Yield: 55%. ^{1}H-NMR ($CDCl_3$): δ 7.37, 7.20 (2×dd, 4H, CH aromatic); 3.06 (s, 1H, HC≡C); 2.90 (t, 2H, CH_2O); 1.66-1.23 (m, 8H, CH_2 aliphatic), 0.88 (t, 3H, CH_3). ^{13}C-NMR ($CDCl_3$) δ 138.93, 132.37, 127.51, 118.76 (aromatic); 83.44, 76.65 (acetylene); 32.80, 31.38, 28.88, 28.54, 22.53, 14.01 (aliphatic).

Heptanoic acid (4-trimethylsilanylethynylphenyl) amide (10). Heptanoyl chloride (67 mmol) was added in 15 minutes to a cooled solution (0 ºC) of mixture of **9** (67 mmol) and triethylamine (100 mmol) in THF (100 mL) in an argon atmosphere. After stirring for 16 hours at room temperature Pd(II)$Cl_2(PPh_3)_2$ (0.57 mmol), PPh_3 (1.14 mmol), ethynyltrimethylsilane (90 mmol), triethylamine (10 mL) and piperidine (20 mL) was added to the reaction mixture. The mixture was stirred for 1 hour at room temperature and a solution of CuI (1.1 mmol) and LiBr (11 mmol) in THF (5 mL) was added via a syringe. After stirring for 24 hours at room temperature, the mixture was poured into a 0.5N HCl solution and extracted with CH_2Cl_2 (3×) . The combined organic layers were washed with a 0.5 N HCl solution (2×) and water (2×) and the solvent was evaporated. The crude product was obtained as a dark brown solid and was used for the deprotection step without further purification.

Heptanoic acid (4-ethynylphenyl) amide (11). To a solution of **10** (all from the previous reaction) in methanol (100 mL) was added solution of NaOH (175 mmol) in methanol (250 mL). The reaction mixture was stirred at room temperature until TLC indicated complete consumption of **10**. Half of the solvent was removed and the mixture was precipitated in water. The product was filtered, dried, dissolved in ether (100 mL) and filtered over Al_2O_3. Pure **11** was obtained after column chromatography (SiO_2, eluent CH_2Cl_2) in 58% overall yield. ^{1}H-NMR ($CDCl_3$): δ 7.65 (s, 1H, amide); 7.50, 7.20 (2×dd, 4H, CH aromatic); 3.04 (s, 1H, HC≡C); 2.34 (t, 2H, CH_2N), 1.75-1.20 (m, 8H, CH_2 aliphatic); 0.88 (t, 3H, CH_3). ^{13}C-NMR ($CDCl_3$) δ 171.81 (C=O); 138.50, 132.90, 119.42, 117.54 (aromatic); 83.40; 76.75 (acetylene); 37.80, 31.54, 28.93, 25.54, 22.49, 14.02 (aliphatic).

11-Pentabromophenoxyundecan-1-ol (12). A mixture of pentabromophenol (75 mmol), 11-bromoundecan-1-ol (100 mmol), K_2CO_3 (100 mmol), KI (10 mmol) and DMF (250 mL) was stirred for 2 hours at 120°C. The volume was reduced by evaporating 150 mL of DMF and the mixture was precipitated in water (500 mL). After filtration and drying, the product was obtained by one or two crystallizations from aceton:THF (9:1) as a white powder in a 75-86% yield. ^{1}H-NMR ($CDCl_3$): δ 3.99 (t, 2H, CH_2OPh); 3.64 (t, 2H, CH_2OH); 1.92-1.25 (m, 18H, CH_2 aliphatic). ^{13}H-NMR ($CDCl_3$): δ 154.60 (Phenyl CO); 128.34, 124.45, 121.90 (C-Br); 73.67 (CH_2OPh); 63.09 (CH_2OH); 32.81-25.74 (CH_2 aliphatic tail).

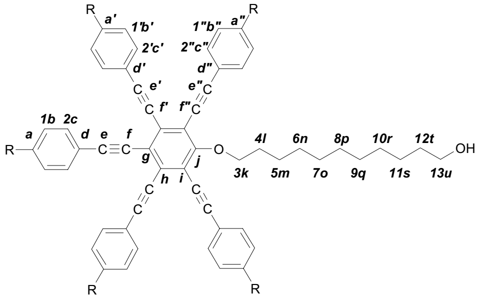

Figure 2.8. ^{1}H and ^{13}H-NMR characterization for **D1**-**D9**.

11-[Pentakis(phenylethynyl)phenoxy]undecan-1-ol (D1). A mixture of **3a** (50 mmol), **12** (5 mmol), PPh_3 (0.95 mmol) and Pd(II)$Cl_2(PPh_3)_2$ (0.43 mmol) in distilled triethylamine (50 mL) was degassed and stirred under an inert atmosphere for 1 hour. A solution of CuI (1.05 mmol) and LiBr (10 mmol) was THF (5 mL) was added to the reaction mixture. After stirring for 8 hours at 90°C, the mixture was cooled, filtered and the salts were washed well with ether (200 mL). The ether solution was cooled to -20°C and the crude product was filtered from the solution. Pure product was obtained after flash chromatography (SiO_2, eluent CH_2Cl_2:hexane 2:1 and repeated crystallizations from ether:hexane and ethanol. Yield: 70% of a pale yellow highly fluorescent powder. T_m = 124°C, lit. 117°C.[24] ^{1}H-NMR ($CDCl_3$): δ 7.65-7.55 (m, 10H, *1*); 7.38-7.26 (m, 15H, *2* and lateral CH); 4.18 (t, 2H, *3*); 3.62 (t, 2H, *13*); 1.98-1.15 (m, 18H, *4-12*).). ^{13}C-NMR ($CDCl_3$): δ 160.53 (*j*); 131.85, 131.75, 131.69 (*c*); 129.06, 128.95, 128.88 (*b*); 128.61, 128.51, 128.44 (*a*); 128.40, 124.58, 119.90 (*g*,*h*,*i*); 123.35, 123.10, 122.77 (*d*); 99.91, 99.48, 97.54 (*f*);87.28, 86.86, 84.24 (*e*); 74.70 (*k*); 63.05 (*u*); 32.80-25.77 (*l-t*).

11-[Pentakis(4-methylphenylethynyl)phenoxy] undecan-1-ol (D2). The procedure as described for **D1** was used. Purification with flash chromatography (SiO_2, eluent CH_2Cl_2:petroleum ether 4:1) and repeated crystallization from methanol yielded a pale yellow, highly fluorescent powder in 73%. ^{1}H-NMR ($CDCl_3$): δ 7.54-7.48, 7.19-7.14 (2×m, 20H, *1*,*2*); 4.37 (t, 2H, *15*); 3.62 (t, 2H, *3*); 2.38 (s, 15H, lateral methyl); 1.98-1.20 (m, 18H, *4-12*). ^{13}C-NMR ($CDCl_3$): δ 160.26 (*j*); 138.97, 138.83, 138.66 (*a*); 131.71, 131.59, 131.53 (*b*); 129.17 (*c*); 120.49, 120.32, 120.26 (*d*); 128.73, 124.02, 120.07 (*g*,*h*,*i*); 99.49, 99.33, 97.27 (*f*); 87.12, 86.66, 84.11 (*e*); 74.72 (*k*); 63.00 (*u*); 32.82, 30.63, 29.68, 29.49, 26.42, 25.79 (*l-t*); 21.58 (CH_3).

11-[Pentakis(4-methylphenylethynyl)phenoxy]undecyl propionate (D2Prop). A mixture of **5** (0.78 mmol) and dry pyridine (4 mmol) was dissolved in THF (25 mL). Freshly distilled propionyl chloride (4 mmol) was added via a syringe. The mixture was stirred overnight, poured into water and extracted with CH_2Cl_2. The combined organic layers were washed with water, dried over $MgSO_4$ and the solvent was evaporated. The pure product was obtained by flash chromatography (SiO_2, eluent CH_2Cl_2:hexane 3:2). Yield: 80% of a pale yellow, highly fluorescent powder. ^{1}H-NMR ($CDCl_3$): δ 7.26-7.18, 7.53-7.47 (m, 20H, *1*,*2*); 4.36 (t, 2H, *3*); 4.05 (t, 2H, *13*); 2.38 (s, 15H, lateral CH_3); 2.33 (q, 2H, CH_2CO_2); 1.96-1.20 (m, 18H, *4-12*); 1.13 (t, 3H, CH_3 propionate). ^{13}C-NMR ($CDCl_3$): δ 174.63 (C=O); 160.26 (inner phenyl, *j*); 138.97, 138.83, 138.66 (*a*); 131.73, 131.59, 131.57 (*b*); 129.20 (*c*); 120.39, 120.34, 120.27 (*d*); 128.75, 124.04, 120.09 (*g*,*h*,*i*); 99.48, 99.32, 97.25 (*f*); 87.04, 86.55, 84.07 (*e*); 74.78 (*k*); 64.51(*u*); 32.8-25.7 (*l-t*, CH_2 propionate); 21.58 (lateral CH_3); 9.18 (CH_3 propionate).

Hexanedioic acid bis-[11-(pentakis(phenylethynyl)phenoxy)undecyl] ester (D2)$_2$. To a solution of **D1** (98 mmol), dry pyridine (1 mL) and DMAP (catalytic amount) in CH_2Cl_2 (25 mL) was added adipoyl chloride (48 mmol) via a syringe. The mixture was stirred for 40 hours under inert conditions poured into water and extracted with CH_2Cl_2. The combined organic layers were with water, dried over $MgSO_4$ and the solvent was evaporated The pure product was obtained by flash chromatography (SiO_2, eluent CH_2Cl_2:hexane 1:1), yielding 88% of a pale yellow, highly fluorescent powder. ^{1}H-NMR ($CDCl_3$): δ 7.53-7.46, 7.16-7.12 (2×m, 2×20H, *1*,*2*); 4.35 (t, 4H, *3*); 4.04 (t, 4H, *13*); 2.37 (s, 30H, CH_3Ph); 1.98-1.18 (m, 40H, *4-12* and CH_2 hexanedioic acid). ^{13}C-NMR ($CDCl_3$) δ 173.41 (CO_2); 160.25 (*j*); 138.98, 138.83, 138.66 (*a*); 131.71; 131.59; 131.54 (*b*); 129.19 (*c*); 128.74, 124.03, 120.07 (*g*,*h*,*i*); 120.50, 120.34, 120.28 (*d*); 99.46, 99.30, 97.24 (*f*); 87.08, 86.60, 84.10 (*e*); 74.74 (*k*); 64.55 (*u*); 33.94 (CH_2CO_2); 30.62-24.44 (*l-t* and CH_2 hexanedioic acid); 21.59 (CH_3Ph).

11-(Pentakis(4-pentylphenylethynyl)phenoxy)undecan-1-ol (D3). The procedure as described for **D1** was used. Purification with flash chromatography (SiO_2, eluent CH_2Cl_2:hexane 1:1) and repeated crystallization from *iso*-propanol yielded a pale yellow, highly fluorescent powder in 37%. ^{1}H-NMR ($CDCl_3$): δ 7.57-7.51, 7.20-7.14 (2×m, 2×10H, *1*,*2*); 4.36 (t, 2H, *3*); 3.62 (t, 2H, *13*); 2.63 (t, 10H, CH_2Ph); 1.98-1.18 (m, 48H, *4-12* and CH_2 tails); 0.90 (t, 15H, CH_3). ^{13}C-NMR ($CDCl_3$) δ 160.26 (*j*); 144.02, 143.90, 143.71 (*a*); 131.78; 131.66; 131.60 (*b*); 128.54 (*c*); 128.77, 124.07, 120.10 (*g*,*h*,*i*); 120.72, 120.56, 120.50 (*d*); 99.54, 99.38, 97.31 (*f*); 87.10, 86.62, 84.11 (*e*); 74.77 (*k*); 63.11 (*u*); 35.98 (CH_2Ph); 32.84-22.54 (*l-t* and CH_2 tails); 14.03 (CH_3).

11-(Pentakis(4-heptylphenylethynyl)phenoxy)undecan-1-ol (D4). The procedure as described for **D1** was used. Pure **D4** was obtained by repeated column chromatography (SiO_2, eluent toluene:ether 40:1) and crystallizations from cold (–20°C) hexane (including fast cold filtration to prevent melting of the substance). Yield: 38% of a yellow solid, obtained from the melt. ^{1}H-NMR ($CDCl_3$): δ 7.55-7.49, 7.19-7.14 (2×m, 2x10H, *1*,*2*); 4.36 (t, 2H, *3*); 3.61 (t, 2H, *13*); 2.63 (t, 10H, CH_2Ph); 1.98-1.28 (m, 68H, *4-12*, CH_2 tails); 0.89 (t, 15H, CH_3). ^{13}H-NMR ($CDCl_3$): δ 160.27 (*j*); 144.01, 143.89, 143.70 (*a*); 131.79, 131.67, 131.61 (*b*); 128.53 (*c*); 128.78, 124.09, 120.11 (*g*,*h*,*i*); 120.75, 120.57, 120.52 (*d*); 99.55, 99.39, 97.32 (*f*); 87.15, 86.66, 84.15 (*e*); 74.76 (*k*); 63.09 (*u*); 36.03 (CH_2Ph, tails); 32.9-22.7 (*l-t*, CH_2 tails); 14.11 (CH_3 tails).

11-[Pentakis(4-methoxyphenylethynyl)phenoxy]undecan-1-ol (D5). The procedure as described for **D1** was used. Purification with flash chromatography (SiO_2, eluent CH_2Cl_2:petroleum ether 4:1) and repeated crystallization from methanol yielded a pale yellow, highly fluorescent powder in a 54% yield. ^{1}H-NMR ($CDCl_3$): δ 7.56-7.51, 6.90-6.86 (2×m, 2×10H, *1,2*); 4.37 (t, 2H, *3*); 3.83 (s,15H, OCH_3); 3.61 (t, 2H, *13*); 1.95-1.10 (m, 9×2H, *4-12*). ^{13}C-NMR ($CDCl_3$) δ 160.0, 159.9 (*a*); 159.8 (*j*); 133.3, 133.1 (*c*); 128.4, 123.8, 119.9 (*g,h,i*); 115.8, 115.6, 115.5 (*d*); 114.1 (*b*); 99.2, 99.0, 97.0 (*f*); 88.7, 86.2, 83.6 (*e*); 74.6 (*k*); 63.1 (*u*); 55.3 (CH_3O); 32.8-25.8 (*l-t*).

11-[Pentakis(4-hexyloxyphenylethynyl)phenoxy]undecan-1-ol (D6). The procedure described for the synthesis of **D1** was used with a reaction time of 8 hours. After the crude work up (yield of ~65%), pure **D6** was obtained by repeated column chromatography (SiO_2, eluent toluene:ether 20:1) and crystallizations from ether: hexane (1:10). Yield 40% of a light yellow, bright fluorescent solid. ^{1}H-NMR (300 MHz, $CDCl_3$): δ 7.54-7.49, 6.88-6.84 (2×m, 2×10H, *1,2*); 4.34 (t, 2H, *3*); 3.97 (t, 10H, CH_2OPh, tails); 3.61 (t, 2H, *13*); 1.95-1.24 (m, 58H, *4-12* and tails); 0.92 (t, 15H, CH_3). ^{13}H-NMR (300 MHz, $CDCl_3$): δ 159.84 (*i*); 159.64, 159.53, 159.44 (*a*); 133.28, 133.14, 133.10 (*c*); 128.40, 123.86, 119.86 (*g,h,i*); 115.54, 115.37, 115.30 (*d*); 114.61 (*b*); 99.25, 99.01, 97.01 (*f*); 86.58, 86.05, 83.47 (*e*); 74.61 (*k*); 68.13 (CH_2OPh, tails); 63.05 (*u*); 23.82-22.62 (*l-t* and CH_2 tails); 14.05 (CH_3 tails).

11-[Pentakis(4-hexylsulfanylphenylethynyl)phenoxy]undecan-1-ol (D7). The procedure described for the synthesis of **D1** was used with a reaction time of 6 hours. After the crude work up (yield ~78%), pure **D6** was obtained by repeated column chromatography (SiO_2, eluent toluene:ether 20:1) and crystallizations from ether: hexane (1:10). Yield: 22% of a yellow, highly fluorescent powder. ^{1}H-NMR ($CDCl_3$): δ 7.49-7.42, 7.28-7.21 (2×m, 2x10H, *1,2*); 4.34 (t, 2H, *3*); 3.62 (t, 2H, *13*); 2.97 (t, 10H, CH_2S); 1.97-1.27 (m, 58H, *4-12* and CH_2 tails); 0.90 (t, 15H, CH_3). ^{13}H-NMR ($CDCl_3$): δ 160.20 (*j*); 139.47, 139.23, 138.98 (*a*); 132.02; 131.88 (*c*); 127.47 (*b*); 128.40, 123.89, 119.39 (*g,h,i*); 119.98, 119.79, 119.66 (*d*); 99.64, 99.27, 99.11 (*f*); 88.05, 87.94, 87.07 (*e*); 74.80 (*k*); 63.08 (*u*); 22.55-32.84 (*l-t* and CH_2 tails); 14.03 (CH_3 tails).

11-[Pentakis[4-(hexylsulfonyl)phenylethynyl]phenoxy]undecan-1-ol (D8). A solution of **D7** (0.37 mmol) in CH_2Cl_2 (25 mL) was cooled in an ice bath. In 3 minutes, *m*-chloroperbenzoic acid (5 mmol) was added and the solid slowly dissolved. The reaction mixture was stirred at room temperature for 4.5 hours. The reaction was stopped by washing the solution with an aqueous Na_2SO_3 solution, an aqueous $NaHCO_3$ solution and pure water subsequently. After drying on $MgSO_4$ and evaporation of the solvent, pure **D8** was obtained by crystallization from methanol. Yield 91% of a yellow, highly fluorescent powder. ^{1}H-NMR ($CDCl_3$): δ 7.98-7.93, 7.75-7.72 (2×m, 2×10H, *1,2*); 4.43 (t, 2H, *3*); 3.62 (t, 2H, *13*); 3.13 (t, 10H, CH_2SO_2); 1.22-1.97 (m, 58H, *4-12* and CH_2 tails); 0.87 (t, 15H, CH_3). ^{13}H-NMR ($CDCl_3$): δ 161.86 (*j*); 139.90, 139.61 (*a*); 132.19, 132.12, 132.07 (*c*); 128.50, 128.47, 128.44 (*b*); 128.18, 128.10, 127.93 (*d*); 129.20,123.87, 120.43 (*g,h,i*); 99.33, 99.28, 96.06 (*f*); 89.77, 89.41, 87.18 (*e*); 75.59 (*k*); 62.95 (*u*); 56.26 (CH_2SO_2); 32.78-22.29 (*l-t* and CH_2 tails); 13.91 (CH_3 tails).

11-[Pentakis[4-(*N*-heptanoylamino)phenylethynyl]phenoxy]undecan-1ol (D9). The procedure described for the synthesis of **D4** was used with a reaction time of 8 hours. The reaction mixture was diluted with CH_2Cl_2 and washed with a 0.5 N HCl solution. To column separations (using silicagel and CH_2Cl_2:MeOH 20:1 as eluent) yielded a crude product in ~40%. A fraction was applied to a subsequent column separation (using silicagel and CH_2Cl_2 with an increasing MeOH content of 2 to 5%), that yielded **D9** in 9% as a yellow, fluorescent solid. Compound **D9** is hardly soluble in CH_2Cl_2, (or $CHCl_3$) or MeOH, but can be dissolved conviniently in combinations of these solvents or polar organic solvent, such as DMSO. ^{1}H NMR ($CDCl_3$ + 10% methanol-*d*4): δ 7.51-7.40 (m, 2x10H, CH aromatic); 4.32 (t, 2H, CH_2OPh); 3.56 (t, 2H, CH_2OH); 2.40 (t, 10H, CH_2CONH); 1.22-1.87 (m, 58H, CH_2 tails and spacer); 0.90 (t, 15H, CH_3). Due to strong aggregation, even in dilute solutions, the ^{13}C NMR is not as detailed as for the other mesogens. ^{13}C NMR ($CDCl_3$ + 10% methanol-*d*4): δ 173.5 (C=O); 138.8 (*a*); 132.6-132.4 (*c*); 120.1 (*b*); 118.9 (*d*); 99.1, 99.0, 96.2 (*f*); 87.8, 87.6, 84.6 (*e*); 77,9 (*k*); 62.6 (*u*); 37.5-22.7 (*l-t*, CH_2 alkyl tails); 14.1 (CH_3). Note that *g-j* were not visible.

1-[2-(2-Ethoxyethoxy)ethoxy]-4-ethynyl-benzene (13a). A mixture of 4-iodophenol (150 mmol), 2-bromo-1-(2-thoxy)ethoxyethane (125 mmol), K_2CO_3 (200 mmol), KI (7 mmol) and butanone (300 mL) was refluxed for 20 hours. After removal of the solvent, water was added and the mixture was extracted with CH_2Cl_2 (2×) and the combined organic layers were washed with 1N NaOH (2×) and brine (1×), dried over $MgSO_4$ and the solvent was evaporated. A solution of the product in CH_2Cl_2 (25 mL) was stirred with powdered KOH (0.5 gram) and extracted over a column (SiO_2, eluent CH_2Cl_2:pet. ether 1:1), yielding the 4-iodophenyl ether as a colorless liquid that solidified upon standing in 78%. A mixture of 3,6-dioxooctyl 4-iodophenyl ether (44.6 mmol), ethynyltrimethylsilane (50 mmol), $Pd(II)Cl_2(PPh_3)_2$ (100 mg, mmol), PPh_3 (75 mg), piperidine (10 mL) and THF (50 mL) was degassed and stirred for 1 hour in an argon atmosphere. A solution of CuI (50 mg) and LiBr (250 mg) in THF (2 mL) was added via a syringe. After stirring for 16 hours, the reaction mixture was filtered and concentrated to a dark brown oil that was dissolved in methanol (50 mL) to which a solution of NaOH (90 mmol) in methanol (50 mL) was added. The mixture was stirred for 5 hours at room temperature, the solvent was evaporated and an 1N HCl solution (400 mL) was added that was extracted with ether (3×). The combined organic layers were washed with brine (3×), dried and the solvent was evaporated. Pure **13a** was obtained by filtration over a column (300 mL SiO_2, eluent CH_2Cl_2:pet. ether 1:1) in 88%. ^1H-NMR ($CDCl_3$): δ 7.41, 6.85 (2×dd, 4H, CH aromatic); 4.12 (t, 2H, CH_2OPh); 3.86, 3.70, 3.62 (3×dd, 6H, glycol); 3.27 (q, 2H, ethoxy); 3.00 (s, 1H, C≡CH); 1.21 (t, 3H, CH_3). ^{13}C-NMR ($CDCl_3$) δ 159.13, 133.52, 114.58, 114.31 (aromatic); 83.63, 75.93 (acetylene); 70.88, 69.81, 69.59, 67.42, 66.69 (CH_2O); 15.11 (CH_3). The five-fold Sonogashira coupling reaction with **12** yielded a yellow oil, containing a high amount of product, identified by the typical blue fluorescent dot on TLC. However, despite multiple column separations, the product was not obtained with a desired purity.

2-(4-Ethynylphenoxy)propionic acid dodecyl ester (13b). To a cooled solution (-15 ºC) of PPh_3 (100 mmol) in THF (85 mL) was added diethylazodicarboxilic acid (100 mmol). The reaction mixture was stirred for 3 minutes, *S*-ethyllactate (100 mmol) and 4-iodophenol (100 mmol) were added. After removal of the cooling bath, the mixture was stirred for 6 hours at room temperature. The product was obtained after an usual work-up in 56%. The acetylene group was introduced as described for **13a** and the trimethylsilyl group was in-situ removed by addition of a 10% solution of NaOH in ethanol. Deprotection also resulted in saponification to the free acid. ^1H-NMR ($CDCl_3$): δ 10.78 (s, 1H, CO_2H); 7.42, 6.82 (2×dd, 4H, CH aromatic); 4.47 (q, 1H, CHOPh); 3.00 (s, 1H, HC≡C); 1.65 (d, 3H, CH_3). Product **13b**, obtained after reaction of the free carboxylic acid with an excess of dodecanol and dicyclohexylcarbodiimide in CH_2Cl_2, has not been treated with **12**, due to the low overall yield.

(4-Ethynylphenyl)-(4-hexyloxyphenyl)diazene (13c). 4-Hydroxy-4'-iodoazobenzene, obtained from a standard diazotation reaction of 4-iodoaniline with phenol was alkylated with bromohexane under standard conditions (see product **6b**) to obtain 4-hexyloxy-4'-iodoazobenzene in a 78% overall yield. ^1H-NMR ($CDCl_3$): δ 7.88, 7.81, 7.59, 6.98 (4×dd, 8H, CH aromatic); 4.01 (t, 2H, CH_2O); 1.85-1.25 (m, 8H, CH_2 aliphatic); 0.91 (t, 3H, CH_3). The acetylene group was introduced by method 3 and deprotected using KOH in methanol. Pure **13c** was obtained by dissolving the reaction mixture in hot acetone, cooling the solution to –20°C and remove the impurities by suction. ^1H-NMR ($CDCl_3$) δ 7.91, 7.83, 7.61, 7.00 (4×dd, 8H, CH aromatic); 4.04 (t, 2H, CH_2O); 3.20 (s, 1H, HC≡C); 1.90-1.25 (m, 8H, CH_2 aliphatic); 0.92 (t, 3H, CH_3). Reactions of **13c** with **12** under the usual or even milder conditions showed fast consumption of the acetylene and no traces of product.

4-Ethynyl-1-nitrobenzene (13d). The acetylene was prepared via method 2, shown in Scheme 2.2, starting from 4'-nitroacetophenone. Pure **13d** was obtained after crystallization from methanol:aceton 1:1 in a 48% overall yield. ^1H-NMR ($CDCl_3$): δ 8.20, 7.64 (2×dd, 4H, CH aromatic); 3.37 (s, 1H, HC≡C). ^{13}C-NMR ($CDCl_3$) δ 147.54, 132.98, 128.93, 123.57 (aromatic); 82.36, 81.62 (acetylene). Reactions of **13e** with **12** under the usual or even milder conditions showed fast consumption of the acetylene and no traces of product.

2,4-Dimethoxy-6-ethynyl-1,3,5-triazine (13e). A mixture of 6-chloro-2,4-dimethoxy-1,3,5-triazine (90 mmol), ethynyltrimethylsilane (100 mmol), $Pd(II)Cl_2(PPh_3)_2$ (300 mg), PPh_3 (200 mg), ethyldiisopropylamine (30 mL) and dry toluene (100 mL) was stirred for 15 minutes in an argon atmosphere. A solution of CuI (150 mg) and LiBr (600 mg) in THF (5 mL) was added and the mixture was stirred for 40 hours. The solvent was evaporated, and the residue was poured into water, extracted with ether (2×) and the combined organic layers were washed with an 1N HCl solution (2×) and water, dried over $MgSO_4$ and the solvent was evaporated. Half of the residue was dissolved in dry CH_2Cl_2 (250 mL) and cooled to 0 ºC. A solution of tetrabutylammonium fluoride hydrate (TBAF) (50 mmol) in CH_2Cl_2 (75 mL) was added in 1 hour and the dark solution was stirred for 2 hours. An usual work-up followed by a column separation yielded the free acetylene in a 47% overall yield. ^{1}H-NMR ($CDCl_3$): δ 4.15 (s, 6H, OCH_3); 3.27 (s, 1H, HC≡C). Reactions of **13e** with **12** under the usual or even milder conditions showed fast consumption of the acetylene and no traces of product.

Ethynylferrocene (13f). The product was prepared from acetylferrocene analogous to the procedure to prepare **8**. Purification using column chromatography (SiO_2, eluent CH_2Cl_2: hexane 1:3) gave the product as red crystals in a 71% overall yield. ^{1}H-NMR ($CDCl_3$): δ 6.86-6.90, 7.51-7.56 (2×m, 2×10H, *1,2*); 4.37 (t, 2H, *3*); 3.83 (s,15H, OCH_3); 3.61 (t, 2H, *13*); 1.10-1.95 (m, 9×2H, *4-12*). Subsequent reaction with **12** under the usual conditions led to a average substitution of only three ethynylferrocyl groups, as indicated by ^{1}H-NMR.

Heptanoic acid (3-ethynylphenyl) amide (13g). The procedure as described for **10** was used, only starting from 3-iodoaniline. Subsequent deprotection to the terminal acetylene was performed with 1.2 eq. TBAF in THF as described for **13e**. After purification with column chromatography (Al_2O_3, eluent CH_2Cl_2) an off-white solid was obtained in a 57% overall yield. ^{1}H-NMR ($CDCl_3$): δ 7.91 (s, 1H, amide); 7.57-7.21 (m, 4H, CH aromatic); 3.05 (s, 1H, HC≡C); 2.34 (r, 2H, CH_2N); 1.80-1.25 (m, 8H, CH_2 aliphatic); 0.88 (t, 3H, CH_3). Treatment of **12** with **13g** under standard conditions yielded the 5-fold substituted product, however despite multiple column separations, the product was not obtained with a desired purity.

4-Hexyloxy-*N*-(4-ethynylphenyl)benzamide (13h). First commercially available 4-hexyloxybenzoic acid was treated with $SOCl_2$ to yield the corresponding acid chloride. The product was added to 4-iodoaniline and the ethynylation and deprotection to the free acetylene was performed under conditions as described for **11**. After purification by multiple crystallizations from methanol:aceton (1:1), pure **13h** was obtained as a white solid in a 25% overall yield (apart from various impure fractions). ^{1}H-NMR (DMSO-d_6): δ 10.23 (s, 1H, amide); 7.94, 7.80, 7.45, 7.06 (4×dd, 8H, CH aromatic); 4.09 (s, 1H, HC≡C); 4.05 (r, 2H, CH_2O); 1.78-1.25 (m, 8H, CH_2 aliphatic); 0.88 (t, 3H, CH_3). Treatment of **12** with **13h** under standard conditions yielded the 5-fold substituted product, however despite many column separations and crystallizations, the product was not obtained with a desired purity. Preliminary microscopy studies revealed liquid crystalline textures at high temperatures.

3,4,5-Trihexyloxy-*N*-(4-ethynylphenyl)benzamide (13i). Ethyl gallate (100 mmol) was three-fold alkylated under standard conditions (see preparation of **6**) and the ester group was converted to the acid chloride by subsequent treatment with KOH in 96% ethanol (reflux for 4 hours, removal of the solvent, neutralization and extraction with ether) and $SOCl_2$ (200 mL, reflux 2 hours and evaporation of the solvent). A solution of the acid chloride (42 mmol) in THF was added to a solution of 4-iodoaniline (42 mmol) and triethylamine (15 mL) in THF (200 mL) and stirred over night. To the mixture was added ethynyltrimethylsilane (60 mmol), $Pd(II)Cl_2(PPh_3)_2$ (400 mg), PPh_3 (300 mg), piperidine (15 mL) and THF (200 mL). The mixture was stirred for 1 hour in argon atmosphere, a solution of CuI (250 mg) and LiBr (1.25 g) in THF (5 mL) was introduced and the mixture was stirred for 20 hours. After the usual work-up, the crude product was dissolved in THF (150 mL) and a solution of tetrabutylammonium fluoride (63 mmol) was added in 1 hour. After the work-up as described for **13g**, pure acetylene was obtained after column chromatography (SiO_2, eluent CH_2Cl_2:methanol 99:1). ^{1}H-NMR ($CDCl_3$): δ 8.41 (s, 1H, amide); 7.63, 7.43 (2×dd, 4H, CH aromatic); 6.98 (s, 2H, CH aromatic); 3.98, 3.88 (2×t, 6H, CH_2OPh); 3.06 (s, 1H, HC≡C); 1.80-1.20 (m, 24H, CH_2 aliphatic); 0.92-0.88 (m, 9H, CH_3). ^{13}C-NMR ($CDCl_3$) δ 166.13 (C=O); 153.11, 141.36, 138.68, 132.88, 129.50, 119.93, 117.80, 105.67 (aromatic); 83.41; 76.93 (acetylene); 31.75, 31.59, 30.28, 29.31, 25.73, 22.69, 22.62, 14.08, 14.03 (aliphatic). Treatment of **12** with **13i** under standard conditions yielded the 5-fold substituted product, however despite multiple column separations, the product was not obtained with a desired purity.

Propan-2-one *O*-(11-hydroxyundecyl)oxime (14). Sodium hydride (45 mmol) was added to a solution of acetoxim (41 mmol) in DMF (100 mL). The mixture was stirred for 30 minutes at room temperature, 1 hour at 80°C and cooled again. A solution of 11-bromoundecanol (41 mmol) in DMF (50 mL) was added. The mixture was stirred for 30 minutes at 110°C, cooled and poured into ice (1 kg) and extracted with ether (2×). The combined organic layers were washed with brine (2×), dried on Na_2SO_4 and the solvent was evaporated. Pure **14** was obtained after column chromatography ($S1O_2$, eluent ether) as a colorless oil in a 72% yield. ^{1}H-NMR ($CDCl_3$) δ 4.0 (t, 2H, CH_2OH); 3.6 (t, 2H, CH_2ON); 1.9 (s, 6H, CH_3); 1.9-1.2 (m, 18H, CH_2).

***E*/*Z*-11-(2,4,7-trinitro-9-fluorenylideneaminooxy)undecan-1-ol (A1).** A solution of 2,4,7-trinitro-9-fluorenone (**A2**) (1.0 g, 3.2 mmol) and propane-2-one-*O*-(11-hydroxyundecyl)oxim (1.5 g, 6 mmol) and *p*-toluenesulfonic acid (catalytic amount) were refluxed in glacial acetic (25 mL) until TLC indicated complete conversion. Water (25 mL) was added to the cooled reaction mixture and the crude product (acetylated **A2**) was obtained by filtration, washed with water and dried. Acetylated **A2** and *p*-toluenesulfonic acid (catalytic amount) were refluxed in ethanol (50 mL) for 16 hours. Water (200 mL) was added to the cooled solution and the crystallized product was filtered, washed with water and dried. Pure **A2** was obtained after column chromatography (SiO_2, eluent: toluene to toluene:aceton 95:5), yielding pale yellow crystals (1.16 g, 73%). ^{1}H-NMR ($CDCl_3$): due to the presence of *E*/*Z* isomers, multiple peaks have two positions. δ 9.42, 9.21, 8.92, 8.87, 8.83, 8.72, 8.44, 8.33, 8.31, 8.17 (10×d/dd, 5H, CH fluorene); 4.63, 4.62 (2×t, 2H, CH_2NO); 3.63 (t, 2H, CH_2OH); 1.96-1.25 (m, 18H, CH_2 aliphatic). ^{13}C-NMR ($CDCl_3$): δ 149.39, 148.00, 147.71, 146.73, 146.50, 145.00, 144.73, 141.05, 139.35, 138.98, 138.13, 135.38, 134.22, 133.87, 132.18, 126.74, 126.70, 126.64, 126.44, 125.22, 123.34, 121.77, 120.94, 120.23, 116.80 (2×13C/CH fluorene); 78.54 (CH_2ON); 63.04 (CH_2OH); 32.78, 29.57, 29.53, 29.49, 29.39, 29.23, 25.89, 25.73 (aliphatic).

Carbonic acid bis[11-(2,4,7-trinitro-9-fluorenylideneaminooxy)undecyl] ester (A1)$_2$. To a solution of **A1** (2.14 mmol) and pyridine (2.14 mmol) in CH_2Cl_2 (10 mL) was added diphosgene (0.9 mmol) via a syringe. The mixture was stirred for 12 hours at room temperature, diluted with CH_2Cl_2 and washed with water. Pure **(A1)$_2$** was obtained after purification by column chromatography (SiO_2, eluent toluene: pet. ether 40-60 1:1) as a pale yellow powder in a 54% yield. ^{1}H-NMR ($CDCl_3$) δ 9.46-8.21 (m of *E*/*Z* isomers, 10H, CH fluorene); 4.63 (t, 4H, CH_2ON); 3.52 (t, 4H, CH_2OCO); 1.96-128 (m, 36H, CH_2 spacer).

Succinic acid mono-[11-(2,4,7-trinitro--9-fluorenylideneaminooxy)undecyl] ester (A1-CO_2H). A mixture of **A1** (10 mmol), succinic acid anhydride (20 mmol), dimethylaminopyridine (catalytic amount), pyridine (3 mL) and THF (20 mL) was stirred for 5 days at room temperature. The reaction mixture was diluted with $CHCl_3$, extracted with water (2×) , 1N HCl solution (2×) and brine and the solvent was evaporated. Pure product was obtained after crystallization from CH_2Cl_2:hexane. ^{1}H-NMR ($CDCl_3$): δ 9.43-8.33 (10×d/dd, 5H, CH fluorene); 4.63 (t, 2H, CH_2ON); 4.08 (t, 2H, CH_2OCO); 2.66-2.63 (2×t, 4H, CH_2CO_2); 1.95-1.30 (m, 18H, CH_2 aliphatic). ^{13}C-NMR ($CDCl_3$) δ 178.1 (CO_2H); 172.2 (CO_2R); 149.4-116.8 (2×13 fluorene); 7.5 (CH_2ON); 65.0 (CH_2OCO); 29.5-25.8 (CH_2 aliphatic).

Succinic acid 11-[pentakis(phenylethynyl)phenoxy]undecyl ester 11-(2,4,7-trinitro-9-fluorenylideneaminooxy)undecyl ester (D1A1). A solution of **D1** (0.42 mmol), **A1** (0.42 mmol), 4-(dimethylamino)pyridine (catalytic amount) dicyclohexylcarbodiimide (2 mmol) and CH_2Cl_2 (10 mL) was stirred for 40 hours at room temperature. The mixture was diluted with CH_2Cl_2 and washed with water (2×) , a 0.5N HCl solution (2×) and brine (1×) , dried over $MgSO_4$ and the solvent was evaporated. Pure **D1A1** was obtained after a two-fold column separation (SiO_2, eluent CH_2Cl_2) in a 33% yield. ^{1}H-NMR ($CDCl_3$): δ 9.21-8.01 (10×d/dd, 5H, CH fluorene); 7.52, 7.37 (2×m, 25H, CH aromatic); 4.37 (t, 2H, CH_2ON); 4.26 (t, 2H, CH_2OCO); 4.09-4.08 (2×t, 4H, CH_2OCO); 2.63 (s, 4H, CH_2CO_2); 1.90-1.23 (m, 36H, CH_2 aliphatic).

Succinic acid 11-[pentakis(4-methylphenylethynyl)phenoxy]undecyl ester 11-(2,4,7-trinitro-9-fluorenylidene aminooxy)undecyl ester (D2A1). The procedure as described for **D1A1** was used. After column chromatography (SiO_2, eluent CH_2Cl_2), pure **D2A1** was obtained in a 64% yield. ^{1}H-NMR ($CDCl_3$): δ 9.10-7.93 (m, 5H, fluorene); 7.44-7.33 (m, 10H, *1*); 7.20-7.13 (m, 10H, *1*); 4.29 (t, 2H, CH_2ON); 4.20 (t, CH_2OPh); 4.09, 4.08 (2t, 4H, CH_2OCO); 2.63 (s, 4H, CH_2CO_2); 2.41 (s, 15H, CH_3); 1.90-1.23 (m, 36H, CH_2 aliphatic). ^{13}C-NMR ($CDCl_3$): δ 172.31 (C=O); 159.75-119.90 (25×fluorene); 139.19, 138.96, 138.89 (*a*); 131.57, 131.47, 131.40 (*b*); 129.21 (*c*); 128.04, 124.61, 119.58 (*g*,*h*,*i*); 120.14, 120.08, 119.95 (*d*); 99.42, 99.39, 97.33 (*f*); 86.58, 86.15, 83.68 (*e*); 78.11 (CH_2ON); 74.37 (*k*); 64.90, 64.84 (2×CH_2 in CH_2OCO); 30.61-25.84 (other CH_2 aliphatic); 21.63 (CH_3).

Poly(acryloyl chloride) (18). To 10.0 grams double distilled acryloyl chloride in 10.0 gram distilled 1,4-dioxane was added 0.272 g. (1.5%) AIBN. The reaction mixture was stirred at 58°C under an argon atmosphere. Using FT-IR spectroscopy (25 μm films between NaCl plates) the progress of the reaction was monitored. After 66 hours the reaction was completed; the carbonyl absorption was shifted from 1762 cm^{-1} to 1785 cm^{-1} and the typical monomer absorptions at 1609, 1369 and 704 cm^{-1} were absent. A specific polymer absorption emerged at 946 cm^{-1}. After reaction, the slightly yellow, viscous polymer solution was diluted with 10.0 gram THF, stored at –20°C and used without further purification.

Polymer analogous reaction. General procedure. Alcohol **D1-D6** or **A1** (2 mmol), pyridine (1 mL) and a catalytic amount of 4-(dimethylamino)pyridine were dissolved in 20 ml of anhydrous THF under an argon atmosphere. A solution of **18** (amount dependent on the desired degree of substitution) was added through a syringe and the mixture was stirred for 72 hours at room temperature. Dry methanol (1-2 mL) was added and the mixture was stirred for 2 hours more and the polymer was precipitated into dry methanol. The product was purified (removing excess of **D1-D5** or **A1** by repeated precipitation from a chloroform into an appropriate nonsolvent (methanol, hot ethanol, aceton or mixtures of these). Instead of starting with one alcohol, a mixture of alcohols can be used to obtain (random) copolymers, e.g. **P(D1A1)** and **P(D2A1)**. In the series **P(D2f-k)**, before addition of methanol, an excess of pentanol or dodecanol was added and the reaction mixture was stirred for another 24 hours before introducing methanol.

References and notes

(1) Cammidge, A.N.; Bushby, R.J. In *Handbook of Liquid Crystals*; Demus, D., Goodby, J.W., Gray, G.W., Spiess, H.W., Vill, V., Eds.; Wiley VCH: New York, 1998; Vol. 2B, pp 693-748.

(2) Destrade, C.; Mondon, M.C.; Malthête, J. *J. Phys. Paris C3* **1979**, *40*, 17-21.

(3) Tinh, N.H.; Gasparoux, H.; Destrade, C. *Mol. Cryst. Liq. Cryst.* **1981**, *68*, 101-111.

(4) (a) Boden, N.; Movaghar, B. In *Handbook of Liquid Crystals*; Demus, D., Goodby, J.W., Gray, G.W., Spiess, H.W., Vill, V., Eds.; Wiley VCH: New York, 1998; Vol. 2B, pp 781-798. (b) Adam, D. *Nature* **1994**, *371*, 141-143. (c) Kamada, K.; Watanabe, J.; Arakawa, K.; Kozono, H. *Eur. Pat. Appl. EP 646829 A1*; Fuji Photo Film Co., Ltd., 1995. (d) Mori, H.; Itoh, Y.; Nishiura, Y.; Nakamura, T.; Y., S. *Jap. J. Appl. Phys.* **1997**, *36*, 143-147.

(5) (a) Boden, N.; Bushby, R.J.; Cammidge, A.N. *J. Chem. Soc., Chem. Commun.* **1994**, 465-466. (b) Boden, N.; Bushby, R.J.; Cammidge, A.N. *J. Am. Chem. Soc.* **1995**, *117*, 924-927. (c) Henderson, P.; Kumar, S.; Rego, J.; Ringsdorf, H.; Schuhmacher, P. *J. Chem. Soc., Chem. Commun.* **1995**, 1059.

(6) Kreuder, W.; Ringsdorf, H. *Makrom. Chem., Rapid Commun.* **1983**, *4*, 807-815.

(7) (a) Boden, N.; Bushby, R.J.; Cammidge, A.N.; Headdock, G. *J. Mater. Chem.* **1995**, *5*, 2275-2281. (b) Boden, N.; Bushby, R.J.; Cammidge, A.N. *Liq. Cryst.* **1995**, *18*, 673-676.

(8) (a) Destrade, C.; Gasparoux, H.; Babeau, A.; Tinh, N.H. *Mol. Cryst. Liq. Cryst.* **1981**, *67*, 37-48. (b) Warmerdam, T. PhD Thesis, Rijksuniversiteit Utrecht; Utrecht, The Netherlands; 1987. (c) Destrade, C.; Tinh, N.H.; Mamlock, L.; Malthete, J. *Mol. Cryst. Liq. Cryst.* **1984**, *114*, 139-150. (d) Cayuela, R.; Nguyen, H.T.; Destrade, C.; Levelut, A.M. *Mol. Cryst. Liq. Cryst.* **1989**, *177*, 81-91.

(9) Papers concerning discotic LCPs based on triphenylenes but not shown in Figure 2.2: (a) Herrmann-Schönherr, O.; Wendorff, J.H.; Kreuder, W.; Ringsdorf, H. *Makrom. Chem., Rapid Commun.* **1986**, *7*, 97; (b) Herrmann-Schönherr, O.; Wendorff, J.H.; Kreuder, W.; Ringsdorf, H. *Makrom. Chem., Rapid Commun.* **1987**, *7*, 97.

(10) (a) Wenz, G. *Makrom. Chem., Rapid Commun.* **1985**, *6*, 577-584. (b) Boden, N.; Bushby, R.J.; Cammidge, A.N.; Martin, P.S. *J. Mater. Chem.* **1995**, *5*, 1857-1860.

(11) (a) Stewart, D.; McHattie, G.S.; Imrie, C.T. *J. Mater. Chem.* **1998**, *8*, 47-51. (b) Kreuder, W.; Ringsdorf, H.; Tschirner, P. *Makrom. Chem., Rapid Commun.* **1985**, *6*, 367. (c) Boden, N.; Bushby, R.J.; Lu, Z.B. *Liq. Cryst.* **1998**, *25*, 47-58.

(12) Weck, M.; Mohr, B.; Maughon, B.R.; Grubbs, R.H. *Macromolecules* **1997**, *30*, 6430-6437.

(13) Pol, J.F.v.d. PhD Thesis, Rijksuniversitiet Utrecht; Utrecht, The Netherlands, 1990; pp 91-125.

(14) (a) Favre-Nicolin, C.D.; Lub, J. *Macromolecules* **1996**, *29*, 6143-6149. (b) Disch, S.; Finkelmann, H.; Ringsdorf, H.; Schuhmacher, P. *Macromolecules* **1995**, *28*, 2424-2428. (c) Braun, C.D.; Lub, J. *Liq. Cryst.* **1999**, *26*, 1501-1509. (d) Kumar, S.; Schuhmacher, P.; Henderson, P.; Rego, J.; Ringsdorf, H. *Mol. Cryst. Liq. Cryst.* **1996**, *288*, 211-222.

(15) Sonogashira, K.; Tohda, Y.; Nagihara, N. *Tetrahedron Lett.* **1975**, 4467.

(16) Kohne, B.; Praefcke, K. *Chimia* **1987**, *41*, 196-198.

(17) Diercks, R.; Armstrong, J.C.; Boese, R.; Vollhardt, K.P.C. *Angew. Chem.* **1986**, *98*, 270-271.

(18) (a) Mongin, O.; Hoyler, N.; Gossauer, A. *Eur. J. Org. Chem.* **2000**, 1193-1197. (b) Kayser, B.; Altman, J.; Nöth, H.; Knizek, J.; Beck, W. *Eur. J. Inorg. Chem.* **1998**, 1791-1798. (c) Kayser, B.; Altman, J.; Beck, W. *Chem.-Eur. J.* **1999**, *5*, 754-758.

(19) Janietz, D.; Festag, R.; Schmidt, C.; Wendorff, J.H. *Liq. Cryst.* **1996**, *20*, 459-467.

(20) Praefcke, K.; Kohne, B.; Singer, D. *Angew. Chem.* **1990**, *102*, 200-202.

(21) Kumar, S.; Varshney, S.K. *Angew. Chem. Int. ed. Engl.* **2000**, *39*, 3140-3142.

(22) Ebert, M.; Jungbauer, D.A.; Kleppinger, R.; Wendorff, J.H.; Kohne, B.; Praefcke, K. *Liq. Cryst.* **1989**, *4*, 53.

(23) Praefcke, K.; Singer, D.; Gündogan, B.; Gutbier, K.; Langner, M. *Ber. Bunsenges. Phys. Chem.* **1993**, *97*, 1358-1361.

(24) Janietz, D.; Hofmann, D.; Reiche, J. *Thin Solid Films* **1994**, *244*, 794-798.

(25) Janietz, D. *Chem. Commun.* **1996**, 713-714.

(26) Janietz, D.; Praefcke, K.; Singer, D. *Liq. Cryst.* **1993**, *13*, 247-253.

(27) Langner, M.; Praefcke, K.; Krüerke, D.; Heppke, G. *J. Mater. Chem.* **1995**, *5*, 693-699.

(28) (a) Ebert, M. PhD Thesis, Technische Hochschule Darmstadt; Darmstadt, Germany, 1990; p 54. (b) P.H.J. Kouwer, unpublished results. Although a slight change in the absorption spectrum is observed (indicating some CT interactions), complexes of **D2** or **D5** with either hexacyanohexaazatriphenylene or its corresponding hexamethyl and ethyl esters showed phase separation at elevated temperatures.

(29) Weck, M.; Dunn, A.R.; Matsumoto, K.; Coates, G.W.; Lobkovsky, E.B.; Grubbs, R.H. *Angew. Chem. Int. ed. Engl.* **1999**, *38*, 2741-2745.

(30) Orchin, M.; Woolfolk, E.O. *J. Am. Chem. Soc.* **1946**, *68*, 1727.

(31) Mukherjee, T.K.; Levasseur, L.A. *J. Org. Chem.* **1965**, *30*, 644-646.

(32) (a) Newman, M.S.; Lutz, W.B. *J. Am. Chem. Soc.* **1956**, *78*, 2469-2473. (b) Möller, M.; Tsukruk, V.V.; Wendorff, J.H.; Bengs, H.; Ringsdorf, H. *Liq. Cryst.* **1992**, *12*, 17-36.

(33) Sulzberg, T.; Cotter, R. *J. Org. Chem.* **1970**, *35*, 2762-2769.

(34) Wüstefeld, R., PhD Thesis, Johannes Gutenberg Universität; Mainz, Germany; 1990.

(35) Bengs, H.; Renkel, R.; Ringsdorf, H.; Baehr, C.; Ebert, M.; Wendorff, J.H. *Makrom. Chem., Rapid Commun.* **1991**, *12*, 439-446.

(36) Möller, M.; Tsukruk, V.V.; Wendling, J.; Wendorff, J.H.; Bengs, H.; Ringsdorf, H. *Makromol. Chem.* **1992**, *193*, 2659-2668.

(37) Bengs, H.; Ringsdorf, H. *Makromol. Chem.* **1992**, *193*, 2659-2668.

(38) Praefcke, K.; Singer, D.; Kohne, B.; Ebert, M.; Liebmann, A.; Wendorff, J.H. *Liq. Cryst.* **1991**, *10*, 147-159.

(39) Rosenblum, M.; Brawn, N.; Papenmeier, J.; Applebaum, M. *J. Organomet. Chem.* **1966**, *6*, 173-180.

(40) (a) Brandsma, L.; Vasilevsky, S.F.; Verkuijsse, H.D. In *Applications of Transition Metal Catalysis in Organic Synthesis*; Springer Verlag: Berlin Heidelberg, 1998; pp 198-225. (b) Rossi, R.; Carpita, A.; Bellina, F. *Org. Prep. Proced. Int.* **1995**, *27*, 129-160. (c) Brandsma, L.; Verkuijsse, H.D. *Synthesis* **1999**, 1727-1728.

(41) Negishi, E.I.; Kotora, M.; Xu, C. *J. Org. Chem.* **1997**, *62*, 8957-8960.

(42) Michel, P.; Gennet, D.; Rassat, A. *Tetrahedron Lett.* **1999**, *40*, 8575-8578.

(43) (a) Solberg, J.; Undheim, K. *Acta Chem. Scand. B* **1986**, *40*, 381-386. (b) Victor, F.; Brown, T.J.; Campanale, K.; Heinz, B.A.; Shipley, L.A.; Su, K.S.; Tang, J.; Vance, L.M.; Spitzer, W.A. *J. Med. Chem.* **1997**, *40*, 1511-1518.

(44) Otto van den Berg is gratefully acknowledged for the preparation and characterization of **A1** and its corresponding dimer and polymers.

(45) (a) The donor and acceptor moieties have been covalently coupled by an esterification reaction. The triphenylene based intramolecular CT complexes (see Figure 2.9a) show columnar mesophases, similar to their nonlinked counterparts, see reference 32b. The thermal results on the linked complexes with **D1**, **D2** and **D3** (see Figure 2.9b) is much more complex, see references 25 and 46.

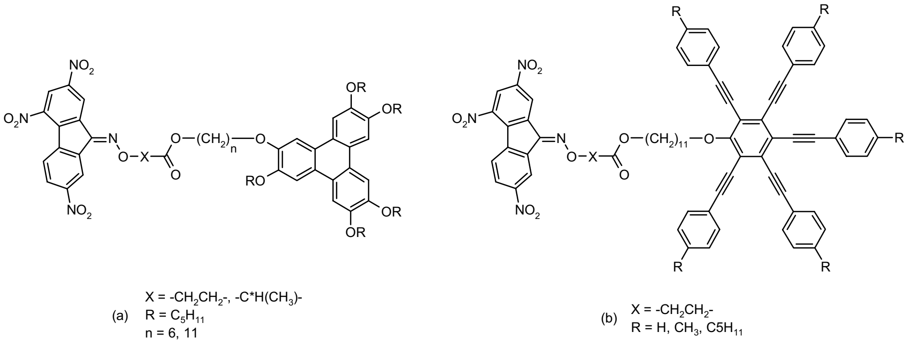

(a) X = -CH$_2$CH$_2$-, -C*H(CH$_3$)-
R = C$_5$H$_{11}$
n = 6, 11

(b) X = -CH$_2$CH$_2$-
R = H, CH$_3$, C5H$_{11}$

Figure 2.9. Structures of the intermolecular CT complexes based on:
(a) triphenylenes and (b) pentakis phenylethynyl benzenes

(46) Mahlstedt, S.; Janietz, D.; Schmidt, C.; Stracke, A.; Wendorff, J.H. *Liq. Cryst.* **1999**, *26*, 1359-1369.

(47) Kouwer, P.H.J.; Mijs, W.J.; Jager, W.F.; Picken, S.J. *Macromolecules* **2000**, *33*, 4336-4342.

(48) Strohriegl, P. *Makromol. Chem.* **1993**, *194*, 363-387.

(49) (a) Yang, Y.S.; Qi, G.R.; Qian, J.W.; Yang, S.L. *J. Appl. Pol. Sci.* **1998**, *68*, 665-670. (b) Schultz, R.C.; Elzer, P.; Kern, W. *Makromol. Chem.* **1960**, *42*, 189-196.

(50) Kouwer, P.H.J.; Gast, J.; Jager, W.F.; Mijs, W.J.; Picken, S.J. *Mol. Cryst. Liq. Cryst.* **2001**, *364*, 225-234.

(51) Kouwer, P.H.J.; Van den Berg, O.; Jager, W.F.; Mijs, W.J.; Picken, S.J. *Macromolecules* **2002**, *35*, 2576-2582.

(52) Reference 40a, p. 10.

(53) Gattermann, L. *Liebigs Ann. Chem.* **1906**, *347*, 359.

3 Methyl substituted mesogens: low molar mass materials and polymers

Parts of this chapter have been published in: (a) Kouwer, P.H.J.; Jager, W.F.; Mijs, W.J.; Picken, S.J. *Macromolecules* **2000**, *33*, 4336-4342. (b) Kouwer, P.H.J.; Gast, J.; Jager, W.F.; Mijs, W.J.; Picken, S.J. *Mol. Cryst. Liq. Cryst.* **2001**, 364, 225-234. (c) Kouwer, P.H.J.; Mijs, W.J.; Jager, W.F.; Picken, S.J. *J. Am. Chem. Soc.* **2001**, *123*, 4645-4646.

Abstract

The liquid crystalline properties of the low molar mass mesogens, based on **D2** were compared with the properties of the corresponding polyacrylates. Many materials showed a N_D phase at high temperatures. While the low molar mass materials crystallized, the polymers showed a transition to the N_{Col} phase. The polymer backbone adequately disturbs the columnar organization and, hence, prevents long-range positional order of the columns. The polymers described in this chapter are the first thermotropic materials for which a nematic-nematic phase transition has been observed. This transition was investigated using various techniques, including DSC, OPM, XRD, DRS and rheology. At the N_{Col} to N_D transition, both DRS and rheology show a large discontinuity in the dynamics of the material. This indicates an efficient network formation in the N_{Col} phase with the columns acting as polyfunctional crosslinks.

In a series of copolymers, the mesogen fraction [M] in the polymer was varied. A master phase diagram was constructed, despite the differences in substitution of the polymer backbone. At mesogen contents [M] > 61 %-wt the polymers showed a N_{Col} *and* a N_D phase, while polymers with smaller mesogen fractions only showed a N_{Col} phase and a direct transition to the isotropic phase. The McMillan theory extended for a columnar to nematic phase transition was used to describe the experimental phase diagram, using simple scaling laws. The strength of the mean-field potential was expressed as a function of [M], and it was found that the clearing temperature is linearly dependent on [M] while the melting of the columns is virtually independent on [M] (dependency $[M]^{0.12}$).

3.1 Introduction

Semi flexible side chain polymer liquid crystals offer distinct advantages over low molar mass mesogens as long as a high mobility is not very important. For example, they are dimensionally stable and can be processed easily, for example to thin films. Often, the polymer backbone efficiently suppresses crystallization, usually resulting in a wide temperature window for the mesophase. Below the glass transition temperature, which can be tuned selectively by the chemical structure of the backbone, the desired liquid crystalline texture can be frozen in. Alternatively, the liquid crystalline order can be stored permanently by means of a chemical crosslinking process.

So far, research in discotic liquid crystalline polymers has mainly focused on substituted triphenylenes; some of these are described in Chapter 2.3. For a series of polymers with only minor changes in the nature of the spacer linking the mesogen to the polymer backbone, a wide range of transition temperatures was reported.[1] Note that, discotic polymers of triphenylenes are difficult to study, since the high order (usually Col$_x$ or occasionally N$_{Col}$) results in materials with a high viscosity and hence, a low mobility of the mesogens.

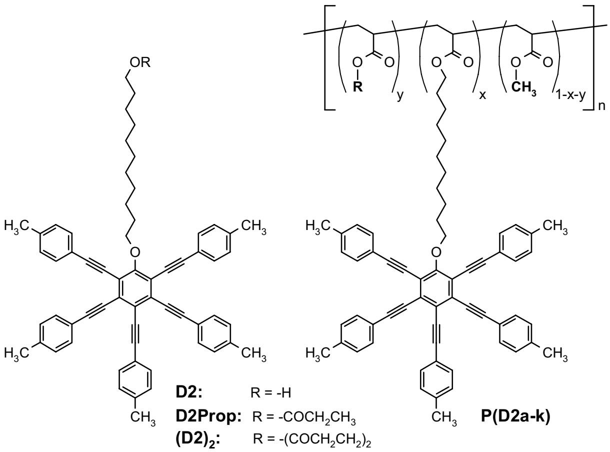

	R	x	y	[M]
P(D2a)	CH_3	0.90	–	0.74
P(D2b)	CH_3	0.64	–	0.71
P(D2c)	CH_3	0.48	–	0.68
P(D2d)	CH_3	0.31	–	0.62
P(D2f)	C_5H_{11}	0.69	0.31	0.70
P(D2g)	C_5H_{11}	0.41	0.43	0.62
P(D2h)	C_5H_{11}	0.42	0.50	0.62
P(D2i)	$C_{12}H_{25}$	0.61	0.11	0.68
P(D2j)	$C_{12}H_{25}$	0.45	0.45	0.58
P(D2k)	$C_{12}H_{25}$	0.33	0.42	0.53

Figure 3.1. Investigated materials.

In this chapter, the liquid crystalline properties of a series of polyacrylates based on the methyl substituted mesogen (**D2**), and their low molar mass equivalents (see Figure 3.1) are discussed. In the series of polymers, the mesogen fraction is controlled by 'copolymerization' of the mesogen with different alkylacrylates. The syntheses of **D2**,[2] the polymers **P(D2a-k)**,[3a] their low molar mass analogue **D2Prop** and the corresponding dimer **(D2)$_2$** are reported in chapter 2. Section 3.2 compares the liquid crystalline properties of polymer **P(D2b)** and low molecular weight analogue **D2Prop**, investigated by DSC, OPM, XRD[3b] and rheological experiments. In section 3.3, the mesophase behavior of the series of (co)polymers is discussed.[3a] The results of dielectric relaxation studies for a selection of polymers and low molar mass materials are reported in 3.4. In section 3.5, modeling of the experimentally obtained results according to the extended McMillan theory is descibed.3c

3.2 Comparison between high and low molar mass materials

DSC. All mesogens showed clear and reproducible thermograms, as shown in Figure 3.2. For the low molar mass compounds **D2Prop** and **(D2)$_2$**, two first order transitions were observed; a strong melting peak and a small clearing peak. Note that the transition temperatures for the dimer are higher than for the corresponding monomer, as would be expected from studies on the phase behavior of liquid crystalline dimers.[4] Polymer **P(D2b)** showed a broad and weak glass transition around 100°C. Furthermore, two first order transitions were observed; a fairly strong transition at 164°C and a small transition at 235°C. Slow decomposition of the polymer was observed at temperatures above 200°C, attributed to crosslinking reactions between the triple bonds in the mesogen. In addition, thermogravitrometric experiments show a loss of weight starting approximately at 190°C.

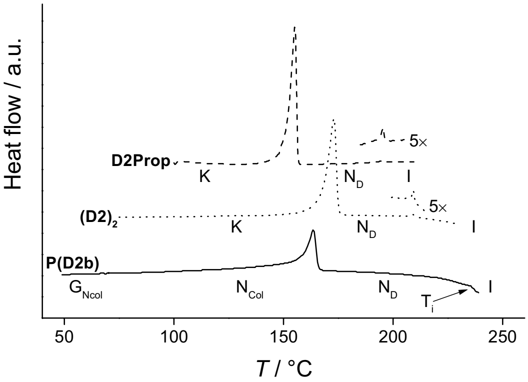

Figure 3.2. Normalized DSC thermograms of **D2Prop** (broken line), **$(D2)_2$** (dotted line) and **P(D2b)** (solid line). All scans are second heating scans. Some thermal degradation occurs at elevated temperatures.

OPM. The low molecular weight compounds **D2Prop** and **$(D2)_2$** showed the typical texture of a nematic phase at temperatures from 153 to 191°C and from 174 to 210°C, respectively. Monomer **D2Prop** had a strong tendency to form a homeotropic texture near the clearing temperature. Samples of polymer **P(D2b)** were heated to the isotropic phase prior to the measurement. On cooling from the isotropic phase, a clear nematic texture of the N_D phase was found (Figure 3.3b), easily characterized by its disclination lines and the low viscosity. Upon further cooling into a second nematic phase (identified as the N_{Col} phase), the texture remained unchanged and a rapid increase in the viscosity was observed. Only annealing for long times at elevated temperatures caused slight changes in the texture (3.3a). The disclination lines are still visible in the background while another smaller texture has developed on top, possibly caused by a local increase in order. The material vitrified by passing the glass transition temperature and the texture remained stable for months. Data from OPM and DSC measurements are summarized in Table 3.1.

Table 3.1. Thermal behavior of **D2**, **D2Prop**, **$(D2)_2$** and **P(D2b)** obtained by DSC and OPM.

Sample	Transition temperatures [°C] and (enthalpy changes) [kJ·mol^{-1}]						
D2			K	177 (48.0)	N_D	228 (0.4)	I
D2Prop			K	155 (32.3)	N_D	195 (0.3)	I
$(D2)_2$			K	173 (35.2)	N_D	209 (0.3)	I
P(D2b)	G_{NCol}	~100	N_{Col}	165 (12.0)	N_D	233 (0.3)	I

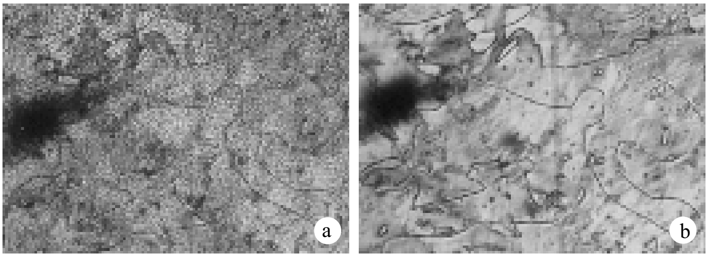

Figure 3.3. OPM photographs of the nematic textures of **P(D2b)** at (a) 140°C (N_{Col} phase, after annealing for 10 hrs at 140°C) and 170°C (N_D phase). Photographs taken at exactly the same spot, magnification 120×.

XRD. The mesophases of **P(D2b)** were studied by X-ray diffraction in the presence of a magnetic field.[5] The diffractograms are shown in Figure 3.4. Because of the negative diamagnetic anisotropy of the disk-shaped materials, the director alignment was found to be perpendicular to the magnetic field lines. Although director alignment by a magnetic field is not unusual for calamitic nematic samples, it is uncommon for discotic nematics.

The X-ray diffractogram of **P(D2b)**, recorded at 170°C (Figure 3.4b) shows the typical pattern of an N_D phase, i.e., two weakly oriented, diffuse reflections (similar to the diffraction pattern of the low molar mass **D2Prop** at 170°C). From the reflections, attributed to the planar [001] and the lateral [100] disk-disk distance, the spacings were calculated: d_{001} = 4.2 Å [A] and d_{100} = 16.5 Å [D]. The correlation length – a measure for the local order – of both reflections is typical for low ordered nematics: ξ_{001} = 12 Å and ξ_{100} = 55 Å. Furthermore, a nonoriented weak halo at 5-5.5 Å [C] is observed, attributed to the disordered alkyl chains, i.e. the spacer and the backbone.

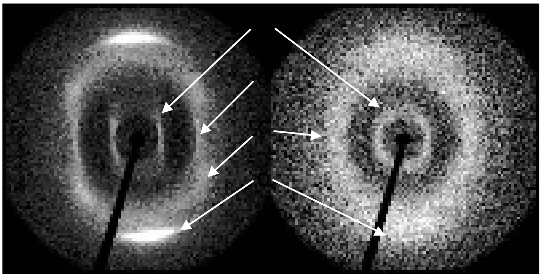

Figure 3.4a,b. XRD patterns of **P(D2b)** at (a) 140°C (N_{Col} phase) and (b) 170°C (N_D phase). The reflections marked A-D are discussed in the text.

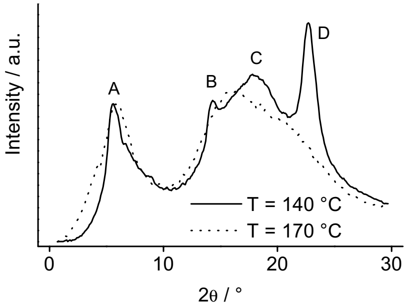

Figure 3.4c. Radial scan of the XRD patterns of **P(D2b)** at 140°C (dotted line) and 170°C (solid line).

X-ray measurements at 140°C revealed a well-aligned and much more complex pattern (Figure 3.4a). Reflections [A], [C] and [D] are still clearly visible. The slight sharpening of [A] (d_{100} = 16.0 Å and ξ_{100} = 67 Å) compared to [D] (d_{001} = 3.8 Å and ξ_{001} = 54 Å) suggests an increased order, particularly in the columnar [001] direction. This is even more clear from the radially integrated patterns shown in Figure 3.4. An extra reflection is visible at 6.2 Å [B], attributed to a higher order reflection. The, at first sight, remarkable shape of the reflections [A] and [B] strongly support the presence of columns aligned (randomly) perpendicular to a magnetic field. A detailed explanation is given in appendix A3 at the end of this chapter. Also note that the diffuse reflection of the alkyl chains shows the polymer backbone to be slightly oriented along the director (parallel to the columns of the N_{Col} phase).

Discussion on the phase behavior of P(D2b). By combining the experimental results a detailed picture of the mesomorphic behavior of **D2Prop**, **(D2)$_2$** and **P(D2b)** can be constructed. For the low molar mass materials **D2Prop** and **(D2)$_2$**, the results obtained are consistent with a N_D phase assignment. For the N to I phase transitions, the latent heat values, the diffuse X-ray diffraction patterns and the optical texture of liquid crystalline phase are similar to those reported for different substituted analogues of **D2Prop**.[6] At lower temperatures, the mesogens crystallized.

For **P(D2b)**, a more complex phase behavior was observed. The diffuse X-ray diffraction pattern taken at 170°C, the small change in enthalpy at the clearing point (0.3 kJmol^{-1}) and the texture observed in optical microscopy strongly are indicative of a N_D phase at high temperatures. This is similar to what was observed for the low molar mass mesogens. Upon cooling from the N_D phase, a transition into a second nematic phase was observed at 165 °C. The unchanged optical texture indicates the formation of another nematic phase. Since a transition between two nematic phases will not alter the director field of the molecules, no significant changes of the optical texture are anticipated. XRD studies of **P(D2b)** below 165 °C reveal a sharp reflection at 3.8 Å for the periodic intracolumnar disk distances and a somewhat more diffuse reflection at 16.6 Å for the less ordered intercolumnar distances. The diffraction pattern corresponds to a nematic columnar (N_{Col}) phase with a well-defined intracolumnar order and absence of long-range intercolumnar order. The assignment to a N_{Col} phase is in full agreement with the DSC and OPM data. At the transition from N_{Col} to N_D, the columns melt, but the mesogens retain the nematic orientation. It should be noted that the latent heat at the N_{Col} to N_D transition (8.4 kJ·mol^{-1}) is rather high compared to literature values. For polymers containing other discotic side groups, enthalpies of N_{Col} to I transitions on the order of 1-3 kJ·mol^{-1} were reported,[1c] while enthalpies close to 8 kJ·mol^{-1} have been reported for Col_h to I transitions.[1b,7] The N_{Col} phase is preserved on cooling below the glass transition of the polymer.

Theoretical studies on the phase behavior of nematic liquid crystalline polymers have elucidated that for side chain polymers with a flexible backbone multiple nematic phases are expected.[8] The backbone can be aligned along the director of the phase (that is perpendicular to the plane of the disk) or, alternatively, perpendicular to the director. First order phase transitions between the nematic phases are predicted by these studies,[8c] which could provide an alternative explanation of our experimental results (a first order nematic-nematic phase transition). However, we cannot explain our experimental data only in terms of modification of the order of the backbone for various reasons: (*i*) The latent heat values observed in our materials is rather high. A transition of the order of the backbone with respect to the mesogens is expected to be very small,[8c] particularly when the small fraction of backbone in our systems is considered. (*ii*) Structural analysis (XRD diffraction) clearly shows that below the N_D to N_{Col} transition a strong difference in the intracolumnar order between the mesogens is observed. This difference clearly indicates a transition in the columnar ordering of the mesogens rather than a small change in the order of the backbone. These observations are strongly supported by the evidence obtained from the dynamic measurements, in particular DRS.

The phase behavior of **D2Prop** (or **(D2)$_2$**) and **P(D2b)** is qualitatively comparable. At high temperatures, both formed a N_D phase, due to the large anisotropy of the disk-shaped groups and the absence of strong attractive π-π interactions (that would promote columnar phases). To our knowledge, **P(D2b)** is one of the very few polymers for which a N_D phase is reported.[9] The low molecular weight compounds **D2Prop** and **(D2)$_2$** crystallized, whereas **P(D2b)** formed the less ordered nematic columnar phase. This difference in phase behavior between **D2Prop** and **P(D2b)** cannot be traced back to spatial arguments, since the volume per mesogenic unit in **D2Prop** and **P(D2b)** is virtually identical.[10] More likely the effect of covalent attachment to the polymer backbone results in topological constraints and a strongly reduced mobility. In addition, the physical presence of the backbone itself between the columns prevents the columnar structure to reach long-range order and, hence, 'frustrates' the formation of higher ordered columnar or semi-crystalline phases.

Rheology. Polymer **P(D2b)** was subjected to a rheological analysis in the bulk.[11] Unfortunately, the sample suffered from thermal degradation at elevated temperatures, so only a limited number of experiments could be performed. In Figure 3.5, the storage modulus (*G′*) is plotted as a function of temperature in a dynamic mechanical experiment.

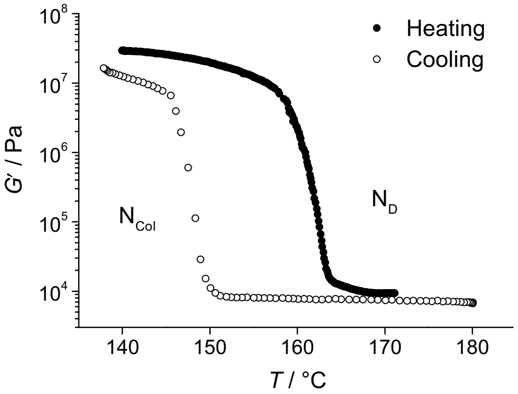

Figure 3.5. Dynamic mechanical analysis of **P(D2b)**

In the N_{Col} phase the sample showed a high modulus of 20-30 MPa that drops to low values at the phase transition (164°C) and remains nearly constant in the N_D phase at a value of 7-8 kPa. Initial experiments indicate that the modulus hardly drops further in the isotropic phase, but because of the strong degradation reactions no reliable values could be obtained. Cooling down from the N_D phase, the modulus increases with three orders of magnitude at ~150°C. Despite the low cooling rates (5°C·min^{-1}) a pronounced thermal hysteresis of more than 15°C was observed. This is similar to what was observed in DSC experiments (ΔT = 17°C at cooling rates of 10°C·min^{-1}) and dielectric relaxation spectroscopy experiments (ΔT = 15°C at cooling rates of 0.5 to 1°C·min^{-1}).

The high modulus in the nematic columnar phase can be explained in terms of (physical) network formation. Because of the flexibility of polyacrylate main chain and the length and flexibility of the undecanyl spacer, disks attached to one chain are not expected to be ordered in one stack, but rather form a three-dimensional network. Now the columns act as physical crosslinks, resulting in a dense network, due to the high functionality of the columns.

To gain extra information on the molecular interactions, present in the material, additional rheological experiments were performed in solutions of 1,1,2-trichloroethane.[11] At sufficient concentrations the polymer forms a physical network. The network formation in the gels can be explained by intermolecular interactions, like π-π interactions and solvofobic effects, i.e. repulsive forces between the aromatic cores and the aliphatic parts of the polymer. Preliminary results indicate that the measurements can be explained by solubility parameter theories that comprise both effects.[12]

3.3 Polymers with various mesogen contents

A series of polymers, **P(D2a-k)**, see Figure 3.1, with a varying degree of mesogen substitution was prepared similar to **P(D2b)**. The observed phase behavior of these polymers, characterized by OPM and DSC, was analogous with that of **P(D2b)**, comprehensively discussed in the previous paragraph.

Table 3.2. Phase behavior of polymers **P(D2)** obtained by DSC and OPM. The weight fraction of rigid mesogen is calculated in Table 2.2, Chapter 2.2.5. [a] n.d.: not determined. [b] Monotropic phase transition.

Polymer	Rigid Mesogen [%-wt]	Transition temperatures [°C] and (latent heat values [kJ·mol^{-1}])								
		G_{NCol}		N_{Col}			N_D			I
P(D2a)	73.8	•	n.d.[a]	•	164	(9.6)	•	235	(0.3)	•
P(D2b)	70.8	•	n.d.[a]	•	165	(12)	•	233	(0.3)	•
P(D2c)	67.5	•	92	•	158	(9.1)	•	204	(0.2)	•
P(D2d)	61.5	•	62	•	149	(8.5)	[•[b]	148	(0.1)]	•
P(D2e)	64.5	•	74	•	155	(8.3)	•	175	(0.1)	•
P(D2f)	69.7	•	77	•	169	(8.6)	•	209	(0.1)	•
P(D2g)	62.0	•	70	•	157	(8.7)				•
P(D2h)	61.7	•	51	•	157	(8.3)				•
P(D2i)	68.3	•	86	•	155	(8.2)	•	210	(0.1)	•
P(D2j)	57.8	•	50	•	154	(8.1)				•
P(D2k)	52.9	•	49	•	136	(8.3)				•

The results show that all polymers exhibit a N_{Col} mesophase at low temperatures (T ≤ 150°C). On cooling from this phase, a weak transition into a glass was found for most polymers and the optical texture was frozen in.[13] As expected, the glass transition temperature increases with increasing degree of mesogen substitution. On heating from the N_{Col} phase, a transition to the N_D phase was found for a limited number of polymers (polymers **a-c**,**e**,**f**,**i**) only, while the others turn isotropic. Interestingly, these transitions took place in the same temperature range (~150-170°C) and with nearly constant enthalpy changes. On the other hand, the transition temperature from N_D to isotropic was strongly dependent on the degree of mesogen substitution. For **P(D2d)**, a narrow monotropic N_D phase was found.

Mesogen content. In order to make a fair comparison between the liquid crystalline polymers **P(D2)**, the different molecular constituents were expressed in weight fractions, see Table 3.2). The polymers were divided in two parts: (*i*) a rigid part of the mesogen (without the flexible spacer) and (*ii*) all flexible parts of the polymer, including the spacer, backbone and dangling ends of the methyl, pentyl and dodecyl side chains.[14]

Due to the high molecular weight of the mesogen, compared to that of the backbone, the mesogen weight fraction in polymer series **P(D2a-d)** only slightly decreases with decreasing degree of substitution. Note that the maximum mesogen fraction would be 0.746 for the fully substituted polyacrylate. By the introduction of the longer alkyl groups along the polymer backbone, the mesogen content was reduced further to 0.53 (for **P(D2k)** with the lowest mesogen weight fraction). Using the mesogen weight fraction, the liquid crystalline properties of all materials can be represented in a master phase diagram as shown in Figure 3.6.

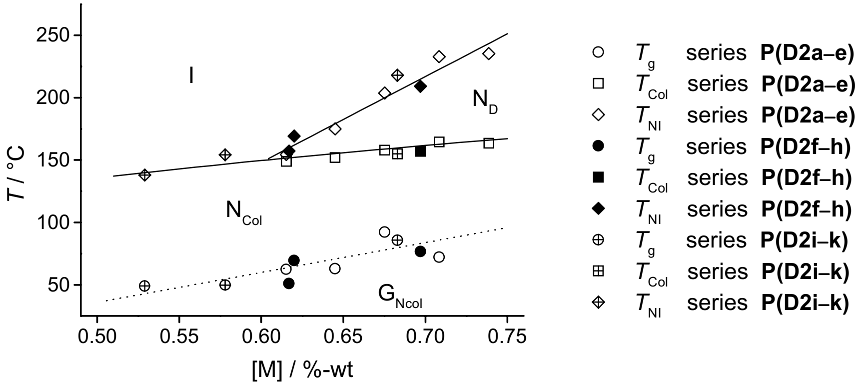

Figure 3.6. Phase diagram of copolymers with methyl acrylate (open); pentyl acrylate (solid) and dodecyl acrylate (swith cross). Transitions: T_g: circles; T_{Col}: squares and T_i: diamonds. The drawn curves are calculated using the extended McMillan theory (see section 3.5), the dotted curve is just a guide to the eye.

The figure clearly shows that the thermal properties of the materials are strongly dependent on the mesogen content in the material and much less on the kind of alkyl acrylate co-monomer. When a certain amount of mesogen is present in the material (> 61%) an extra mesophase is observed at high temperatures, the N_D phase. The clearing temperatures of these polymers are again, strongly dependent on the mesogen content. However, the melting of the columnar structure is much more concentration independent. These results have been described by the McMillan theory, extended for columnar and nematic mesophases, and will be discussed in Section 3.5.

3.4 Dielectric relaxation spectroscopy

The monomer **D2**, dimer **(D2)$_2$** and several polymers **P(D2b-d,j)** have been studied using dielectric relaxation spectroscopy (DRS) measurements. Some fundamentals of this technique and the procedure for data analysis are explained in Appendix B of this chapter. Using DRS, insight in the dynamics of the materials is gained.

The two characteristic spectra shown Figure 3.7, show the 'conduction-free' dielectric loss[15] $\varepsilon''_{\mathrm{deriv}}(f,T)$ as a function of frequency f and temperature T for **D2** and **P(D2j)**. The crystalline compound **D2** (in 3.7a) shows several relaxation processes at low temperatures, for which the assignment to particular molecular motions is still under discussion. In contrast, the loss spectrum of the polymer (Figure 3.7b) looks less complicated. The relaxation processes indicated here are characteristic for the series of polymers. They have been analyzed according to the methods discussed in Appendix B and the results are discussed separately for the individual relaxation processes in the following section.

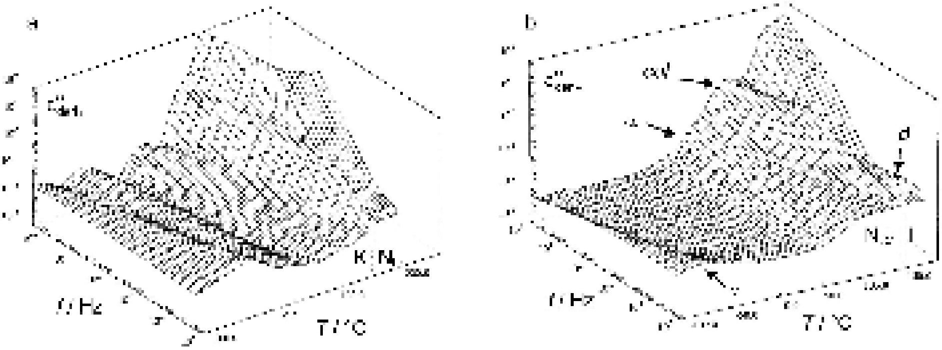

Figure 3.7. Conduction-free dielectric loss $\varepsilon''_{\mathrm{deriv}}$ diagram of (a) **D2** and (b) polymer **P(D2j)**.

γ-relaxation. The γ-relaxation process was ascribed to the spacer motions involving the single oxygen atom that links the spacer to the rigid mesogenic unit in analogy to the γ-process frequently found in calamitic side-chain liquid crystalline polymers.[16,17] Figure 3.8 displays the relaxation times of the γ-relaxation process for the series of materials based on **D2** in an Arrhenius diagram.

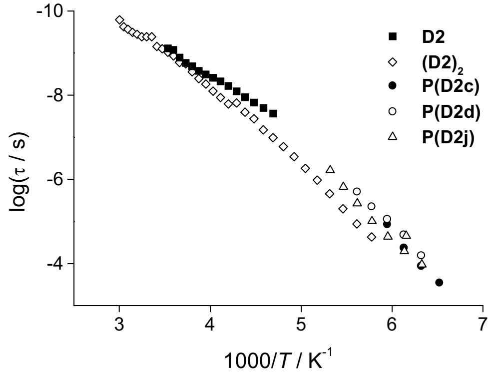

Figure 3.8. Arrhenius plot of the relaxation time for the γ-process of the investigated series.

The low molar mass compounds **D2** and **(D2)$_2$** posses somewhat different relaxation characteristics, which will be discussed later in this section. All polymers however, show very similar γ-relaxation data, which have been fitted to the Arrhenius equation. By using an Eyring analysis,[18] values for the zero-entropy activation energy ($E_{A,0}$) and the activation entropy (ΔS) were obtained, see Table 3.3. Interestingly, all polymers show an almost identical zero-entropy activation energy $E_{A,0}$ of (29 ± 1) kJ·mol^{-1}, which implies the existence of an identical energy barrier involved in the γ-process for all polymers. However, strong variations in the pre-exponential factor and thus the activation entropy ΔS indicate that the γ-relaxation cannot be regarded as a true local, non-cooperative relaxation process. Most likely, fluctuations in the local (mesogenic) order are required to overcome unfavorable conformational states of the methylene spacers resulting in a non-zero activation entropy.

Table 3.3. Details of the γ- and α-relaxation process of the investigated series of materials.

Material	**γ-relaxation**				**α-relaxation**		
	E_A [kJ·mol^{-1}]	**log(τ_∞)**	**$E_{A,0}$ [kJ·mol^{-1}]**	**ΔS [kJ·mol^{-1}K^{-1}]**	**$T_{g,VFT}$ [°C]**	**$T_{g,Eapp}$ [°C]**	**$T_{g,DSC}$ [°C]**
D2	25.2	–13.7	23.4	0.018	–	–	–
(D2)$_2$ γ_1	24.0	–13.5	22.6	0.014	–	–	–
γ_2	43.2	–17.6	31.0	0.091	–	–	–
P(D2b)	34.6	–15.4	28.5	0.049	–	87	–
P(D2c)	46.1	–19.2	30.2	0.121	–	100	92
P(D2d)	40.1	–17.5	29.0	0.089	59	65	62
P(D2j)	42.8	–18.0	30.0	0.098	55	77	50

α-relaxation. The dielectric α-relaxation was exclusively found in the polymeric materials and was identified as the dielectric manifestation of the dynamic glass transition, mainly involving the polymer backbone/spacer fraction. The characteristic feature of the α-process is its typical temperature dependence of the relaxation time $\tau_\alpha(T)$, which obeys the Vogel-Fulcher-Tammann (VFT) law (see Figure 3.9a). From the VFT-curve we were able to determine an 'operationally defined' glass transition temperature $T_{\mathrm{g,VFT}}$ being the temperature at which the relaxation time reaches τ_α = 100 Hz. This 'dielectric' T_g is particularly useful since calorimetric measurements often showed only broad or ill-defined glass transitions.

The polymer-rich (i.e. the mesogen-poor) materials showed the expected VFT behavior, resulting in T_g's of 59 and 55 °C for **P(D2d)** and **P(D2j)**, respectively. Both values correspond to the T_g's determined by DSC in the previous section (see Table 3.3). The α-process of the more densely substituted polymers could not be fitted using the VFT equation because of the poor quality of the relaxation data (weak or nonseparable α-relaxation). Instead, they show a nice Arrhenius behavior, as shown in Figure 3.9 for **P(D2c)**. Here, as an alternative route, the glass transition temperature was obtained from the apparent activation energy E_{App} showing a local maximum at the glass transition temperature.[19] The $E_{\mathrm{App}}(T)$ curves for all polymers, calculated from ε' at f = 28 Hz, are shown in Figure 3.9b and the calculated T_g's in Table 3.3

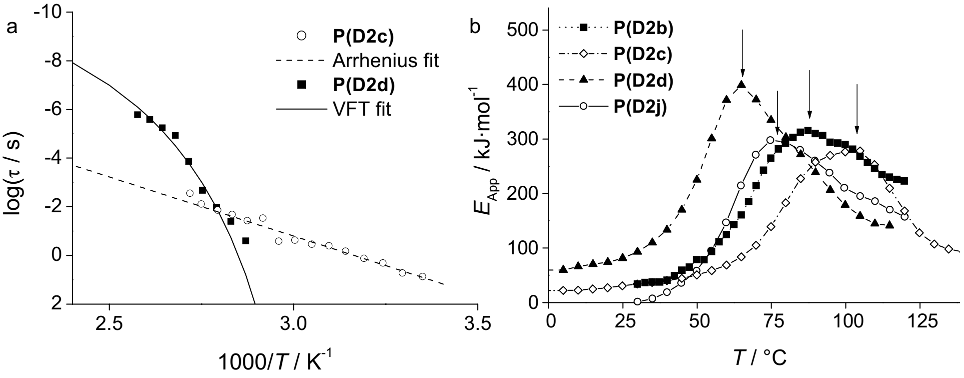

Figure 3.9. (a) The α-relaxation of **P(D2c)**, fitted with the Arrhenius equation (dashed line) and of **P(D2j)**, fitted with the VFT relation (curved line). (b) The apparent activation energy E_{App} as a function of T (at f = 28 Hz) for determining the T_g's (indicated by arrows).

Mesogen relaxations. The most important information regarding the order in the materials can be abstracted from the relaxation processes involving the mesogens themselves. As discussed in the appendix, several relaxation modes can be distinguished for the mesogens and their (columnar) assemblies. As yet, it is not clear which of the (combination of) suggested modes are cause the observed relaxation behavior. Figure 3.10 shows the Arrhenius plot of the (fastest) mesogenic relaxation mode for all materials. Again, all polymers behave very similar. At the phase transition from the N_{Col} to the N_D or I phase, a discontinuity in the relaxation time of roughly one order of magnitude is observed, accompanied by a decrease in the activation energy of the relaxation. Both features are consistent with the idea that during melting of the columns (i.e. upon vanishing of the columnar order), the mesogenic dynamics changes from highly cooperative (slow motions and high E_A) to almost single molecule dynamics (faster motions and lower E_A). As discussed before for the γ-relaxation process, the relaxation data of the low molar mass mesogens deviate significantly from those of the polymeric compounds. Presumably, the unusually short relaxation times of **(D2)₂** in the N_D phase can be attributed to fast motions of the aliphatic intermesogenic bridge, containing two highly polar linear ester groups, rather than to molecular motions of the adjacent discotic moieties.

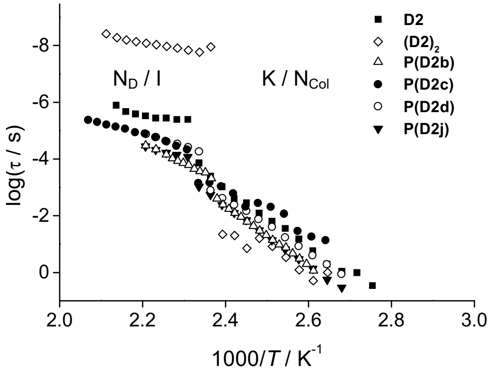

Figure 3.10. Arrhenius plot of the relaxation time for the mesogenic relaxations of the investigated series.

Most mesogenic compounds revealed several relaxation processes in their columnar phase which beyond any doubt are related to the dynamics of the mesogenic units. The different relaxation modes can be classified with respect to their cooperative character.[18] Based on the Eyring equation, the Starkweather analysis enables the evaluation of the activation entropy ΔS and the zero-entropy activation energy $E_{A,0}$ from the experimentally obtained Arrhenius parameters E_A and τ_∞. This procedure was carried out for all relaxation processes encountered in the series of materials based on **D2**, the results are given in a Figure 3.11.

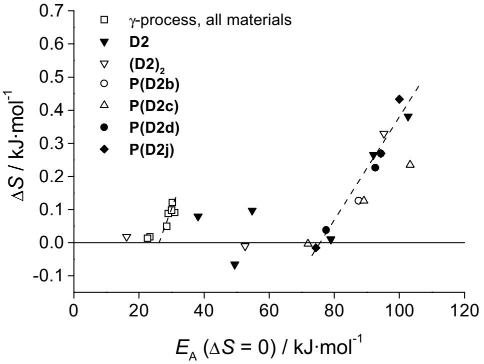

Figure 3.11. Activation entropy ΔS versus zero-entropy activation energy $E_{A,0}$ for all relaxation processes found for the series of material based on **D2**. Note that all parameters relate to the temperature at which the relaxation frequency equals 1 Hz. The two trendlines were drawn manually and are intended as guide to eye.

Two groups of relaxations showing a strong correlation between ΔS vs. $E_{A,0}$ (located around the trendlines) can be identified. The remaining points with $\Delta S \neq 0$ belong to the low molecular **D2** and **(D2)$_2$** and will not be discussed further. The left group located around $E_{A,0}$ = 30 kJ·mol^{-1} represents the γ-relaxation of the polymer materials which was already discussed. More interestingly, the second group which spans the $E_{A,0}$-range from 70–100 kJ·mol^{-1}, is characterized by a huge variation in ΔS between zero and ~0.5 J·mol^{-1}K^{-1}. Here, the data points with the low ΔS values refer to relaxations in the isotropic or N_D-state, whereas the high activation entropies were found for the slow relaxations in the crystalline or N_{Col} phase.
Such a correlation, a variation in the (measured) activation energy mainly caused by a variation in the activation entropy, was found in the recent years in various side-chain LCPs, and is also known as compensation behavior from cooperative dynamics of polymers in their glassy state near T_g. The phenomenon can be rationalized by the picture that the degree of molecular order determines the degree of cooperativity of an associated molecular motion, which is connected with a perturbation of the local order on the length scale of the cooperative motion. A positive activation entropy means that the motional process requires a temporary higher disorder in its excited state provided by entropy fluctuations. It is clear that the improved columnar order will affect the mesogenic relaxation processes much more than the γ-relaxations, which is expressed by minor variations in $E_{A,0}$ of the latter.

Relaxation strength. Another useful quantity that can be determined from the relaxation spectra is the relaxation strength $\Delta\varepsilon$. The relaxation strength is related to the concentration, the dipole moment and possible correlations of molecular dipoles by the Onsager equation (see Appendix B). Therefore, $\Delta\varepsilon$ contains information on the degree of cooperativity of a certain relaxation process, which is manifested by the Kirkwood correlation factor g.
In the present case of a columnar order, the parameter g can be related to the typical length of the columnar order by a simple consideration. Assuming an columnar arrangement of disk-like moieties which possess exclusively an in-plane dipole moment perpendicular to the column axis (the normal component of the ether-dipole averages out at the time-scale of the γ-process), collective rotations of the mesogens around the column axis in combination with a perfect stacking of the polar groups would result in a Kirkwood correlation factor being roughly equal to the (relative) stack length $N_{C,DRS}$. However, since rotational correlations will be imperfect and certainly get lost over long stacking periods, the experimentally determined g will be less or equal to the actual column length $N_{C,DRS}$. In other words, in this simple picture g can be identified as a lower limit of the stack number $N_{C,DRS}$. In the N_D phase, the meaning of g is clearly different. Instead of laterally correlated dynamics within a well-developed columnar arrangement, lateral correlations might persist induced by the presence of short columns, short-range disk-disk interactions or topological reasons (bridges via the polymer backbone).

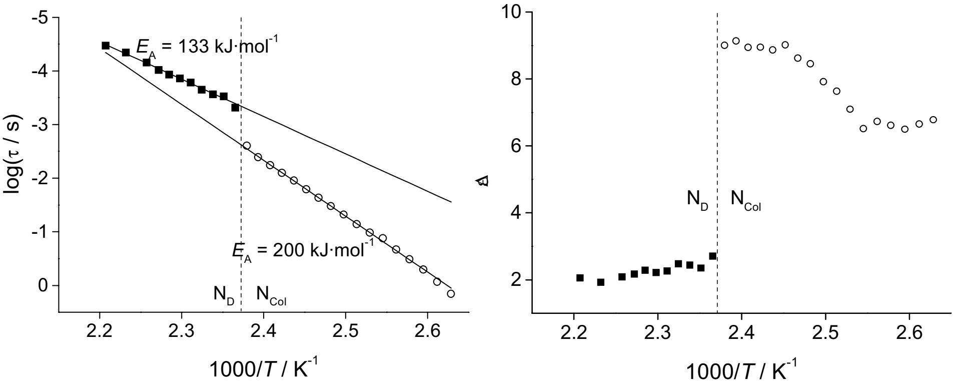

Figure 3.12. Example of the changes in relaxation characteristics of **P(D2b)** at the N_D to N_{Col} phase transition: Arrhenius plots of (a) the relaxation time and (b) the relaxation strength.

An example is given in Figure 3.12b, showing the relaxation strength below and above the N_{Col} to N_D phase transition. As expected, $\Delta\varepsilon$ drops sharply from ~ 9 to 2.5, which corresponds to a drop in g from ~ 34 to 8. These values can be compared with the results of the detailed XRD measurements. By taking into account that the columns have a finite length, an actual column length can be estimated from the correlation length.[21] Subsequent division by the measured spacing gives the column length in number of mesogens:

$$N_{\mathrm{C,XRD}} = 2.78\frac{\xi_{001}}{d_{001}} \tag{3.1}$$

For the N_{Col} phase, equation 3.1 yields $N_{\mathrm{C,XRD}} = 39$ and for the N_D phase is found $N_{\mathrm{C,XRD}} = 8$. It should be realized that in both methods to calculate N_{C}, many assumptions have been made and the their absolute values are questionable. Nevertheless, is striking to see that the *ratio* of the values in the N_{Col} and in the N_D phase, as well as the absolute values themselves, are more or less identical.

3.5 Modeling of the N_D and N_{Col} phase transitions

The Maier-Saupe model,[22] developed to describe the nematic to isotropic phase transition as a function of temperature, is based on a mean-field potential U that is experienced by an average test particle:

$$U = -V_0 S P_2(\cos\theta) \tag{3.2}$$

Here, the parameter V_0 represents the absolute strength of the potential and serves to fix the absolute temperature scale. The $P_2(\cos\theta)$ term, describes the dependence of the potential on the mesogen orientation (at angle θ) with respect to the director, and S is the order parameter, defining the orientational order: $S = \langle P_2(\cos\theta)\rangle \equiv \langle \tfrac{1}{2}(3\cos^2\theta - 1)\rangle$. Calculation of the self-consistent set of equations and taking the solution of the lowest free energy gives a good description of the order parameter with temperature in the nematic phase.

The McMillan theory[23] is an extension of the Maier-Saupe model that describes the I, N and the SmA phase. Accordingly, a positional order term is added to the potential:

$$U = -V_0\left\{S + \alpha\sigma\cos(2\pi z/d)\right\}P_2(\cos\theta) \tag{3.3}$$

where $\cos(2\pi z/d)$ describes the locally layered structure, σ is the positional order parameter and α is the interaction parameter describing the strength of smectic ordering: $\alpha = 2\exp[-(\pi r_0/d)^2]$, with r_0 is the rod-length and d is the lattice constant. Self-consistency demands that: $S = \langle P_2(\cos\theta)\rangle$ and $\sigma = \langle \cos(2\pi z/d)P_2(\cos\theta)\rangle$. Numerical calculations to solve the set of equations give solutions of the type: (*i*) $\sigma = 0$ and $S = 0$ (I phase); (*ii*) $\sigma = 0$ and $S \neq 0$ (N phase) and (*iii*) $\sigma \neq 0$ and $S \neq 0$ (SmA phase). The stable solution corresponds to the solution with the lowest free energy.

The McMillan model was recalculated for a discotic liquid crystalline system, consisting of a columnar and nematic phase. This extended McMillan theory,[24] discussed here in somewhat more detail, is based on the McMillan model, but now using a two-dimensional positional order function. The mean-field potential U of a test molecule at position $\mathbf{r}$ and oriented at an angle θ with respect to the z-axis is now described as:

$$U = -V_0\left\{S + \alpha\sigma\left[\cos(\mathbf{A}\cdot\mathbf{r}) + \cos(\mathbf{B}\cdot\mathbf{r}) + \cos(\mathbf{C}\cdot\mathbf{r})\right]\right\}P_2(\cos\theta) \tag{3.4}$$

where again parameter α determines the relative contribution of the columnar potential, but now: $\alpha = 2\exp[-(\pi r_0/\sqrt{3}d^2)^2]$ and d is the disk-radius. The columnar phase is described by a superposition of three density waves with the primitive vectors **A**, **B** and **C** in which $\mathbf{A} = (4\pi/\sqrt{3}d)\mathbf{j}$, $\mathbf{B} = (4\pi/\sqrt{3}d)(\sqrt{3}\mathbf{i}/2 - \mathbf{j}/2)$ and $\mathbf{C} = \mathbf{A} + \mathbf{B}$, with **i** and **j** being the unit vectors along the x and y-axis.

It is noted that the polymers, described here, do not exhibit a columnar hexagonal phase, but rather a nematic columnar phase. Clearly, the lack of long-range hexagonal order makes the here described model unfit to apply to our polymers. However, because of the high local organization of the N_{Col} phase, found in these materials (observed by DSC, XRD and DRS), we will assume that locally, the columnar order is well established. Therefore, on a local scale the deviations from the hexagonal patterns are small and the use of this theory as a first step towards a full description appears reasonable .[25]

The order parameters S and σ respectively describe the orientational order and positional order, via:

$$S = \langle P_2(\cos\theta)\rangle \tag{3.5}$$

$$\sigma = \tfrac{1}{3}\langle\{\cos(\mathbf{A}\cdot\mathbf{r}) + \cos(\mathbf{B}\cdot\mathbf{r}) + \cos(\mathbf{C}\cdot\mathbf{r})\}\, P_2(\cos\theta)\rangle \tag{3.6}$$

In this case the averaging process for calculating the order parameters as indicated by the brackets involves integration over the angle θ and the position coordinates x and y. Solving the McMillan model involves finding self-consistent solutions for the orientational and positional order parameters. The stable solution corresponds to the lowest free energy, using:

$$F = U - TS = \tfrac{1}{2}\left(S^2 + \alpha\sigma^2\right) - \frac{k_B T}{V_0}\log(Z) \tag{3.7}$$

where Z is the partition function given by:

$$Z = \frac{2}{\sqrt{3}d^2}\int \mathrm{d}x\,\mathrm{d}y \int_0^{\pi} \mathrm{d}(\cos\theta)\; e^{-U(x,y,\theta)/k_B T} \tag{3.8}$$

The phase diagram resulting from the extended McMillan theory as a function of the scaled temperature and the interaction parameter α, is shown in Figure 3.13. Note that for high values of α a nematic columnar to isotropic transition is observed, and lower α values yield the required $N_{Col} - N_D - I$ sequence.

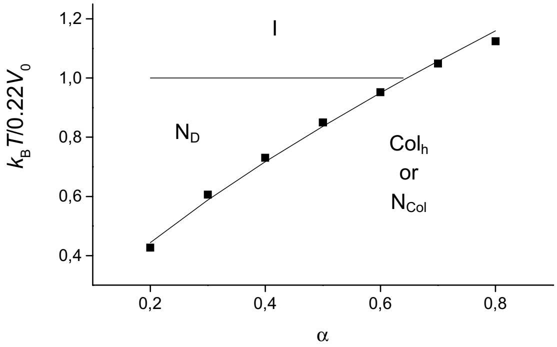

Figure 3.13. Phase diagram from the extended McMillan theory. The symbols match the exact result, the drawn horizontal line represents the N_D to I transition at $T_{NI} = 0.22V_0/k_B$. The drawn curve is a power law fit to $\kappa\alpha^{0.69}$, with $\kappa = 0.30$.

Apart from a proposed application of the extended McMillan theory,[26a] the model has only been used before to describe phase transitions in a homologous series of substituted triphenylenes, where the potential is written as a function of the length of the alkyl tails.[26b,c] Here, the effectiveness of the model is illustrated by describing the phase transitions as a function of the rigid mesogen fraction [M] as calculated in the previous paragraph. To fit our experimental data we have to determine the dependence of the model parameters V_0 and α on [M]. To this end we will assume that the transition temperatures T_{NI} and T_{Col} show a power-law dependence on [M]. The advantage of this form is that the terms disappear for [M] = 0 as required. Using a simple scaling analysis that correlates the transition temperatures with V_0 and α, a system of equations is obtained:

$$T_{\mathrm{NI}} = A[\mathrm{M}]^{\gamma} = 695[\mathrm{M}]^{0.98} \tag{3.9}$$

$$T_{\mathrm{Col}} = B[\mathrm{M}]^{\delta} = 465[\mathrm{M}]^{0.18} \tag{3.10}$$

The numbers given are obtained from fitting the power-law expressions to the experimental data. Because $k_{\mathrm{B}}T_{\mathrm{NI}}/V_0 = 0.2202$ in the theory, we find that V_0 is a nearly linear function of [M], i.e., $V_0 \propto A[\mathrm{M}]$. From fitting a power law to McMillan theory we find that $k_{\mathrm{B}}T_{\mathrm{Col}}/V_0$ scales as $\alpha^{0.69}$ for a reasonable range of α values. This fit is shown in Figure 3.13 together with the exact values of T_{Col}/V_0 versus α. Combining the various power-law expressions then leads to the following relation for the scaling behavior of α as a function of [M] (using equation 3.9): $T_{\mathrm{NI}} = A[\mathrm{M}]^{\gamma}$ and the power-law $\alpha = c_2[\mathrm{M}]^{\varepsilon}$):

$$B[\mathrm{M}]^{\delta} = T_{\mathrm{Col}} = T_{\mathrm{NI}}\kappa\alpha^{0.69} = A[\mathrm{M}]^{\gamma}\kappa\left(C[\mathrm{M}]^{\varepsilon}\right)^{0.69} \tag{3.11}$$

Solving ε, we find: δ = γ + 0.69ε and thus ε = (δ–γ)/0.69 = (0.18–0.98)/0.69 = –1.16. Now the mean-field potential from equation 3.4 can be written as a function of [M]:

$$\begin{aligned} U &= -V_0\left\{S + \alpha\sigma f(\mathbf{r})\right\} P_2(\cos\theta) \\ &= -k_{\mathrm{B}}c_1[\mathrm{M}]^{0.98}\left\{S + \frac{c_2}{[\mathrm{M}]^{1.16}}\sigma f(\mathbf{r})\right\} P_2(\cos\theta) \end{aligned} \tag{3.12}$$

where $f(\mathbf{r}) = [\cos(\mathbf{A}\cdot\mathbf{r}) + \cos(\mathbf{B}\cdot\mathbf{r}) + \cos(\mathbf{C}\cdot\mathbf{r})]$ and c_1 and c_2 are constants: $c_1 = A/0.2202 = 3156$ K and $c_2 = (B/\kappa A)^{1/0.69} = 3.2$.

3.6 Conclusions

A series of differently substituted polyacrylates has been prepared using a polymer analogous substitution reaction. At high temperatures, the polymers with a high mesogen content showed the N_D phase (Figure 3.14b), similar to the low molar mass equivalents **D2**, **D2Prop** and the dimer **(D2)$_2$**. Where the low molar mass equivalents crystallized at 177, 155 and 175°C, respectively, the polymers exhibited a transition to the N_{Col} phase (Figure 3.14a) around 155°C. To our knowledge these are the first thermotropic materials for which nematic-nematic phase transitions are observed. Polymers with a lower mesogen content ([M] < 61%-wt) did not show a N_D phase, but exhibited a direct N_{Col} to I phase transition. The phase behavior of the series of polymers could be fitted perfectly with the McMillan theory extended for columnar and nematic phases. By using simple scaling laws, the model was described in terms of the mesogen fraction [M]. It was found that the N_D to I transition was almost linearly dependent on the mesogen fraction, whereas the melting of the columns showed a much weaker [M] dependency.

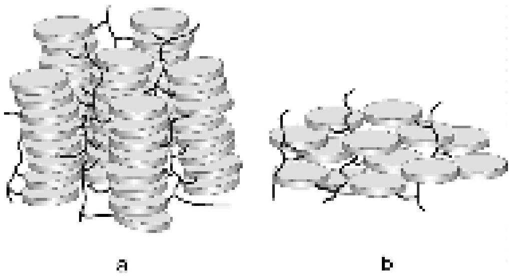

Figure 3.14. Schematic representation of the (a) N_{Col} and (b) N_D phase observed in polymers **P(D2a-k)**.

XRD experiments showed a well-developed intracolumnar organization in the N_{Col} phase, resulting in rather long stacks of molecules. Independently from XRD and DRS studies, an average column length of the N_{Col} phase of **P(D2b)** could be estimated; both values are in good agreement with another. At the N_D to N_{Col} transition a strong change in the dynamics was observed in dielectric and rheological studies. The lack of long-range order in the other two dimensions must be attributed to the presence of the polymer backbone. The physical presence of the backbone in between the well-ordered columns presumably imposes topological constraints on the system and prevents long-range order.[27] While at small length scales, a two-dimensional columnar organization might exist, at longer length scales the order is disrupted by the backbone. Clearly this aspect requires a more detailed analysis, which is however beyond the scope of this thesis.

Appendix A: X-ray diffraction[28,29]

A.1 Introduction

The extent of positional and orientational order is used to classify the type of mesophase. Sometimes the type of phase can be easily determined from microscopy experiments, by their characteristic optical textures. In other cases, XRD is essential to unambiguously characterize the phase, for example to distinguish the various SmA phases or the various nematic phases. In our studies, XRD was used as a technique to study the order in disk-shaped liquid crystals. This appendix offers some extra background in fundamentals of diffraction and the calculation of the correlation length that was used to determine the extent of positional order in the materials.

A.2 Fundamentals

Bragg's law can be visualized by the scattering of X-rays from a set of lattice plane, see Figure 3.15a. For one particular set of planes, constructive interference will occur when Bragg's law is satisfied:

$$2d\sin(\theta) = n\lambda \tag{3.13}$$

Here d is the distance between the planes, θ is the angle of incidence, n is an integer and λ is the wavelength ($\lambda \approx 1.54$ Å for CuKα radiation). The incident and the diffracted beam are characterized by their wavevectors $\mathbf{k_i}$ and $\mathbf{k_s}$, with moduli $|\mathbf{k_i}| = |\mathbf{k_s}| = 2\pi/\lambda$. The scattering wavevector $\mathbf{q}$ represents the change in wavevector of the diffracted beam $\mathbf{q} = \mathbf{k_s} - \mathbf{k_i}$, see Figure 3.15b.

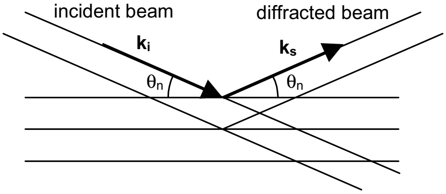

Figure 3.15a. Bragg diffraction process.

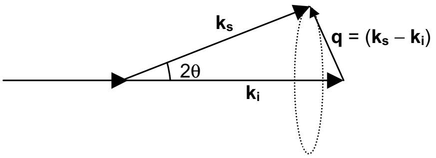

Figure 3.15b. Definition scattering wave vector **q**.

Using eq. 3.13, its modulus q can be written as:

$$q \equiv |\mathbf{q}| = \frac{4\pi\sin(\theta)}{\lambda} = \frac{2\pi n}{d} \tag{3.14}$$

Bragg's law predicts the direction of the diffracted wave and the reciprocal relationship between the diffraction angle θ and the plane separation *d*. The **F** amplitude is given by the Fourier transform of the structure, i.e. the electron density distribution ρ(**r**) in the sample:

$$\mathbf{F}(\mathbf{q}) = \int_V \rho(\mathbf{r}) e^{i\mathbf{q}\cdot\mathbf{r}} \mathrm{d}^3\mathbf{r} \qquad (3.15)$$

The observed intensity is derived from the amplitude $I(\mathbf{q}) = |\mathbf{F}(\mathbf{q})|^2$. For a periodic structure (such as a crystal) **F**(**q**) is non-zero for the discrete diffraction conditions where the Bragg law is satisfied. These conditions can be expressed by the reciprocal lattice vectors $\mathbf{q}_{hkl}$, which constitute a periodic set of δ-functions, called the reciprocal lattice. The set of integers ($h,k,l \in \mathbb{Z}$) are the Miller indices of the various sets of lattice planes in the material. The reciprocal lattice can be related to the real lattice. The real lattice, with lattice vectors **a**, **b** an **c**, is defined as:

$$\rho(\mathbf{r}+\mathbf{R}) = \rho(\mathbf{r}) \qquad \mathbf{R} = u\mathbf{a} + v\mathbf{b} + w\mathbf{c} \qquad u,v,w \in \mathbb{Z} \qquad (3.16)$$

The reciprocal lattice vectors are defined as:

$$\mathbf{A} = 2\pi\frac{\mathbf{b}\times\mathbf{c}}{\mathbf{a}\cdot(\mathbf{b}\times\mathbf{c})}, \quad \mathbf{B} = 2\pi\frac{\mathbf{c}\times\mathbf{a}}{\mathbf{a}\cdot(\mathbf{b}\times\mathbf{c})}, \quad \mathbf{C} = 2\pi\frac{\mathbf{a}\times\mathbf{b}}{\mathbf{a}\cdot(\mathbf{b}\times\mathbf{c})} \qquad (3.17)$$

The scattering wavevector $\mathbf{q}_{hkl}$ can be written as a function of the reciprocal lattice vectors:

$$\mathbf{q}_{hkl} = h\mathbf{A} + k\mathbf{B} + l\mathbf{C} \qquad h,k,l \in \mathbb{Z} \qquad (3.18)$$

Invariance of the solution for transformation over a lattice vector implies that:

$$\begin{aligned} \mathbf{q}\cdot\mathbf{R} &= (u\mathbf{a} + v\mathbf{b} + w\mathbf{c})(h\mathbf{A} + k\mathbf{B} + l\mathbf{C}) \\ &= 2\pi(uh + vk + wl) = 2\pi n \qquad n \in \mathbb{Z} \end{aligned} \qquad (3.19)$$

To summarize, a crystal with lattice parameters **a**, **b** and **c** shows diffraction peaks when the scattering wave vector coincides with the reciprocal lattice, i.e. when $\mathbf{q} = h\mathbf{A} + k\mathbf{B} + l\mathbf{C}$.

A.3 Diffraction pattern of the nematic columnar phase of P(D2b)

Fourier transformation of a series of (infinitely wide) planes (smectic phases!) results in a set of points normal to the planes. A two (Col_x) or three (K) dimensional lattice in real space transforms into a two or three-dimensional lattice in the reciprocal space, respectively. For example a hexagonal lattice of infinite rods (lattice parameter *a*) corresponds to another hexagonal lattice, but of points (lattice parameter $4\pi/\sqrt{3}a$). For long, but not infinite rods, the points in the reciprocal lattice are smeared out along the normal direction see Figure 3.16.

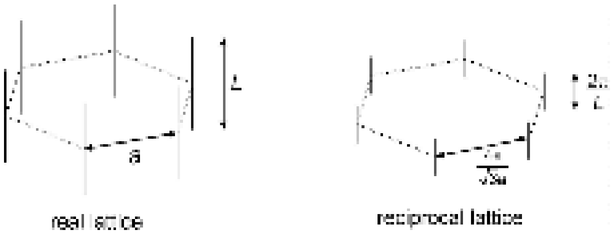

Figure 3.16. Transformation of a real hexagonal lattice of finite rods into its reciprocal lattice.

This may help to understand the complex XRD pattern of **P(D2b)**, (see Figure 3.18 and Chapter 3.2). At 140°C, the mesogens are assembled in columns that align in a magnetic field **B**. By approximation, the phase may be regarded as a two dimensionally ordered set of rods (far from infinitely long), which will give in the reciprocal space also a two dimensional lattice. Rotation of the reciprocal lattice around an axis perpendicular to the two-dimensional plane results in a series of concentric cylinders. Assuming that the two dimensional reciprocal lattice is perpendicular to the incident beam, the intersection of the (rotating) rods with the Ewald sphere results in a circle (see Figure 3.17) that, correspondingly, gives rise to a spherical diffraction pattern.

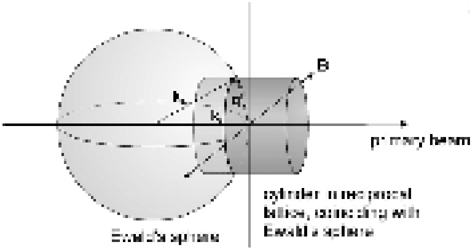

Figure 3.17. Schematic representation of the two-dimensional reciprocal lattice, rotating around an axis perpendicular with the lattice (giving rise to a cylinder), and intersecting Ewald's sphere. The incident beam $\mathbf{k_i}$ is parallel to the rods and the magnetic field **B** is directed toward- the reader.

Now the assumption of the two-dimensional lattice adjusted perpendicular to the incident beam is released and the columns align freely, but in planes perpendicular to the magnetic field. Rotation of the rods perpendicular to the field results in a spreading of circles in only one direction (vertical), as is observed in the XRD diagram. Apart from the [100] reflection, that gives rise to the pattern sketched in Figure 3.19, also a similar pattern is visible at higher diffraction angles, most probably from the [210] reflection. Note that the attribution of the two bright spots at wide angles in the pattern to the [001] reflections corresponds completely to the proposed perpendicular alignment of the rods with respect to the magnetic field.

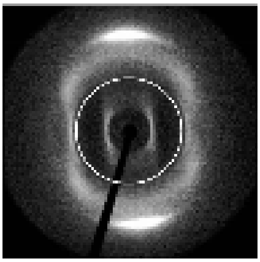

Figure 3.18. Observed diffraction pattern of **P(D2b)** at 140°C. Note that the area within the inner circle (the [100] reflection) is discussed.

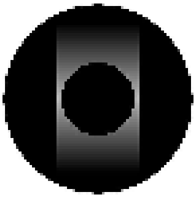

Figure 3.19. Schematic drawing of the inner [100] reflection of the diffraction pattern of **P(D2b)** at 140°C, resulting from the analysis described above.

A.4 The Scherrer equation

For a partially ordered system (typical for liquid crystals) there is no three dimensional lattice. Instead the electron density in the sample can be described by a distribution function $D(\mathbf{r})$, which is the probability of finding a center of mass of a molecule at position **r** with respect to a test molecule at $\mathbf{r} = 0$. For systems with true long-range positional order the intensity plot shows a series of δ-functions. For systems with where the periodicity is lost at larger distances, the positional correlations undergo a algebraic decay with distance, e.g. $D(r) \propto r^{-\eta}$ or $D(r) \propto e^{-r/\xi}$. The latter corresponds to liquid-like materials with only short-range order (e.g. nematic phases). The exponential decay results in a Lorenzian distribution, see Figure 3.20.

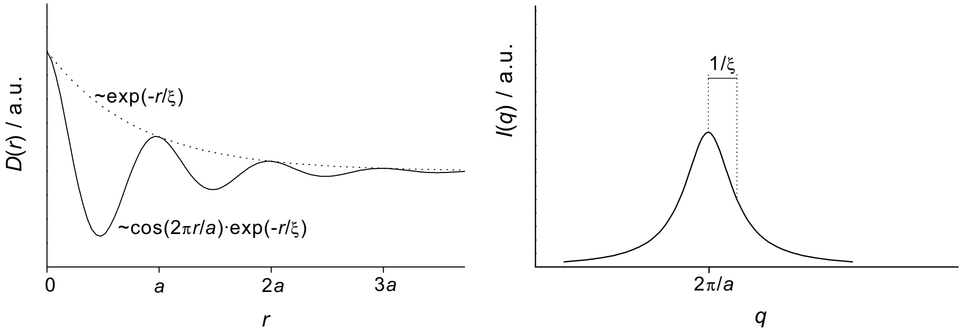

Figure 3.20. Electron density distribution function (one dimensional), based on a exponential decay of a sinusoidal function of periodicity *a* (left) and the corresponding Lorenzian intensity plot with the half width of the distribution function related to the correlation length ξ (right).

The correlation length ξ is a measure for the extent of positional order in the material. It can be calculated from the XRD patterns. The patterns are radially integrated and fitted with a Lorenzian function from which the width at half peak maximum ($\omega_{½}$) of a reflection at diffraction angle θ_0 is calculated:

$$\left|\theta_0 - \theta\right| = \Delta_{HW} = \frac{1}{2}\omega_{½} \tag{3.20}$$

Now the correlation length can be calculated from:

$$\xi = \frac{2\pi}{q-q_0} = \frac{\lambda/2}{\sin(\theta_{\mathrm{HW}}) - \sin(\theta_0)} = \frac{\lambda/2}{2\cos\frac{1}{2}(\theta_0+\theta_{\mathrm{HW}})\sin\frac{1}{2}(\theta_{\mathrm{HW}}-\theta_0)} \tag{3.21}$$

Since $\theta_{HW} \approx \theta_0 \Rightarrow \frac{1}{2}(\theta_{HW}+\theta_0) \approx \theta_0$, $\frac{1}{2}(\theta_{HW}-\theta_0) = \frac{1}{2}\Delta_{HW}$ and $\sin(\frac{1}{2}\Delta_{HW}) \approx \frac{1}{2}\Delta_{HW}$ apply, ξ can be written as:

$$\xi = \frac{\lambda/2}{\Delta_{\mathrm{HW}}\cos(\theta_0)} = \frac{\lambda}{\omega_{½}\cos(\theta_0)} \tag{3.22}$$

The standard description of the Scherrer equation (eq. 3.22) includes an extra constant and this is used in this thesis:

$$\xi = \frac{0.89\lambda}{\omega_{½}\cos(\theta_0)} \tag{3.23}$$

A5 Estimation of the column length from the correlation length

The column length N_C of a stack of columns, built up from mesogens at a regular distance d can be estimated from convolution of the Fourier transforms of the function for an infinite lattice $f(x)$ with periodicity d and a function of a block $h(x)$ with a finite block length L. The calculation is schematically shown in Figure 3.21. Note that this (crude) calculation assumes a uniform block size, corresponding to a uniform column length. The calculation could be improved by considering a distribution of block sizes.

An infinite lattice with periodicity d can be described by:

$$f(x) = \sum_{l\in\mathbb{Z}} \delta(x - ld) \tag{3.24}$$

The Fourier transform is written as:

$$F(q) = \frac{1}{\sqrt{2\pi}}\int_{-\infty}^{\infty} \mathrm{d}x \sum_{l\in\mathbb{Z}} \delta(x-ld)\, e^{-iqx} = \frac{1}{\sqrt{2\pi}}\sum_{l\in\mathbb{Z}} e^{-iqld} \propto \sum_{k\in\mathbb{Z}} \delta\left(q - \frac{2\pi k}{d}\right) \tag{3.25}$$

From which follows that the spacing of the reciprocal lattice $q = 2\pi/d$.
The second function, now for a block with length L can be written as:

$$h(x) = H\left(x+\tfrac{1}{2}L\right) - H\left(x-\tfrac{1}{2}L\right) \tag{3.26}$$

where H is the Heaviside step function and its Fourier transform is written as:

$$H(q) = \frac{1}{\sqrt{2\pi}}\int_{-\infty}^{\infty} \mathrm{d}x\, h(x)\, e^{iqx} = \frac{1}{\sqrt{2\pi}}\int_{-\frac{L}{2}}^{\frac{L}{2}} \mathrm{d}x\, e^{iqx} = \frac{L}{\pi\sqrt{2}}\frac{\sin\left(Lq/2\right)}{Lq/2} = \frac{L}{\pi\sqrt{2}}\frac{\sin(u)}{u} \tag{3.27}$$

with $u = \frac{1}{2}Lq$. At the half-maximum of a reflection, the intensity $I(q)$ relates to $\sin^2(u)/u^2 = \frac{1}{2}$, from which follows that $\sin(u) = u/\sqrt{(2\pi)}$, yielding $u_{\mathrm{HM}} = 1.3916 = \frac{1}{2}Lq$. For a Lorentzian distribution, the correlation length is defined as:

$$I(q) \propto \frac{1}{1+\xi^2 q^2} \tag{3.28}$$

Again, at the half-maximum applies $I(q) = \frac{1}{2}$ and hence, $\xi q = 1$. Substitution in the expression for Lq then provides us with an approximate relation between the correlation length and the column length:

$$L = \frac{2.783}{q_{\mathrm{HW}}} = 2.78\xi = N_{\mathrm{C,XRD}} \tag{3.29}$$

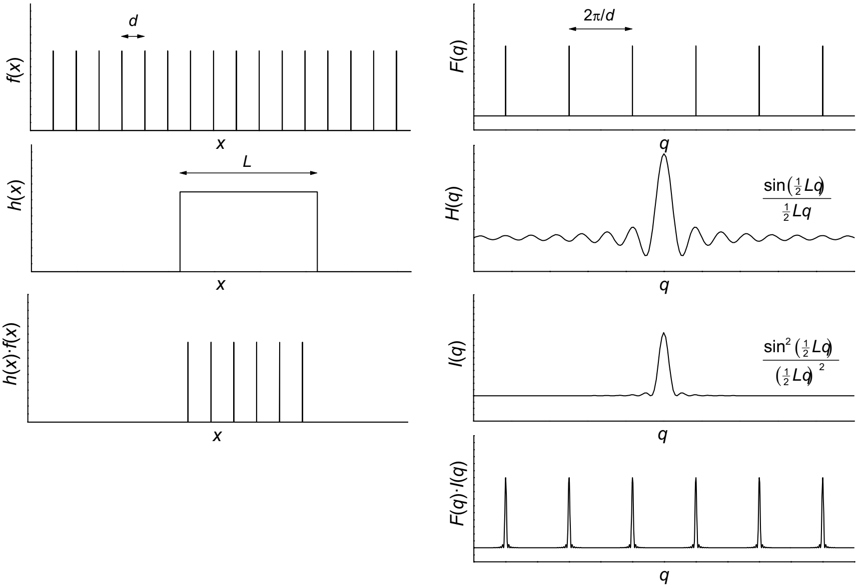

Figure 3.21. Schematic representation of the calculation of the stack length from the correlation length. On the left-hand side the real functions $f(x)$ and $h(x)$ are shown whereas on the right-hand side their corresponding Fourier transforms $F(q)$, $H(q)$ and $I(q)$ are drawn.

Appendix B: Dielectric relaxation spectroscopy

B.1 Introduction

In a dielectric relaxation spectroscopy (DRS) experiment, the time dependent response of an insulating (or weakly conducting) material to an applied electric field is measured. When molecular dipoles are present, various relaxation processes reflecting the orientational dynamics of the polar species can be probed. This orientational dynamics can be non-cooperative, e.g. in gasses or dilute solutions of polar molecules in non-polar solvents, or co-operative due to strong interactions between dipoles. The latter is usually the case in polymers or liquid crystals and their dielectric spectra often reveal relaxation processes caused by collective motions of molecular units.

In a typical experiment, the material is subjected to alternating electric field of various frequencies (0.01 Hz to 10 GHz) at various temperatures (−120 to >200°C). The dipoles in the material, interacting with the field, show frequency and temperature dependent relaxation processes. Every process in the material has its own relaxation characteristics, such as the relaxation time τ and relaxation strength $\Delta\varepsilon$.

B.2 Fundamentals

In a dielectric experiment, the complex capacitance C^* is measured. By knowing the geometrical capacitance C_0 and by using $C^* = C_0\varepsilon^*$, the complex dielectric constant $\varepsilon^* = \varepsilon' - i\varepsilon''$ can be determined. By definition, ε^* consists of a real part ε', the dielectric permittivity, and the imaginary part ε'' the dielectric loss; the latter describes the dissipation of energy caused by 'molecular friction' or by transport of real charge carriers (electrical conduction).

Although the dielectric constant can be measured both in the *time* domain and *frequency* domain, frequency domain spectroscopy is the most common technique since it directly yields the dielectric spectrum $\varepsilon^*(f)$. In case of a relaxation process, the frequency dependence of the dielectric constant can be described by a suitable relaxation function, e.g. the Debye equation:

$$\varepsilon^*(\omega) = \varepsilon_\infty + \frac{\varepsilon_S - \varepsilon_\infty}{1 + i\omega\tau} \tag{3.30}$$

which was originally derived for polar gasses (and isotropic liquids) containing individual dipoles with an identical characteristic relaxation time τ. The other quantities ω, ε_S and ε_∞ denote the angular frequency $\omega = 2\pi f$, the static dielectric constant and the dielectric constant at infinite frequencies. Decomposing equation 3.30 into its real and imaginary part yields the permittivity and the dielectric loss for the 'Debye relaxation':

$$\varepsilon'(\omega) = \varepsilon_\infty + \frac{\varepsilon_S - \varepsilon_\infty}{1 + \omega^2\tau^2} \quad \text{and} \quad \varepsilon''(\omega) = \frac{(\varepsilon_S - \varepsilon_\infty)\,\omega\tau}{1 + \omega^2\tau^2} \tag{3.31}$$

In real materials, e.g. amorphous polymers exhibiting a high degree of structural disorder, the individual dipolar groups experience a variation in their local environment which often causes a distribution in relaxation times. Such broadened relaxation processes can be modeled by e.g. the semi-empirical Havriliak-Negami (HN) function, which extends the Debye equation by two shape parameters *a* and *b* that determine the slope of the tails of the relaxation.

$$\varepsilon^*(\omega) = \varepsilon_\infty + \frac{\varepsilon_S - \varepsilon_\infty}{\left[1+(i\omega\tau)^a\right]^b} \tag{3.32}$$

At high temperatures, usually above the glass transition temperature, polymers might also possess significant electrical conduction (dc-conductivity σ_{dc}) which gives rise to an additional contribution to the loss according to $\varepsilon''(\omega) = \varepsilon''_{lc}(\omega) + \sigma_{dc}/\varepsilon_0\omega$, with ε_0 being the permittivity in vacuum. Owing to its scaling with ω^{-1}, this conduction often obscures dipolar relaxation processes at low frequencies. In order to eliminate the conduction term, it is favorable to calculate the alternative loss spectrum $\varepsilon''_{\mathrm{deriv}}(f)$:

$$\varepsilon''_{\mathrm{deriv}} = -\frac{\pi}{2}\frac{\partial\varepsilon'(\omega)}{\partial\ln\omega} \tag{3.33}$$

which is close to the 'conduction-free' *measured* loss $\varepsilon''_{\mathrm{meas}}$ for broad relaxation peaks. In addition, $\varepsilon''_{\mathrm{deriv}}$ offers an improved method of separating narrowly distributed relaxation, such as a Debye process, which become sharper in the $\varepsilon''_{\mathrm{deriv}}$ representation.
For a quantitative analysis of the relaxation spectra, either $\varepsilon''_{\mathrm{deriv}}$ or ε'' was fitted with the corresponding expression of the HN function, yielding relaxation times and relaxation strengths for each temperature dependent spectrum.

The temperature dependence of the relaxation time $\tau = 1/2\pi f$ (where f is the frequency) can usually be described by either the Arrhenius equation 3.34 or the Vogel-Fulcher-Tammann (VFT) relation 3.35:

$$\tau(T) = \frac{1}{2\pi f(T)} = \tau_\infty e^{E_A/RT} \tag{3.34}$$

$$\tau(T) = \tau_\infty e^{E_A/R(T-T_V)} \tag{3.35}$$

Here, $\tau(T)$ is the relaxation time at temperature T, τ_∞ the relaxation time at infinite temperatures and R is the gas constant. In contrast to the Arrhenius equation, the VFT-relation is only defined for temperatures above the Vogel temperature T_V and can be regarded as an Arrhenius equation scaled to T_V instead of the absolute temperature 0 K. The occurrence of VFT behavior, i.e. bended curves in the log(τ) vs. $1/T$ presentation (Arrhenius diagram or activation plot) is the signature of a dynamic glass transition, or a process related to a glass transition. For relaxation processes which obey the Arrhenius law, an alternative relationship was derived from the theory of absolute reaction rates:[30]

$$f(T) = \frac{k_{\mathrm{B}}T}{2\pi h} e^{-\Delta H/RT} e^{\Delta S/R} \tag{3.36}$$

where h, k_{B} and R are Planck's constant, the Boltzmann constant and the gas constant, respectively. ΔH and ΔS are the activation enthalpy and entropy. From a comparison between the Arrhenius and the absolute reaction rate theories one obtains[31]

$$E_{\mathrm{A}} = \Delta H + RT - P\Delta V \tag{3.37}$$

in which the term $P\Delta V$ can be neglected because of its low magnitude. Combining eqs. 3.36 and 3.37 results in expression 3.38:

$$E_{\mathrm{A}} = RT\left(1 + \ln\frac{k_{\mathrm{B}}}{2\pi h} + \ln\frac{T}{f}\right) + T\Delta S \tag{3.38}$$

which relates the activation energy to the activation entropy ΔS and the relaxation time (or frequency) at a given temperature T. A classification of relaxation processes with respect to the degree of cooperativity is based on the difference between the measured activation energy E_{A} and the activation energy $E_{\mathrm{A},0}$ obtained from equation 3.38 assuming $\Delta S = 0$ (zero-activation energy limit).[18] This criterion is used for the assignment of the relaxation processes observed for the mesogens described in this thesis.

As discussed earlier, the relaxation strength $\Delta\varepsilon$ (defined as: $\Delta\varepsilon = \varepsilon_{\mathrm{S}} - \varepsilon_\infty$) can experimentally be determined either from the permittivity $\varepsilon'(f)$ or the loss spectrum $\varepsilon''(f)$ by fitting with e.g. the HN relaxation function. $\Delta\varepsilon$ is related to the molecular parameters by equation 3.39 developed by Onsager and Fröhlich,

$$\frac{(\varepsilon_{\mathrm{S}} - \varepsilon_\infty)(2\varepsilon_{\mathrm{S}} + \varepsilon_\infty)}{\varepsilon_{\mathrm{S}}(\varepsilon_\infty + 2)^2}\frac{M_{\mathrm{W}}}{\rho} = \frac{N_{\mathrm{A}} g \mu^2}{9\varepsilon_0 k_{\mathrm{B}} T} \tag{3.39}$$

which takes in account local order of the dipoles by means of the Kirkwood correlation factor g. Further parameters are the molar mass per dipolar unit M_{W}, the density ρ (here: $\rho = 10^3$ kg·m^{-3}), Avogadro's number N_{A} and the dipole moment μ involved in a specific relaxation process. The correlation factor g is a measure for the orientation correlation between individual dipoles, which can vary from less than unity (e.g. anti-parallel oriented dipoles) to far above unity in case of collective motions of dipoles in a polar arrangement. Practically, the correlation factor can be obtained by comparing the calculated relaxation strength ($\Delta\varepsilon_{\text{calc}}$) according to equation 3.33 with the experimental value $\Delta\varepsilon_{\text{exp}}$, provided that the value of the dipole moment and the other molecular parameters are known. From 3.40 the relaxation strength can be explicitly obtained for two special cases (weak and strong relaxations):

$$\begin{aligned} \Delta\varepsilon &\approx \frac{(\varepsilon_\infty + 2)^2}{3}\frac{\rho}{M_W}\frac{N_A\mu^2 g}{9\varepsilon_0 k_B T}, \quad \Delta\varepsilon \quad \varepsilon \quad 0 \quad {}_\infty \\ \Delta\varepsilon &\approx \frac{(\varepsilon_\infty + 2)^2}{2}\frac{\rho}{M_W}\frac{N_A\mu^2 g}{9\varepsilon_0 k_B T}, \quad \Delta\varepsilon \quad \varepsilon \quad 2 \quad {}_\infty \end{aligned} \tag{3.40}$$

B.3 Data analysis

In order to distil the results from the measurements, the dielectric spectra of all samples have been treated by a three-step procedure using the individual techniques described above. First, the loss spectra were 'cleaned', if necessary, from the conduction contribution by means of the derivative technique, yielding $\varepsilon''_{\text{deriv}}$. Next, either the $\varepsilon''_{\text{deriv}}$ spectra or the genuine loss data ε'' (at low temperatures) were fitted with an appropriate set of HN functions, varying from 1 to 3 terms depending on the number of (partially) overlapping relaxation peaks. In this way, the mean relaxation time $\tau(T)$, the relaxation strength $\Delta\varepsilon_{\text{exp}}$ and the HN shape parameters *a* and *b* (not further analyzed in this thesis) of all distinct relaxation processes were obtained. As a third step, the temperature dependence of the relaxation time was fitted by the Arrhenius or the VFT equation. For processes that obeyed the Arrhenius law, an additional Eyring analysis was made, yielding the zero-entropy activation energy $E_{A,0}$ as well as the activation entropy ΔS.

The activation parameters and the relaxation strengths formed the basis for the subsequent assignment of the several relaxation processes to specific molecular motions in the different materials. In some materials – interestingly including the compound with the simplest molecular structure (**D2**) – up to *seven* different relaxations were found, indicating a multilevel hierarchy in the molecular dynamics. A first overview of dynamic processes that can be expected in analogy to the dynamics of rod-like mesogens is given in Figure 3.21. Note that only motions are dielectrically active which involve changes of the dipole moment in the direction of the external electrical field.

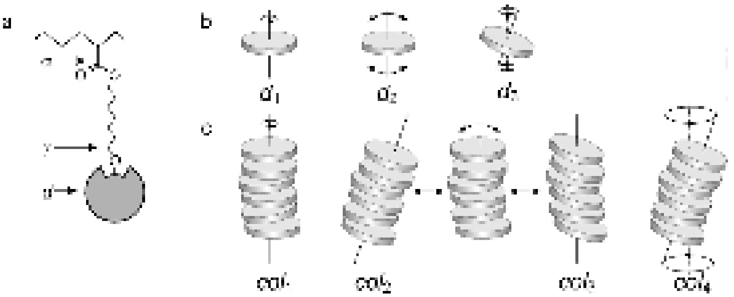

Figure 3.22. Various suggested molecular and cooperative relaxation modes expected for nematic discotic and nematic columnar phases: (a) The dielectrically active position of the molecule (dipoles) and the nomenclature of the corresponding relaxation processes: α: backbone relaxation, γ: spacer relaxation, *d*: mesogenic relaxation. (b) various modes of single molecule mesogenic relaxation: rotation around the mesogen's short and long axis and tumbling around the short axis. (c) the corresponding relaxation modes for an (one-dimensional) columnar assembly of mesogens. Note that two forms of rotation around the long axis can be distinguished: a rotation of the entire column (col_2) and a rotation of all the mesogens in the column resulting in a tilted organization (col_3).

The fastest dielectric relaxation in the discotic mesogenic compounds, the γ-process, originates from motions of the methylene spacer involving the adjacent ether linkage to the mesogenic unit. This process is characterized by the lowest activation energy and thus shows up in the low temperature and high frequency area of the relaxation spectrum. Since the γ-process basically involves local conformational changes extending over a few bonds lengths, this relaxation is almost non-cooperative as indicated by a nearly zero activation entropy.

For amorphous polymers, at higher temperatures, a second process involving segmental motions of the backbone is usually observed. This process, the α-relaxation, is strongly correlated with the glass transition of the polymer. Typically, the α-relaxation is fitted with a VFT relation, resulting in a curved $\tau(T)$ dependence in an Arrhenius diagram. From the VFT parameters, an operationally defined glass transition temperature T_g can be deduced: $T_{g,\mathrm{VFT}} \equiv T(\tau = 100\ \mathrm{s})$. Furthermore, the steepness of the $\tau(T)$ curve at T_g or the curvature itself contains information on the degree of intermolecular cooperativity of the α-process, i.e. the intermolecular coupling of the polymers chains caused by covalent or physical crosslinks, steric hindrance or other inter-chain interactions. A useful measure of the intermolecular cooperativity is the steepness index *m* defined by 3.41:

$$m = \left.\frac{d\log\tau}{d(T_{\mathrm{g}}/T)}\right|_{T=T_{\mathrm{g}}} \tag{3.41}$$

The steepness index can be related to the VFT-parameters:

$$m = \frac{E_{\mathrm{V}}}{2.30R} \frac{T_{\mathrm{g}}}{(T_{\mathrm{g}} - T_{\mathrm{V}})^2} \tag{3.42}$$

Here, E_{V} is the VFT activation energy and T_{V} is the Vogel temperature. When the steepness of the VFT curve decreases, the polymer chains loose intermolecular coupling, possibly caused by increased chain confinement effects. Ultimately, for systems with high topological constraints, the motions of the backbone are so restricted that the α-relaxation can be fitted more satisfactory with the Arrhenius equation. In these cases, the glass transition is determined as the temperature at which a maximum in the apparent activation energy (E_{App}) obtained from differential sampling[19] is found. This technique was exclusively applied for the polymers, discussed in Chapter 3.4.

The most specific relaxation processes involve the motions of the mesogens themselves. According to Figure 3.21, both single molecule relaxation modes (in all phases including $\mathrm{N_D}$ and I phase) and cooperative modes (exclusively in the $\mathrm{N_{Col}}$, $\mathrm{N_L}$ and columnar phases) are likely to be found. Usually, the mesogenic relaxations are well described by an Arrhenius equation. A subsequent Eyring analysis yields interesting parameters, such as the activation enthalpy and entropy. However, in some cases the mesogenic relaxation processes show a typical VFT behavior, indicating that the mesogenic dynamics is dominated by the long-range dynamics of the polymer backbone. At a phase transition, the local environment of a mesogen changes drastically, and hence, a discontinuity in the relaxation process is expected. This makes DRS an excellent technique to determine phase transitions. The transitions observed for the various analyzed materials show a good agreement with the transitions found with other techniques, like DSC en OPM.

References and notes

(1) (a) Kreuder, W.; Ringsdorf, H.; Tschirner, P. *Makrom. Chem., Rapid Commun.* **1985**, *6*, 367. (b) Stewart, D.; McHattie, G.S.; Imrie, C.T. *J. Mater. Chem.* **1998**, *8*, 47-51. (c) Boden, N.; Bushby, R.J.; Lu, Z.B. *Liq. Cryst.* **1998**, *25*, 47-58.

(2) Janietz, D. *Chem. Commun.* **1996**, 713-714.

(3) (a) Kouwer, P.H.J.; Gast, J.; Jager, W.F.; Mijs, W.J.; Picken, S.J. *Mol. Cryst. Liq. Cryst.* **2001**, *364*, 225-234. (b) Kouwer, P.H.J.; Jager, W.F.; Mijs, W.J.; Picken, S.J. *Macromolecules* **2000**, *33*, 4336-4342. (c) Kouwer, P.H.J.; Mijs, W.J.; Jager, W.F.; Picken, S.J. *J. Am. Chem. Soc.* **2001**, *123*, 4645-4646.

(4) Imrie, C.T.; Luckhurst, G.R. In *Handbook of Liquid Crystals*; Demus, D., Goodby, J.W., Gray, G.W., Spiess, H.W., Vill, V., Eds.; Wiley VCH: New York, 1998; Vol. 2B, pp 801-833.

(5) A detailed discussion on X-ray diffraction is given in Appendix A of Chapter3.

(6) Praefcke, K. In *Physical properties of liquid crystals : nematics*; Dunmur, D., Fukuda, A., Luckhurst, G.R., Eds.; INSPEC: London, 2001; pp 17-35.

(7) (a) Kreuder, W.; Ringsdorf, H. *Makrom. Chem., Rapid Commun.* **1983**, *4*, 807-815. (b) Wenz, G. *Makrom. Chem., Rapid Commun.* **1985**, *6*, 577-584. (c) Weck, M.; Dunn, A.R.; Matsumoto, K.; Coates, G.W.; Lobkovsky, E.B.; Grubbs, R.H. *Angew. Chem. Int. ed. Engl.* **1999**, *38*, 2741-2745.

(8) (a) Valisenko, S.V.; Shibaev, V.P.; Khokhlov, A.R. *Makromol. Chem.* **1985**, *186*, 1951-1960. (b) Wang, X.J.; Warner, M. *J. Phys. A: Math. Gen.* **1987**, *20*, 713-731. (c) Renz, W.; Warner, M. *Proc. R. Soc. London A* **1988**, *417*, 213-233. (d) Semenov, A.N.; Khokhlov, A.R. *Sov. Phys. Usp.* **1988**, *31*, 988-1013.

(9) Favre-Nicolin, C.D.; Lub, J. *Macromolecules* **1996**, *29*, 6143-6149.

(10) This assumes that the presence of 35% of methyl acrylate groups in the backbone (corresponding with only 2% in total mass) does not play a major role, although its influence may not be discarded a priori, since small changes in molecular architecture can have dramatic effects.

(11) (a) Measurements were performed by M.W.C.P. Franse and B. Norder. (b) Experimental setup: Measurements were performed using a Rheometric Mechanical Spectrometer with a parallel plate fixture with plates of 8 and 25 mm diameter. Further details: gap: 1 mm; strain: 0.1%, frequency sweep: 10 rad·s^{-1} and heating/cooling rate: 5°C·min^{-1}. The spectra were analyzed using RMS800 Software Orchestrator version 6.4.4.

(12) Franse, M.W.C.P., *Manuscript in preparation.*

(13) In gerenal, polymers with a higher mesogen content showed a broader glass transition, indicating a slower relaxation process due to a lower mobility of the mesogens.

(14) The classification of the rigid and flexible parts is a bit ambiguous where both are connected. For polymers of **D2**, the lateral methyl substituents are regarded as rigid, since they have no positional flexibility with respect to the mesogen. The oxygen, connecting the spacer to the disk, is arbitrarily also regarded as rigid, for its reduced mobility. Calculations pointed out that addressing this oxygen flexible has only a minor effect on the results.

(15) Wübbenhorst, M.R.; Van Turnhout, J. *J. Non-Cryst. Solids*, *in press*.

(16) Wübbenhorst, M.R.; Van Koten, E.; Jansen, J.C.; Mijs, W.J.; Van Turnhout, J. *Macromol. Rapid Commun.* **1997**, *18*, 139-147.

(17) Simon, G.P. In *Dielectric Spec-troscopy of Polymeric Materials: Fundamentals and Applications*; Runt, J.P., Fitzgerald, J.J., Eds.; ACS: Washington DC, 1997; pp 329-378.

(18) Starkweather, H.W. *Polymer* **1991**, *32*, 2443-2448.

(19) Van Turnhout, J.; Wübbenhorst, M.R. *J. Non-Cryst. Solids*, *in press*.

(20) (a) Wübbenhorst, M.; Nieuwhof, R.P.; Marcelis, A.T.M.; Sudhölter, E.J.R.; van Turnhout , J. *submitted to Polymer*. (b) Wübbenhorst, M.; van Turnhout, J.; Hempenius, M.A.; Lammertink, R.G.H.; Vancso, G.J. *Manuscript in preparation*.

(21) The column length $N_{\mathrm{C,XRD}}$ can be calculated by convolution of a distribution in the one-dimensional periodic lattice with a finite block length, see Appendix A5. Note that the calculation assumes a uniform column length, which makes the absolute outcomes of the calculation at least questionable. However, the calculation can be used for relative quantities, such as the ratio of the column lengths N_{Col} in the $\mathrm{N_{Col}}$ and the $\mathrm{N_D}$ phase.

(22) (a) Maier, W.; Saupe, A. *Z. Naturforsch.* **1958**, *13a*, 564. (b) Maier, W.; Saupe, A. *Z. Naturforsch.* **1960**, *15a*, 287. (c) Maier, W.; Saupe, A. *Z. Naturforsch.* **1959**, *14a*, 882.

(23) McMillan, W.L. *Phys. Rev. A* **1971**, *4*, 1238.

(24) Feldkamp, G.E.; Handschy, M.A.; Clarck, N.A. *Phys. Lett.* **1981**, *85A*, 359-362.

(25) The McMillan theory was originally derived to describe the SmA to N phase transition. It is noted that the order of the layered structure of the SmA phase is not long-range. Still, a sinusoidal function is used to describe the layers, because on a local scale a layered structure will be present. This is similar to what occurs in our systems, where locally a hexagonal order is expected, while no long-range order is observed.

(26) (a) Ebert, M.; Frick, G.; Baehr, C.; Wendorff, J.H.; Wüstefeld, R.; Ringsdorf, H. *Liq. Cryst.* **1992**, *11*, 293-309. (b) Ghose, D.; Bose, T.R.; Mukherjee, C.D.; Roy, M.K.; Saha, M. *Mol. Cryst. Liq. Cryst.* **1986**, *138*, 379-392. (c) Chandrasekhar, S. *Phil. Trans. R. Soc. Lond.* **1983**, *A309*, 93.

(27) In polymers based on substituted triphenylenes, usually columnar phases are formed. Here the backbone can be placed in the disordered sea of alkyl substituents in between the columns. In this way, the polymer backbone does not hinder any long-range organization of the columns.

(28) With the realization of this appendix the following literature was used: (a) Seddon, J.D. In Handbook of Liquid Crystals; Demus, D., Goodby, J.W., Gray, G.W., Spiess, H.W., Vill, V., Eds.; Wiley VCH: New York, 1998; Vol. 1, pp 635-679. (b) Warren, B.E. X-ray diffraction; Addison-Wesley: Reading, 1969.

(29) Enno Klop of the Akzo Nobel Chemical Research Arnhem - department of applied physics is gratefully acknowledged discussions on the results of the XRD experiments, especially the contribution in explaining the complex XRD pattern of the N_{Col} phase of **P(D2b)**.

(30) Eyring, E. *J. Chem. Phys.* **1936**, *4*, 283.

(31) Steinfeld, J.; Hase, W. *Chemical Kinetics and Dynamics*; Prentice-Hall: Englewood cliffs, NJ, 1989.

4 Nonsubstituted mesogens: Properties of the materials and charge transfer complexes

Parts of this chapter have been published in: (a) Kouwer, P.H.J.; Jager, W.F.; Mijs, W.J.; Picken, S.J. *Macromolecules* **2001**, *34*, 7582-7584. (b) Kouwer, P.H.J.; Van den Berg, O., Jager, W.F.; Mijs, W.J.; Picken, S.J. *Macromolecules* **2002**, *35*, 2576-2582.

Abstract

The liquid crystalline properties of charge transfer complexes of disk-shaped electron rich *donors*, based on **D1** (see Figure 4.1), and a series of electron deficient *acceptors*, based on trinitrofluorenone have been investigated. Specific interactions resulted in supramolecular assemblies that exhibit various mesophases, although none of the pure materials showed liquid crystalline properties. Complexes of the low molar mass donor with a weak (**A1**), intermediate (**A2**) and a strong acceptor (**A3**) yielded various mesophases including the N_D, N_{Col} and Col_h phase. Stronger CT complexes showed higher ordered mesophases and accordingly a strong increase in the melting and clearing temperatures. Complexes with the corresponding macromolecular donor **P(D1)** also showed the new nematic lateral (N_L) phase. Decreasing the spacer length attached to the donor or the acceptor results in higher ordered mesophases due to a decrease in steric packing effects. The use of a polymer bound mesogens as well as charge transfer complexing and modification of the spacer length are effective tools to induce a wide variety of unusual mesophases, starting from a limited number of materials.

4.1 Introduction

The charge transfer (CT) interactions between a disk-shaped acceptor with a discotic mesogen were first investigated in the late 1980s.[1a] Early contributions discuss the CT complexes of substituted triphenylenes with TNF (**A2**) that resulted in a considerable broadening of the temperature window of the mesophases, due to a strong increase in the clearing temperatures. Analogous investigations of CT complexes of non-liquid crystalline triphenylene derivatives (including polymers) showed induction of columnar and nematic columnar phases.[1] Obviously, an important factor determining the phase behavior of a CT complex is the interaction strength between the donor and the acceptor. This can easily be manipulated by using acceptors of different electron affinities.[2]

In the early 1990s, the first CT complexes of pentakis(phenylethynyl)benzenes were studied.[3] Various mesophases were reported for a series of non-ring substituted donors (Figure 2.3b, R=H) with TNF.[4] In a later contribution, properties of such donors with alkoxy tails fixed at the central phenyl were investigated.[5] TNF complexes of the mesogens with short spacers, residing within the radius of the core (i.e. $<C_5$) gave rise to columnar hexagonal phases. On the other hand, spacers protruding from the core ($>C_{11}$) prevented the establishment of a well-defined hexagonal packing, which resulted in the formation of a N_{Col} phase. Complexes of mesogens with an intermediate spacer length showed Col_h phases at low temperatures and N_{Col} phases at higher temperatures. This indicates that initially the spacer can adapt to the hexagonal packing, but at increasing temperatures the mobility of the spacer increases and the hexagonal order is destroyed, while the columns remain present due to the CT interactions. These studies were among the first in which the N_{Col} phase was reported.

It is emphasized that the main method of characterization of the N_{Col} phase was measuring the latent heat involved at the clearing point in combination with the observance of the nematic optical texture. We would like to stress that this method is at least unconvincing, since the latent heat only reflects the difference in order in the liquid crystalline and the isotropic phase. Moreover, it is expected and that in the isotropic phase still a substantial amount of local order is present. Appropriate X-ray diffraction measurements should be performed to establish the local order in these systems. Characterization of the N_D, N_{Col} and the N_L phase in this chapter was performed by X-ray diffraction, which probes the local order and therefore, is much more convincing.

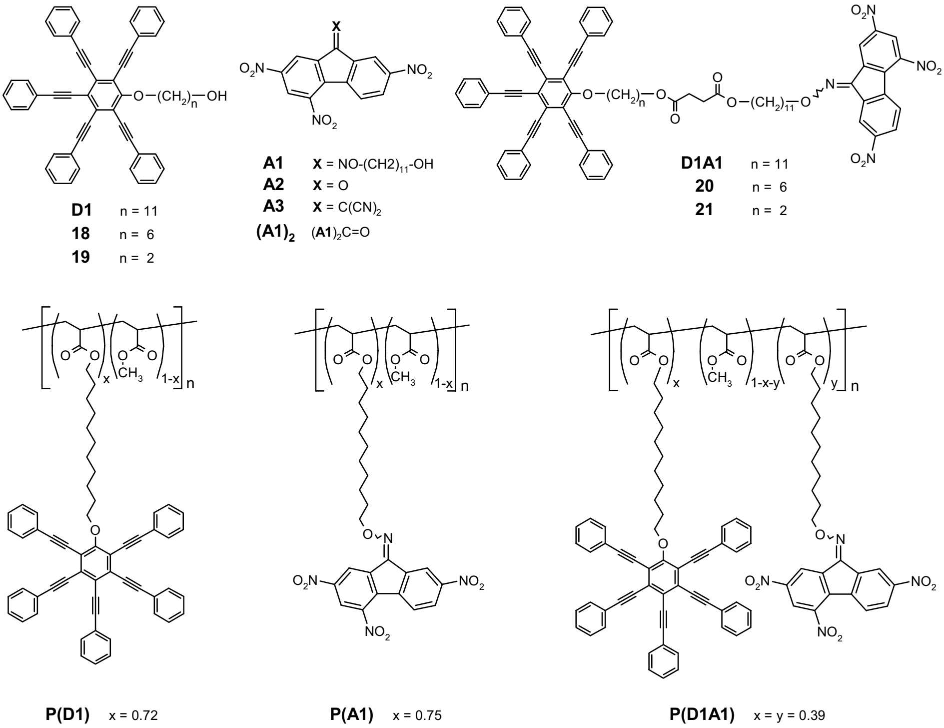

Figure 4.1. Materials discussed in this chapter.

In this chapter, the CT complexes based on **D1** with acceptors **A1**-**A3** and **(A1)$_2$** will be described. Attachment of the mesogen and/or the acceptor to a polyacrylate backbone considerably affects the phase behavior. For reasons of comparison, also the phase behavior of the intramolecular CT dimer **D1A1** and copolymer **P(D1A1)** is included. In section 4.5, a preliminary study on the effect of the spacer length on the phase behavior is reported. The preparation of the materials (Figure 4.1) is discussed in Chapter 2. Compounds **18** and **19**, short chain equivalents of **D1** were synthesized analogously to **D1,**[6] Intramolecular charge transfer complexes **20** and **21** were synthesized by the same procedures as **D1A1**.[7]

4.2 Liquid crystalline properties of the charge transfer complexes

The results on the thermal analysis of the pure materials are summarized in Table 4.1. All the low molar mass compounds are crystalline solids whereas the polymers are amorphous materials. None of the pure donors or acceptors showed liquid crystalline behavior. Note that the broad melting trajectories of **A1** and **(A1)$_2$** are due to the presence of isomers in these materials, as already discussed in Chapter 2.2.3.

Table 4.1. Thermal behavior of the pure compounds obtained by DSC.

Material	Transition temperatures [°C] and (latent heat [kJ·mol^{-1}])				Material	Transition temperatures [°C] and (latent heat [kJ·mol^{-1}])			
D1 (n=11)	K	122	(39)	I	**A1**	K	98-109	(54)	I
18 (n=6)	K	197	(23)	I	**(A1)$_2$**	K	71-88	(57)	I
19 (n=2)	K	179	(46)	I	**A2**	K	176	(59)	I
P(D1)	G_I	53		I	**A3**	K	276	(78)	I
					P(A1a)	G_I	50		I

The thermal properties of CT complexes of **D1**:**A2** and **P(D1)**:**A2** as a function of acceptor concentration were investigated. In addition to multiple mixtures that were analyzed by DSC and OPM, contact samples of the donors with **A2** were examined with OPM. From the resulting (simplified) phase diagrams (see Figure 4.2), it is evident that at equimolar ratios the best properties are found, i.e. absence of biphasic regions and a maximum in the transition temperatures. Deviation from the 1:1 ratio results in the formation of distinct biphases. For this reason, only the equimolar complexes have been investigated in more detail. Optimal properties at 1:1 ratios have been reported for similar materials before, but remarkably, in other cases the best properties were obtained from ratios deviating from 1:1.[8]

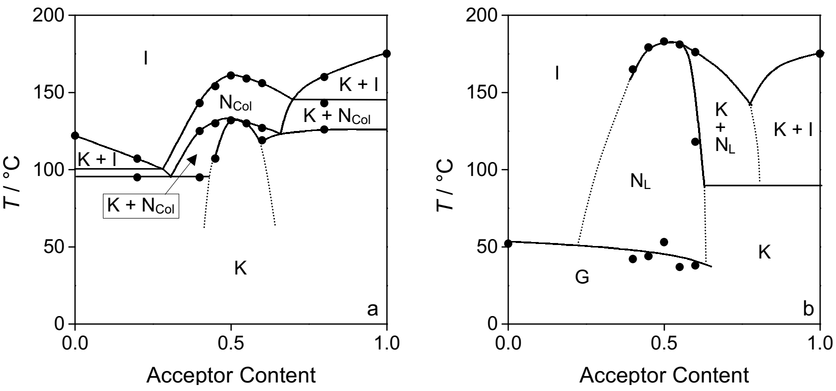

Figure 4.2. Simplified phase diagrams of (a) **D1**:**A2** and (b) **P(D1)**:**A2**. The dotted curves are estimated.

2 All materials showed reproducible DSC diagrams; some examples, all second heating curves, are depicted in Figure 4. Complexes with **A3** (not shown) exhibit dissimilar second heating runs, since substantial thermal degradation was observed during the first run.

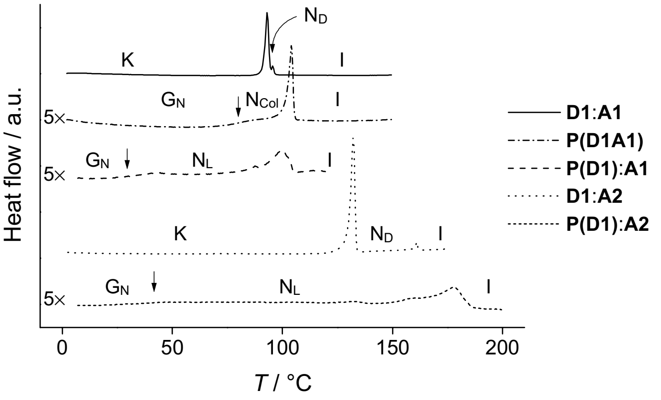

Figure 4.2. Normalized DSC thermograms of various CT complexes. From top to bottom: **D1**:**A1**, **P(D1A1)**, **P(D1)**:**A1**, **D1**:**A2** and **P(D1)**:**A2**. Note that the DSC traces of the polymeric systems have been magnified. The arrows in these traces indicate the glass transitions.

The OPM and DSC results of the equimolar CT complexes are summarized in Table 4.2. The CT complexes of **D1** and **P(D1)** with **A1** and **P(A1a)** and their intramolecular analogues **D1A1** and **P(D1A1)** all displayed nematic mesophases. Low molar mass complexes **D1**:**A1** and **D1A1** crystallized upon cooling, whereas the macromolecular complexes showed a glass transition and their optical textures were frozen in. Except for **D1A1**, the clearing temperatures were close to each other. Only the latent heat values at the N to I transitions, roughly corresponding to the extent of order in the nematic phase, varied considerably.

The transition temperatures and latent heat values of **P(D1)**:**P(A1a)** were measured after annealing for 10 hours at 100°C.

Table 4.2. Thermal behavior of equimolar complexes of **D1** and **P(D1)** with electron acceptors **A1**-**A3** and **P(A1a)** obtained by DSC and OPM. Transition temperatures in [°C], and latent heat in [J·g^{-1}]).

Complex	**D1**					**P(D1)**				
A1	K	93 (20)	N_D	96 (1.2)	I	G_{N_L}	28	N_L	103 (5)	I
P(A1a)	G_{N_L}	33	N_L	101 (5)	I	$G_{N_{Col}}$	65	N_{Col}	94 (3)	I
A1	K	93 (20)	N_D	96 (1.2)	I	G_{N_L}	28	N_L	103 (5)	I
A2	K	132 (39)	N_{Col}	161 (1)	I	G_{N_L}	50	N_L	164 (5)	I
A3	K	200 (10)	Col_h	227 (12)	I	G_{Col_h}	50	Col_h	>250	d
Intramolecular	**D1A1**	K/Col	32 (1.0)	N_D	84 (1)	I				
CT complexes	**P(D1A1)**	$G_{N_{Col}}$	80	N_{Col}	104 (5)	I				

The liquid crystalline properties of CT complexes of **D1** and **P(D1)** with electron acceptors **A2** and **A3** have been investigated at equimolar ratios as well. The observed phases (nematic as well as columnar) and transition temperatures (T_i ranging from ~90 to >250 °C) were strongly dependent on the acceptor. In complexes with the macromolecular donor crystallization was fully suppressed, whereas the clearing temperatures did not change much compared to the low molar mass mesogens. For **P(D1)**:**A2** a strong increase in the latent heat at the N to I transition was observed as compared to the equivalent **D1**:**A2**. Complex **P(D1)**:**A3** revealed a columnar texture in microscopy studies, but no further transitions were found before degradation started at high temperatures.

Powder X-ray diffraction. The low molar mass complex **D1**:**A1** showed a typical N_D pattern with just diffuse reflections, whereas the one-polymer complex **D1**:**P(A1a)** showed the pattern of the newly identified N_L phase,[9,10] i.e. much sharper reflections in the columnar and lateral direction as well as a clearly visible [200] reflection at small angles. The related **P(D1)**: **A1** complex showed a nearly identical pattern. In addition, the polymer mixture **P(D1)**:**P(A1a)** as well as the copolymer **P(D1A1)** exhibited sharp reflections in the intracolumnar direction, though their intercolumnar reflections were much more diffuse. CT complexes with **A3** showed further peak narrowing, as would be expected for columnar phases. In Figure 4.4 the XRD patterns of the observed liquid crystalline phases are presented.

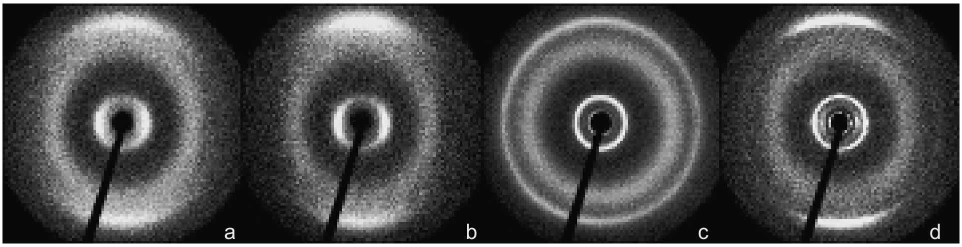

Figure 4.4 XRD patterns of observed mesophases a: (a) N_D phase (**D1**:**A1** at 95°C); (b) N_{Col} phase (**D1**:**A2** at 150°C); (c) N_L phase (**D1**:**P(A1a)** at 90°C) and (d) Col_h phase (**D1**:**A3** at 210°C).

For a more quantitative analysis, the spacings d were calculated using Bragg's Law: $2d\sin\theta = n\lambda$, where θ is the diffraction angle and λ the wavelength (1.54 Å). To calculate the correlation length ξ, which is a measure for the extent of spatial order in one direction, the Scherrer equation was used: $\xi\omega_{1/2}\cos(\theta) = 0.89\lambda$, with $\omega_{1/2}$ is the full width at half height of a reflection. Correlation lengths for the various spacings are summarized in Tables 4.3 and 4.4. More details on X-ray diffraction are given in Appendix A of Chapter 3.

Table 4.3. XRD Results of high and low molar mass CT complexes.

Complex	T [°C]	Phase	Miller Indices	d [Å]	ξ [Å]	ξ/d [-]
D1:**A1**	95	N_D	200	13.4	59	4.4
			alkyl	4.8	23	4.8
			001	3.56	36	10
D1 : **P(A1a)**	90	N_L	200	12.6	212	17
			alkyl	4.7	26	5.5
			001	3.57	61	17
P(D1):**A1**	90	N_L	200	12.8	242	19
			alkyl	4.8	26	5.4
			001	3.52	63	18
P(D1) : **P(A1a)**	90	N_{Col}	200	13.1	100	7.7
			alkyl	4.9	31	6.5
			001	3.58	58	16
P(D1A1)	90	N_{Col}	200	13.0	106	8.2
			alkyl	4.8	24	5.0
			001	3.57	59	16

Table 4.4. XRD Results of CT complexes with an increasing donor-acceptor interaction strength.

Complex	T [°C]	Phase	Miller Indices	d [Å]	ξ [Å]	ξ/d [-]
D1:**A2**	150	N_{Col}	200	13.5	82	6.0
			alkyl	4.9	22	4.5
			001	3.53	60	17
P(D1):**A2**	150	N_L	200	12.7	179	14
			alkyl	4.8	22	4.6
			001	3.52	43	12
D1:**A3**	210	Col_h	200	13.0	308	24
			alkyl	5.0	21	4.1
			001	3.48	134	38
P(D1):**A3**	200	Col_h	200	12.6	261	21
			alkyl	5.0	29	5.8
			001	3.54	80	23

4.3 Discussion on the phase assignment

Complexes of D1 with A1 and their corresponding polymer analogues. CT complex **D1**:**A1** showed an induced nematic discotic phase in a very small temperature range. By incorporating one of the constituents to a polyacrylate backbone, the phase behavior changed dramatically. Crystallization was suppressed and, due to the plasticizing effect of the tail of **A1**, the glass transition of the complex dropped to room temperature. This resulted in an increased mesophase window from 3°C to about 70°C, since the N to I transition temperature remained nearly constant. The strong rise of the latent heat at the clearing temperature resulted from the increased order of the novel N_L phase.[10] This is clearly demonstrated by the high correlation lengths in both the [200] and the [001] direction. The thermal data of **D1**:**P(A1a)** and **P(D1)**:**A1** are nearly identical, indicating that it is of no importance which of the constituents, donor or acceptor, is bound to the polymer backbone.

The complex of polymers **P(D1)** and **P(A1a)** was highly viscous and, therefore, it was difficult to obtain a homogeneous mixture.[11] DSC experiments showed sharper transitions at higher temperatures after increased annealing times, indicating a continuing homogenization process, but on very long time scales. An annealed sample of the complex showed an increase in T_g and a slight decrease in T_i, accompanied by a decrease in the latent heat, as compared to the one-polymer complexes **D1**:**P(A1a)** and **P(D1)**:**A1**. In contrast to the polymer mixture, the copolymer **P(D1A1)** was much easier to handle. Thin films for microscopy experiments were obtained by simply shearing the polymer in the nematic phase between two glass slides. The latent heat at the clearing point is similar to the one-polymer complexes, and thus in harmony with the N_L to I transition. However, for both **P(D1A1)** and **P(D1)**:**P(A1a)**, powder X-ray diffraction measurements indicate a N_{Col} phase. The combined observation of a high correlation length in the [001] direction and a much lower correlation length in the [200] direction corresponds better to the N_{Col} phase by using the classification that we made after measuring a series of mesogens and CT complexes.[8,12] Another argument in favor of a N_{Col} phase and opposing a N_L phase results from miscibility studies of the nematic phase of **P(DA)** with the N_L phases of **P(D1)**:**A1** or **D1**:**P(A1)**. Although miscibility would be expected based on the resembling molecular structures and other miscibility studies (e.g. the N_L phases of **P(D1)**:**A1** and **D1**:**P(A1)** are perfectly miscible), contact samples clearly show that both nematic phases are immiscible. Taking into account all our experimental data, we conclude that for both macromolecular CT complexes an N_{Col} phase is most likely.

Complexes of D1 and corresponding polymer analogues with A2 and A3. Complexing **D1** and **P(D1)** with the stronger acceptor **A2** resulted in strong increases in the clearing temperatures. The CT complex **D1**:**A2** was reported previously to exhibit a N_{Col} phase.[13] This result is confirmed by our XRD experiments. The macromolecular complex **P(D1)**:**A2** showed suppression of crystallization. From the high latent heat at the clearing point and the increased lateral ordering (in the [200] direction), the formation of a N_L phase was deduced.[10] Moreover, contact samples of **P(D1)**:**A2** and **P(D1)**:**A1** showed the formation of well-mixed interfaces. Complexes with **A3** resulted in columnar phases. Where the low molar mass complex crystallized at 200°C, the polymer did not show any transition before decomposition started at elevated temperatures. This is a clear example of the extension of the temperature window of the mesophase to ~200°C by using a macromolecular compound.

4.4 Dielectric relaxation spectroscopy

A selection of materials was studied by DRS. To investigate the dynamics of the associated nematic mesophase, the donor-acceptor copolymer **P(D1A1)** (N_{Col} phase) was compared with the amorphous donor and acceptor polymers **(PD1)** and **P(A1c)**. Furthermore, complexes of **P(D1)** with the low molar mass acceptors **A1**-**A3** have been investigated. The two series are discussed separately. For details on DRS, the analysis of the raw spectra and peak assignment, the reader is referred to Appendix B of Chapter 3.

The γ-relaxations of **P(D1)**, **P(A1c)** and **P(D1A1)** are shown in Figure 4.5a. The process, originating from low-temperature spacer motions, is similar for all materials. The slight deviation observed for **P(A1c)** can be explained easily by taking the very different chemical structure of the donor and the acceptor into account. The α-relaxation process (Figure 4.5b) clearly shows the impact of the phase formation on the dynamics of the systems. Both the donor and the polymer show a well-developed VFT behavior over the complete temperature range, as would be expected for amorphous polymers. However, the low-temperature relaxation time of the DA-copolymer can be fitted easily with the Arrhenius equation. Moreover, at the phase transition the backbone dynamics speeds-up by orders of magnitude to the level of that of the amorphous polymers. Speeding up the backbone dynamics at the phase transition is accompanied by a decrease the relaxation strength Δ by a factor of 3.

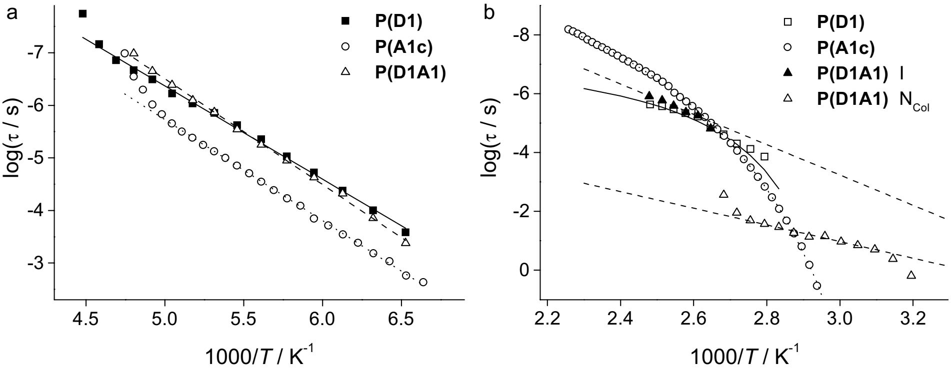

Figure 4.5. Arrhenius plot of the relaxation time for: (a) the γ-relaxation and (b) the α-relaxation. Note that the relaxation behavior of the DA-copolymer shows a discontinuity at the transition from the N_{Col} to the I phase.

Also the mesogen relaxation of the DA-copolymer (not shown) has discontinuity in the relaxation time at the phase transition. The side group relaxation of the amorphous polymers turned out to be highly coupled to the backbone dynamics. The relaxations showed VFT behavior, usually found for α-relaxation process, see Figure 4.6. Hence, the backbone governs the motions of the side groups, or alternatively, the side groups themselves can be considered as molecular probes for the backbone dynamics!

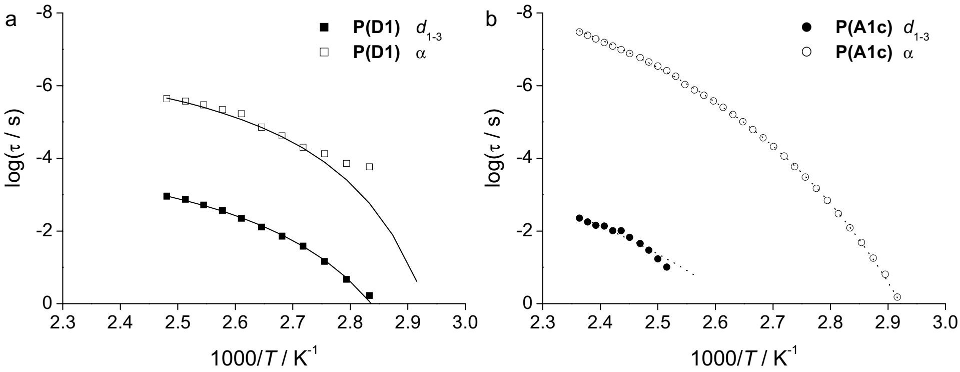

Figure 4.6. Arrhenius plot of the relaxation time of the dielectric α relaxation (open symbols) and the (amorphous) mesogenic relaxations $d_{1\text{-}3}$ (solid symbols), all fitted with the VFT relation.

The influence of the strength of the CT complex was investigated in the second series, containing the complexes of **P(D1)** with **A1**, **A2** and **A3**. As in the previous series, this effect is clearly seen in the α-relaxation, see Figure 4.7. All relaxations could be fitted with the VFT equation. The steepness of the VFT curve at T_g, quantified by the steepness index *m,* yields direct information on the degree of intermolecular cooperativity of the polymeric segmental motions, see Table 4.5. Clearly, *m* decreases with increasing donor-acceptor interaction. This indicates a loss of intermolecular coupling between the polymer chains, caused by increasing chain confinement effects induced by an increased mesogenic order. Note that at high confinement, the actual glass transition temperature drops sharply. The second order transition observed in DSC experiments at much higher temperatures should be attributed to the vitrification process that involves the mesogens.

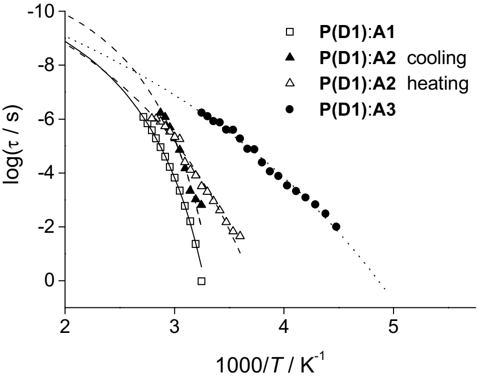

Figure 4.7. Arrhenius plot of the α-relaxation and the VFT fits of the investigated series CT complexes.

Table 4.5. Glass transition temperatures calculated with the VFT relation[14] $T_{g,VFT}$ (compared with the glass transition temperature determined by DSC $T_{g,DSC}$) and the corresponding steepness index *m* for the CT complexes. As a comparison, the steepness indices of the amorphous polymers **P(D1)** and **P(A1a)** are indicated as well.

CT complex	$T_{g,DSC}$ [°C]	$T_{g,VFT}$ [°C]	*m*	Homopolymer	$T_{g,DSC}$ [°C]	$T_{g,VFT}$ [°C]	*m*
P(D1):**A1**	28	24	85	**P(D1)**	50	63	202
P(D1):**A2** (cooling)	45	50	64	**P(A1a)**	53	62	108
P(D1):**A2** (heating)	50	−15	50				
P(D1):**A3**	50	−81	33				

A remarkable feature was observed for the relaxation data of complex **P(D1)**:**A2**. While other materials normally showed similar heating and cooling curves, the loss spectra for **P(D1)**:**A2** revealed remarkable differences between the heating and cooling run, shown in Figure 4.8. Although the γ-relaxation (Arrhenius behavior) remains unaltered during the subsequent heating and cooling runs, the α-process (VFT behavior) clearly reveals changes in its temperature dependence which is manifested by significant differences in the steepness index *m*. The latter observation is already an indication for the higher backbone mobility in the cooled sample. This effect is even more pronounced in the mesogenic relaxation processes. The *col*-relaxation of the cooled sample showed VFT behavior, i.e. it follows the dynamics of the polymer backbone. Conversely, the corresponding relaxation of the heated sample obeys an Arrhenius law rather than the VFT dependence, clearly indicating that the dynamics of the mesogens is almost decoupled from that of the polymer backbone. This observation emphasizes the particular sensitivity of the cooperative relaxation processes (α and mesogenic processes) to the actual degree of molecular order, which obviously depends strongly on the thermal history.

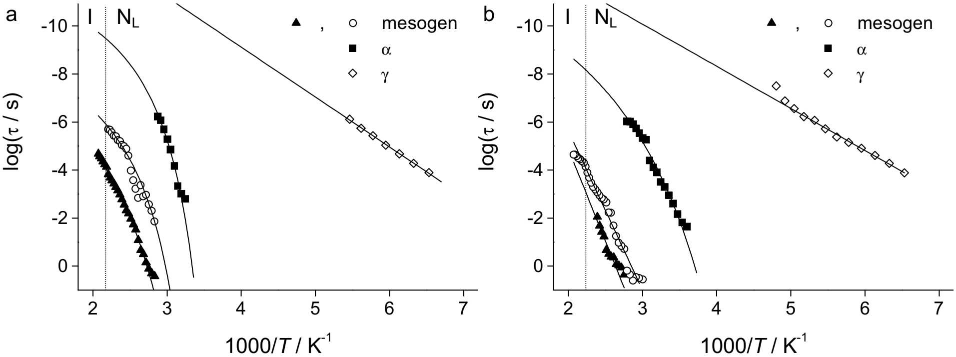

Figure 4.8. Arrhenius plots for the various relaxation processes for **P(D1)**:**A2** for the (a) cooling run and (b) heating run.

4.5 Variation of the spacer length

Previous studies on the steric effect of the spacer in complexes very similar to **D1**:**A2** show that high ordered mesophases (Col_{ho}) are suppressed at sufficient spacer lengths ($>C_{11}$).[4a] The results, outlined in the previous section show that upon improving the donor-acceptor interaction (i.e. by employing the stronger electron acceptor **A3**) a columnar phase could be achieved, despite the presence of the protruding tails. Hence, some extra investigations on the role of the spacer length were performed. For this study, the short spacer donors **18** and **19** were prepared[6] as well as their complexes with acceptors **A1**, **A2** and **A3**.

Charge transfer complexes of **18** and **19** with **A3** resulted in highly stable complexes with transitions from a crystalline to a columnar phase at high temperatures (T_m > 200°C). Unfortunately, the materials suffered from thermal degradation at elevated temperatures and hence the exact melting and clearing temperatures could not be determined. Well-defined results were obtained from CT complexes with **A1** and **A2**; they are summarized in Table 4.6.

The weak acceptor **A1**, bearing a C_{11} tail gave nematic phases with all donors at similar temperatures. The type of nematic phase could not be determined, since no XRD studies were performed on complexes with **18** and **19**. Upon cooling **18**:**A1** and **19**:**A1** from the nematic phase, a grainy texture and a solidification process was observed during microscopy studies; both are indicative for the formation of a crystalline phase. However, the latent heat values at the crystallization temperature are far too small for a real crystallization process. Probably these phases are either highly ordered columnar phases or ill-defined crystalline phases.

Table 4.6. Thermal behavior of equimolar complexes of **D1**, **18** and **19** with electron acceptors **A1** and **A2** obtained by DSC and OPM. Transition temperatures in [°C] and latent heat (between the brackets) in [$J \cdot g^{-1}$]).

Complex	A1					A2				
D1 (n=11)	K	93 (20)	N_D	96 (1.2)	I	K	132 (39)	N_{Col}	164 (5)	I
18 (n=6)	K/Col	88 (3)	N_X	113 (2,1)	I	K	160 (40)	Col_h	215 (2)	I
19 (n=2)	K/Col	79 (6)	N_X	106 (0,9)	I	phase separation				
Intramolecular CT complexes										
D1A1 (n=11)	K/Col	32 (1.0)	N_D	84 (1)	I					
20 (n=6)	K/Col	65 (4.5)	N_X	90 (1.1)	I					
21 (n=2)	K/Col	45 (1.1)	N_X	89 (0.5)	I					

Moreover, the corresponding intramolecular CT complexes[7] **20** and **21** showed nematic mesophases with clearing temperatures close to those of the non-linked complexes. However, mesophases with a much wider temperature range are obtained, because solidification takes place at a much lower temperature. Remarkably, the results of the intramolecular CT complexes differ substantially from the results of a CT complex based on **D1** and an oxim substituted TNF derivative (coupled with a slightly shorter spacer), giving rise to a columnar mesophase.[15]

By complexing the donors with the stronger acceptor **A2**, the intracolumnar order improved. For the complex **18**:**A2**, where none of the constituents has a protruding tail, this resulted in formation of a two-dimensionally ordered columnar phase. In contrast, the complex **D1**:**A2** shows a N_{Col} phase, since the columnar order is disrupted by the long tail of **D1**.

4.6 Conclusions

Mixing electron donors, based on **D1**, with electron acceptors, based on **A2**, resulted in the formation of charge transfer complexes. Phase diagrams of **D1** and **P(D1)** with **A2** show that at exact equimolar ratios, stable complexes were found that effectively behave as a single mesogenic species. By incorporating the mesogens into polyacrylates and by variation of the strength of the CT complex, it was possible to gain insight in the structural parameters determining mesophase formation.

In the low molecular weight complex, the traditional N_D phase was induced. If only one of the species is a polymer, a recently discovered N_L phase with increased columnar and lateral order was observed. Finally, fully polymeric systems formed N_{Col} phases with mainly columnar order. Interestingly, the asymmetric dimer **D1A1** showed a lower clearing point than **D1**:**A1** and **P(D1A1)** and hence, it is an exception in this series of materials.[16] Therefore, its use as a model compound is limited.

The effect of the donor-acceptor interaction strength was studied by a series of different substituted TNF-based acceptors. Complexing **D1** with a weak, intermediate and a strong acceptor resulted in the formation of a N_D, N_{Col} and a Col_h phase, respectively. A strong increase both of the melting temperature and the clearing temperature was found with increasing acceptor strength. When **P(D1)** was substituted for **D1**, a N_L phase and Col_h phase were obtained. In addition, suppression of crystallization led to the formation of broad temperature windows of liquid crystalline phases.

A preliminary study on the effect of he spacer on the phase behavior showed that the phase behavior can be manipulated by steric factors as well. We have demonstrated that there is a balance between the charge transfer interactions, promoting (highly ordered) columnar mesophases and steric effects suppressing the formation of columnar order. These results strongly support the observations in literature where spacer lengths and not the acceptor strengths were varied.[4a,5]

Using only a limited number of non-liquid crystalline materials, we have been able to prepare a series of CT complexes with a wide range of mesophases and transition temperatures. This clearly demonstrates the versatility of non-covalent interactions, such as charge transfer complexing and steric packing effects. The liquid crystalline diversity expands even further when macromolecular species are applied.

References and notes

(1) (a) Ringsdorf, H.; Wüstefeld, R.; Zerta, E.; Ebert, M.; Wendorff, J.H. *Angew. Chem. Int. ed. Engl.* **1989**, *28*, 914-918. (b) Bengs, H.; Ebert, M.; Karthaus, O.; Kohne, B.; Praefcke, K.; Ringsdorf, H.; Wendorff, J.H.; Wüstefeld, R. *Adv. Mater.* **1990**, *2*, 141-144.

(2) (a) Ebert, M. PhD Thesis: Technische Hochschule Darmstadt, Darmstadt, Germany, 1990; p 54. (b) Wüstefeld, R. PhD Thesis, Johannes Gutenberg Universität, Mainz, Germany, 1990.

(3) Praefcke, K.; Singer, D.; Kohne, B.; Ebert, M.; Liebmann, A.; Wendorff, J.H. *Liq. Cryst.* **1991**, *10*, 147-159.

(4) (a) Praefcke, K.; Singer, D.; Langner, M.; Kohne, B.; Ebert, M.; Liebmann, A.; Wendorff, J.H. *Mol. Cryst. Liq. Cryst.* **1992**, *215*, 121-126. (b) These donors are similar to **D1**, but with various substituents anchored at the central phenyl ring, including CH_3, CF_3, CN and OC_nH_{2n+1}.

(5) Praefcke, K.; Singer, D.; Eckert, A. *Liq. Cryst.* **1994**, *16*, 53.

(6) The syntheses of **18** and **19** were performed analogously to the synthesis of **D1**. In the first step pentabromophenol was etherified with 6-chlorohexanol or 2-bromoethanol in a 68 and 60% yield, respectively. The second step was the coupling reaction with phenylacetylene, that produced the products after the usual work-up in a 48 and 31% yield, respectively.

(7) The syntheses of **20** and **21** were performed analogously to the synthesis of **D1A1**, i.e. coupling of equimolar amounts of **A1-CO_2H** with **18** and **19** respectively, using DCC as a coupling agent and DMAP as a catalyst. The materials were purified, using column chromatography and only the very pure samples were used for analysis, which resulted in low yields of 18 and 9% respectively.

(8) (a) Praefcke, K.; Holbrey, J.D. *J. Inclusion Phenom.* **1996**, *24*, 19-41. (b) Ringsdorf, H.; Wüstefeld, R. *Phil. Trans. R. Soc. Lond.* **1990**, *A 330*, 95-108.

(9) Kouwer, P.H.J.; Jager, W.F.; Mijs, W.J.; Picken, S.J. *Macromolecules* **2001**, *34*, 7582-7584.

(10) The characteristics of the recently discovered N_L phase are comprehensively discussed in Chapter 5.3.3. The reader is referred to this chapter for more information.

(11) A mixture of two polymers is hard to make due to immediate precipitation of the polymers when the two solutions are poured together. After removal of the solvent, the precipitate was annealed for several hours prior to the DSC measurement to allow optimal mixing of the two polymer materials.

(12) This classification is found to be general for the class of mesogens and CT complexes described in this thesis. It is discussed in the final chapter: General considerations.

(13) Janietz, D.; Hofmann, D.; Reiche, J. *Thin Solid Films* **1994**, *244*, 794-798.

(14) It is stressed that at high backbone confinement the α-process separates in a faster backbone relaxation and other relaxations that involve the mesogen. Since the first are real backbone relaxations, they are observed by DRS, resulting in a low-temperature T_g. The related mesogenic relaxations show a much larger step in the heat capacity and they are therefore observed in the DSC experiments

(15) (a) Janietz, D. *Chem. Commun.* **1996**, 713-714. (b) The reported phase behavior for the asymmetric donor acceptor dimer, based on pentakis(phenylethynylbenzene and TNF (shown in Figure 4.9) is G_M 60 M ~125 N_{Col} 134 I (where M is an unknown mesophase).

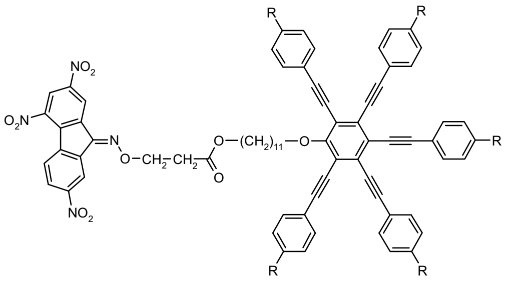

Figure 4.9. Intramolecular CT complex, investigated by Janietz (R = H).

(16) (a) From theory of dimers, a clearing temperature higher than for the complex D1:A1 was expected. On the other hand, the comparison between **D1**:**A1** and **D1A1** is not entirely valid, since the non-linked complex has hydroxyl groups at the terminal end of the spacer, which in principle are able to stabilize the mesophase. (b) For more information on dimers, read: Imrie, C.T.; Luckhurst, G.R. In *Handbook of Liquid Crystals*; Demus, D., Goodby, J.W., Gray, G.W., Spiess, H.W., Vill, V., Eds.; Wiley VCH: New York, 1998; Vol. 2B, pp. 801-833.

5 Methoxy substituted mesogens: Properties of the materials and charge transfer complexes

Parts of this chapter have been or will be published in: (a) Kouwer, P.H.J.; Jager, W.F.; Mijs, W.J.; Picken, S.J. *Macromolecules* **2001**, *34*, 7582-7584. (b) Kouwer, P.H.J.; Jager, W.F.; Mijs, W.J.; Picken, S.J. *Macromolecules, in press*. (c) Kouwer, P.H.J.; Jager, W.F.; van den Berg, O.; Mijs, W.J.; Picken, S.J., *Polym. Mater. Sci. Eng.* **2001**, *85*, 303-304.

Abstract

We have investigated a new discotic nematogen **D5**, bearing one hydroxyl-functionalized tail and five methoxy substituents. The corresponding side chain polyacrylates **P(D5)** exhibited N_D phases from 50°C until degradation above 200°C. Addition of equimolar amounts of various trinitrofluorenone based acceptors to the mesogen resulted in the formation of charge transfer complexes with a variety of liquid crystalline properties. Depending on the acceptors, different columnar and nematic phases are induced, including the recently discovered nematic lateral phase. The liquid crystalline properties were investigated with differential scanning calorimetry (DSC), optical polarizing microscopy (OPM) and extensive X-ray diffraction. In some cases, the XRD results showed discrepancies with the results obtained by OPM and DSC. These discrepancies can be explained, taking into account that XRD mainly probes the regularity of the local molecular arrangement.

5.1 Introduction

The thermal properties of charge transfer (CT) complexes are strongly dependent on the interaction strength between the donor and the acceptor involved. In the previous chapter, these effects were investigated by the application of acceptors with variable electron affinities to the same donor **D1**. Some complexes of **D2** with various acceptors have been studied as well.[1] Addition of an acceptor to **D2Prop** or **P(D2a)** resulted in the formation of CT complexes, which in all cases showed nematic mesophases with a decrease in clearing temperatures, compared to the pure **D2** derivatives. This indicates that for **D2** (derivatives), CT complexing rather destabilizes the mesophase, in contrast to what was observed in Chapter 4.

Therefore, we decided to improve the CT interaction, not by changing the acceptor, but by preparing a more electron rich donor, i.e. **D5**. From complexation studies of dilute solutions ($CH_2ClCHCl_2$) at various temperatures, the complexation constant K_C and the complexation enthalpy ΔH_C were determined,[2] using the Hildebrand equation[3a-c] (5.2) and an Arrhenius equation[3d] (5.3), respectively:

$$\mathrm{D} + \mathrm{A} \xrightleftharpoons{K_C} \mathrm{DA} \qquad K_C = \frac{[\mathrm{DA}]}{[\mathrm{D}][\mathrm{A}]} \tag{5.1}$$

$$\frac{[\mathrm{A}]_0}{D} = \frac{1}{K_{\mathrm{C}}[\mathrm{D}]_0 \varepsilon_{\mathrm{DA}}^{\mathrm{opt}}} + \frac{1}{\varepsilon_{\mathrm{DA}}^{\mathrm{opt}}} \tag{5.2}$$

$$K_{\mathrm{C}} = K_{\mathrm{C},0} \exp\left(-\frac{\Delta H_C}{RT} \right) \tag{5.3}$$

As expected both the complexation constant (at 30°C) and the complexation enthalpy of **D5**:**A2** showed an increase with respect to the **D2**:**A2** complex ($K_{\mathrm{C},\mathbf{D5:A2}} = 12.6$ l·mol^{-1}, $K_{\mathrm{C},\mathbf{D2:A2}} = 9.9$ l·mol^{-1}; $\Delta H_{\mathrm{C},\mathbf{D5:A2}} = -13.7$ kJ·mol^{-1}, $\Delta H_{\mathrm{C},\mathbf{D2:A2}} = -11.2$ kJ·mol^{-1}).[2] It should be noticed that these values are obtained from experiments in dilute (1,1,2-trichloroethane) solutions and that they may not be exact for concentrated systems. However, these experiments give a clear indication of an increased interaction in complexes of **D5**.

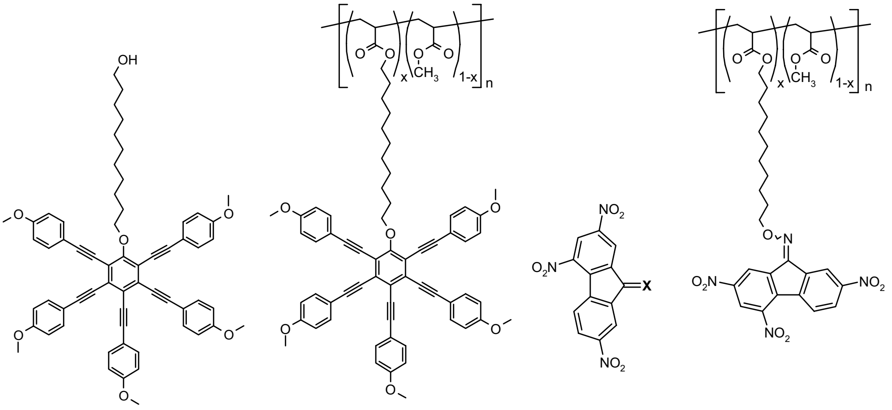

A1 X: =NO(CH$_2$)$_{11}$OH

P(D5a) x = 0.64 **(A1)$_2$** X: [=NO(CH$_2$)$_{11}$O]$_2$CO

P(D5b) x = 0.71 **A2** X: =O

D5 **P(D5c)** x = 0.83 **A3** X: =C(CN)$_2$ **P(A1a)** x = 0.77

Figure 5.1. Investigated materials. The synthesis of the materials is discussed in Chapter 2.

In this chapter, we discuss the liquid crystalline properties of the novel discotic mesogen **D5** and the corresponding polyacrylates **P(D5)**, see Figure 5.1. The properties of the polymers are compared to those of the low molar mass compound **D5**. The effect of CT complexation was studied by the preparation of a series of CT complexes of **D5** with the non-liquid crystalline acceptors **A1**-**A3**, **(A1)$_2$** and **P(A1a)**. The liquid crystalline behavior of the supramolecular CT complexes is investigated by OPM, DSC and XRD. It is clearly demonstrated that the use of CT interactions offers a simple as well as versatile approach to obtain a broad variety of liquid crystalline phases, using only a limited number of compounds.

5.2 Liquid crystalline properties of the pure mesogens

The thermal behavior of the pure compounds was determined by OPM and DSC. The results are summarized in Table 5.1.

Table 5.1. Thermal behavior of D5 and **P(D5)** obtained by DSC and OPM.

Material	**Transition temperatures in [°C] and (latent heat in [kJ mol^{-1}])**				
D5	K	132 (37)	N_D	246 (0.2)	I/d
P(D5a)	G_N	41	N_D	> 200	d
P(D5b)	G_N	50	N_D	> 200	d
P(D5c)	G_N	45	N_D	> 200	d

Despite the absence of multiple long tails, **D5** showed a N_D mesophase over a broad temperature range. Mesogens with the pentakis(phenylethynyl)benzene cores are known to display liquid crystalline behavior in the absence of multiple long tails, that are usually required for discotic liquid crystals. The mesogen with the methyl substituted core, that we investigated thoroughly before,[4,5] is another example of such behavior. The corresponding side chain polymers **P(D5)** did not crystallize, but their mesophases froze in below the glass transition temperature. The observed T_g's are close to each other, suggesting a rather independent behavior towards the degree of substitution; where we should bear in mind that only three polymers have been investigated. This resulted in materials with nematic discotic mesophases over a temperature range of more than 160°C, which is unusually wide.[6] The acceptors did not show any liquid crystalline behavior: **A1-A3** and **(A1)$_2$** are crystalline solids, melting at 98-109, 176, 276 and 71-88°C, respectively,[7] and **P(A1a)** is an amorphous polymer with a glass transition temperature of 50°C.[8]

5.3 Liquid crystalline properties of the charge transfer complexes

Charge transfer complexes. Charge transfer (CT) complexes were prepared by dissolving the appropriate amounts of donor and acceptor in a common solvent (CH_2Cl_2 or $CHCl_3$) and subsequent evaporation. Unfortunately, the thermal results of CT complexes with **P(D5)** were hard to interpret, due to the weak phase transitions and the slowly developing optical textures. For example, the complex **P(D5a)**:**A1** was similar in phase behavior to the opposite complex **D5**:**P(A1a)**, but the phase transitions in **D5**:**P(D1a)** were much sharper and larger. This is in contrast to what was observed in the previous chapter, where the mesophase behavior of **P(D1)**:**A1** was nearly identical to the behavior of **D1**:**P(A1a)**.

5.3.1 OPM and DSC

OPM studies of donor-acceptor contact samples, combined with DSC of CT complexes at various molar ratios, were used to investigate the phase behavior of the complexes as a function of acceptor concentration. It appeared that at exact equimolar concentrations the best properties were found, i.e. the highest clearing temperature and no biphasic temperature trajectories. This indicates that a stable complex is formed at such concentrations, that effectively induce a single liquid crystalline CT species, similar to what was reported before in other CT complexes,[8,9] including the complexes in Chapter 4.

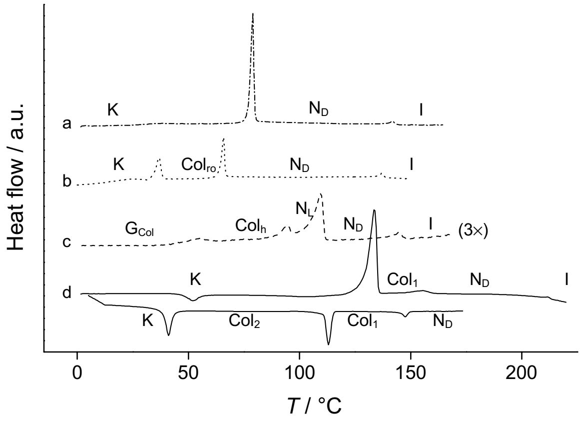

Figure 5.2. DSC thermograms of (a) **D5**:**A1** (–   ); (b) **D5**:**(A2)$_2$** (·   ); (c) **D5**:**P(A1)** (– – –) and (d) **D5**:**A2** (—   ).

Combining the acceptors with **D5** induced several liquid crystalline phases, see Table 5.2. Interaction with acceptor **A1** reduced the melting point of **D5**, but even more the clearing temperature, which narrowed the temperature window of the mesophase substantially (Figure 5.2a). This is indicative of a strong destabilization of the nematic mesophase. The analogous complex with the dimeric acceptor **D5**: **(A1)$_2$** showed a N_D phase at temperatures, comparable to those of the monomeric species, as well as an additional columnar phase, prior to crystallization at low temperatures (Figure 5.2b).

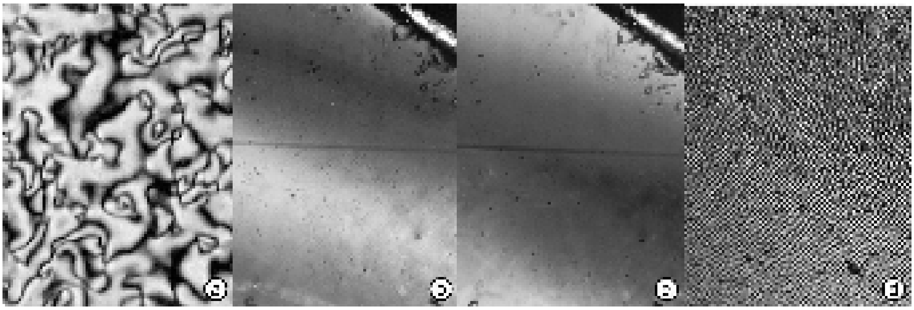

Figure 5.3. Optical textures of **D5**:**P(A1a)**: (a) *schlieren* texture of N_L phase at 100°C; (b) uniform planar aligned texture of N_L phase at 100°C; (c) uniform planar aligned texture of N_D phase at 130°C; (d) fingerprint texture the N_D* phase at 130°C of **D5**:**P(A1a)** doped with 3%-wt chiral dopant. Pictures b and c were taken at the same spot. All pictures taken with crossed polarizers, maginifcation 110× (a), 52× (b-d).

The complex of **D5** with the corresponding **P(A1a)** showed a similar behavior at high temperatures, i.e. a nematic phase and a reduced clearing temperature. At lower temperatures crystallization was suppressed, and a number of mesophases were observed instead, clearly shown by the DSC thermogram (Figure 5.2c). Cooling from the isotropic phase, first the N_D phase was observed. The optical texture (Figure 5.3) did not change at the transition to the new N_L phase.[8a] After further cooling a transition to a columnar hexagonal phase was found, which could be identified by its optical texture after extensive annealing at 80°C.

The role of acceptor strength was investigated by complexing **D5** with acceptors of increasing electron affinities. The acceptor strength sequence is **A1** ≈ **(A1)$_2$** ≈ **P(A1)** < **A2** < **A3**. Compared with **D5**:**A1**, discussed above, the N_D phase of **D5**:**A2** occurred at higher temperatures. The heating curve of the thermogram (Figure 5.2d) showed a columnar phase (Col_1) between the crystalline and the nematic discotic phase. Due to supercooling of the crystalline phase, a second columnar phase (Col_2) was revealed in the cooling run. Both phases were easily recognized as columnar phases by their characteristic optical textures, shown in Figure 5.4. The Col_2 phase is meta-stable, since annealing at 100°C for several hours did not cause crystallization.

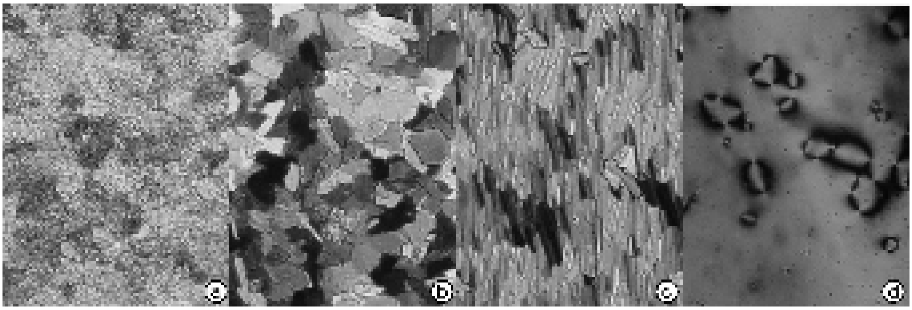

Figure 5.4. Optical textures of **D5**:**A2**: (a) Crystalline phase at 25°C; (b) Col_2 phase at 100°C; (c) Col_1 phase at 130°C; (d) N_D phase at 160°C. All pictures were with crossed polarizers, magnification 140×.

In the complex with the stronger acceptor **D5**:**A3**, the nematic discotic phase was entirely replaced by a columnar mesophase, even at high temperatures. Upon cooling from the isotropic phase, a transition into a columnar phase was observed, showing a highly viscous texture that developed very slowly. At lower temperatures a second order transition was found, where the liquid crystalline phase was frozen in. This is similar to what was observed in derivatives of triphenlenes[10] and CT complexes of substituted triphenylenes with **A2**.[11] In these studies, the second order transition was attributed to a transition into a columnar plastic phase, that is characterized by a three-dimensional positional order of the molecules, while the molecules keep their rotational mobility, analogous to the soft crystal B phase in rod-shaped liquid crystals. The thermal results of the CT complexes of **D5** are summarized in Table 5.2.

Table 5.2. Thermal behavior of charge transfer complexes of **D5** obtained by DSC and OPM with various acceptors. [a] Monotropic phase transition. [b] Col_p: Plastic columnar phase.

Complex D5 with	**Thermal behavior: transition temperatures [°C] and (latent heat) [kJ·mol^{-1}]**									
A1	K	80 (11)						N_D	146 (0.3)	I
$(A1)_2$	G	10	K		37 (3.2)	Col_{ro}	66 (4.0)	N_D	137 (0.5)	I
P(A1a)	G_{Col}	45	Col_h		94 (1.3)	N_L	110 (5.0)	N_D	146 (0.3)	I
A2	K	[41 (6.2)	Col_2	110 (5.0)][a]	134 (43)	Col_1	150 (1.2)	N_D	216 (0.6)	I
A3	Col_p[b]	18	Col_{ro}		148 (4.7)	Col_{hd}			220-230	I/d

5.3.2 Powder X-ray reflection measurements

Temperature dependent X-ray diffraction (XRD) measurements were performed on **D5** and its corresponding side chain polymers as well as on the charge transfer complexes with **D5**. The spacings *d* were calculated, using the Bragg Law: $2d\sin(\theta) = n\lambda$, and the correlation length ξ, using the Scherrer equation: $\xi\phi_{\frac{1}{2}}\cos(\theta_0) = 0.89\lambda$. For details on XRD analysis, the reader is referred to Appendix A of Chapter 3.

Powder XRD patterns of the nematic phases of **D5** and polymers **P(D5)** were nearly identical. They all showed very diffuse reflections and the samples hardly aligned in the ~1.5 T magnetic field in the sample holder. The low order of the N_D phase is clearly demonstrated by the low correlation lengths in the both lateral [$hk0$] and the columnar [$00l$] direction,[12] as shown in Table 3. These correlation lengths were among the lowest that we have measured in our laboratories, compared to X-ray data of N_D phases of other disk-shaped mesogens. Upon heating **D5** slightly above the clearing temperature, the correlation lengths hardly changed. Polymers **P(D5a-c)** show a very broad nematic phase. XRD measurements were performed from 30 to 190 °C to study the temperature dependence of the molecular spacings *d* and correlation lengths ξ in the nematic discotic phase. With increasing temperature, an expected slight increase in the lateral and ‘columnar’ spacings was observed, combined with a small decrease in the corresponding correlation lengths. Unfortunately, the diffuse reflections (low order) were hard to fit, and no quantitative data could be obtained. Furthermore, no differences between the polymers with an increasing degree of substitution could be observed.

Table 5.3. Spacings d_{hkl} and correlation lengths ξ_{hkl} of **D5** based mesogens obtained from XRD experiments.

Discotic mesogen	***T* [°C]**	**Phase**	**lateral direction**		**‘columnar’ direction**	
			d_{100} [Å]	**ξ_{100} [Å]**	**d_{001} [Å]**	**ξ_{001} [Å]**
D5	160	N_D	15.2	22	4.02	11
P(D5b)	50	N_D	15.0	29	4.12	13
P(D5b)	150	N_D	15.2	23	4.25	13
P(D5c)	50	N_D	14.5	23	4.09	9
P(D5c)	150	N_D	14.8	22	4.19	8

Due to the CT interactions in the N_D phase of **D5**:**A1**, the correlation lengths increased slightly, especially in the columnar [001] direction. However, the mesophase was still characterized as N_D. Both the analogous dimer complex **D5**:**(A1)$_2$** and macromolecular complex **D5**:**P(A1)** showed comparable XRD patterns of the N_D phase. At lower temperatures, **D5**:**(A1)$_2$** underwent a transition to a columnar rectangular (Col_{ro}) phase, which was characterized by only two reflections, attributed to the d_{200} and d_{010} spacings. By estimating the volume of a unit cell (using $\rho = 1.05 \cdot 10^3$ kg·m^{-3}) from the molecular mass of the complex, we were able to calculate approximate values of the lattice parameters a, b and the angle α,[13] as presented in Figure 5.5.

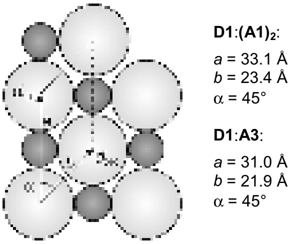

Figure 5.5. Rectangular organization of **D5**:**(A1)$_2$** and **D5**:**A3** and calculated lattice parameters.

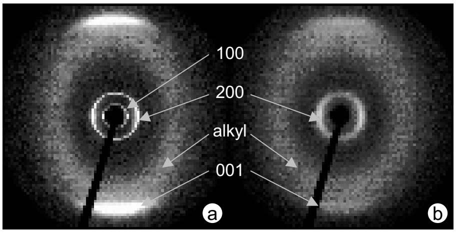

Figure 5.6. XRD patterns of **D5**:**P(A1a)** at (a) 100°C (N_L phase) and (b) 130°C (N_D phase)

Upon cooling **D1**:**P(A1)** from the N_D phase (Figure 5.6b) into the N_L phase (Figure 5.6a), the complex aligned in the 1.5 T magnetic field. In addition, both the [200] and the [001] reflections sharpened considerably and an additional reflection, attributed to the [100] reflection, was observed at small angles.[8a] The difference in order between the two nematic phases is most clearly shown in the radially integrated scans, see Figure 5.7a. By cooling the sample into the columnar phase, further increases of the correlation lengths in both the columnar and lateral direction were observed, see Figure 5.7b.

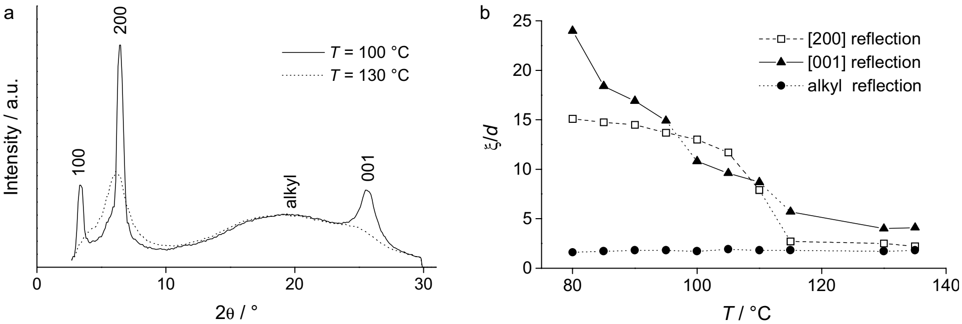

Figure 5.7. XRD results of **D5**:**P(A1a)**: (a) Radially integrated pattern at 100°C (N_L phase, dotted) and 130°C (N_D phase, solid). (b) Temperature dependence of the correlation length of the (200) reflection (intercolumnar direction, broken), (001) reflection (intracolumnar direction, solid) and the alkyl reflections (dotted).

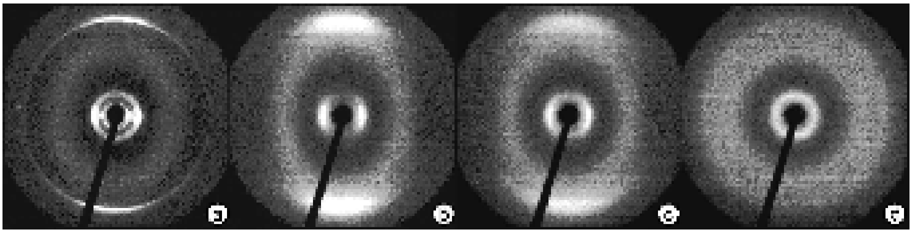

Figure 5.8. XRD patterns of CT complex **D5**:**A2** at (a) 40 °C (K phase); (b) 105 °C (Col_2 phase, obtained from cooling the Col_1 phase); 130 °C (Col_1 phase) and (d) 160 °C (N_D phase). Maximum diffraction angle: $2\theta = 30°$.

Charge transfer complexes of **D5**:**A2** display a very interesting set of XRD results, see Figures 5.8 and 5.9. At high temperatures, **D5**:**A2** showed the diffuse diffraction pattern of a N_D phase (Figure 5.8d). Upon cooling into the columnar phase, the diffraction pattern remained effectively unaltered (Figure 5.8c). Apart from some alignment in the 1.5 T magnetic field, only a slight sharpening of the [001] reflection was observed, best seen in the integrated pattern in Figure 5.9. The intercolumnar reflection (d_{200}) is identical to the reflection observed for the N_D phase at 160°C. Before the sample crystallized at low temperatures (the crystalline pattern with many sharp reflections in the small angle region, is shown in Figure 5.8a), a second (monotropic) mesophase appeared. Peculiarly, again, the XRD pattern (Figure 5.8b) remained very diffuse. In the intercolumnar direction, the radially integrated pattern is still identical to that of the first columnar phase and the N_D phase. In the intracolumnar direction, a slight increase in order is observed with respect to the first columnar phase.

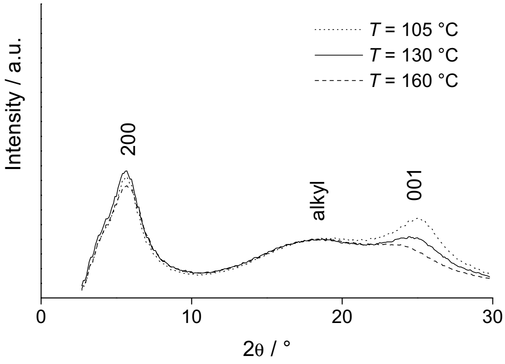

Figure 5.9. Radially integrated diffraction pattern of **D1**:**A2** at 105 °C (Col_{ho} phase, dotted line); 130 °C (Col_{hd} phase, solid line) and 160 °C (N_D phase, dashed line).

XRD experiments on the complex **D5**:**A3** showed the anticipated behavior. The characteristic patterns of well-ordered columnar phases were observed. The Col_{hd} phase shows only one sharp intercolumnar reflection. In the Col_{ro} phase a second reflection in the small angle region appeared that defines the rectangular lattice. At the transition from the Col_{ro} phase to the Col_{hd} phase, the correlation length in the lateral direction (ξ_{200}) remains constant. The correlation length in the columnar direction (ξ_{001}) decreases suddenly, indicating a strong loss of order within the columns. The results of the XRD experiments are summarized in Table 5.4.

Table 5.4. Spacings d_{hkl} and correlation lengths ξ_{hkl} obtained from XRD experiments. The lattice parameters of the hexagonal columnar phases can be calculated from the intercolumnar spacing: $a = b = 4d_{200}/\sqrt{3}$ and $\alpha = 60°$. [a] Rectangular phase with lattice parameters $a = 33.1$, $b = 23.4$, $\alpha = 45°$. [b] Rectangular phase with lattice parameters $a = 31.0$, $b = 21.9$, $\alpha = 45°$. For the rectangular phases, see Figure 5.5.

CT complex	***T*** **[°C]**	**Phase**	**Lateral direction**				**Columnar direction**	
			d_{200} **[Å]**	ξ_{200} **[Å]**	d_{010} **[Å]**	ξ_{010} **[Å]**	d_{001} **Å]**	ξ_{001} **[Å]**
D5:A1	130	$\mathrm{N_D}$	15.5	25	–	–	3.6	19
D5:(A1)$_2$	50	$\mathrm{Col_{ro}}^{a}$	16.2	126	11.8	74	3.6	80
	100	$\mathrm{N_D}$	16.3	41	–	–	3.8	13
D5:P(A1a)	80	$\mathrm{Col_{ho}}$	13.6	206	–	–	3.5	87
	100	$\mathrm{N_L}$	13.7	148	–	–	3.6	43
	130	$\mathrm{N_D}$	14.3	36	–	–	3.7	16
D5:A2	105	$\mathrm{Col_2}$	15.7	35	–	–	3.5	16
	130	$\mathrm{Col_1}$	15.6	31	–	–	3.6	12
	160	$\mathrm{N_D}$	15.5	28	–	–	3.7	11
D5:A3	130	$\mathrm{Col_{ro}}^{b}$	15.3	21	11.1	15	3.6	68
	160	$\mathrm{Col_{hd}}$	14.2	21	–	–	3.6	32

5.3.3 Discussion on the observed mesophases

Complex D5 with P(A1a): The $\mathrm{N_L}$ phase. Combining our experimental data (DSC, OPM and XRD) we can conclude the following: Even after extensive annealing, the $\mathrm{N_L}$ phase shows all the required features to unambiguously identify it as a nematic phase, i.e. *schlieren* of ±½ and ±1 disclinations,[14a] occasional disclination lines, a smooth appearance and due to a low viscosity spontaneous flow and fast texture coarsening.[14b] Even after deformation, the *schlieren* texture returned rapidly. However, to our surprise, we found a large latent heat values at the transition, i.e. 5 $\mathrm{J{\cdot}g^{-1}}$) in combination with a strong sharpening of both the [200] and the [001] reflections in the XRD diagrams. The latter is a strong indication for a locally highly ordered material. Seemingly, this is in contrast with the lack of positional order of the nematic phase. However, we proposed that in the $\mathrm{N_L}$ phase, the disc-shaped molecules assemble in disc-shaped superstructures. It is these supramolecular assemblies that exhibit a nematic arrangement. The transition from the $\mathrm{N_L}$ phase to the $\mathrm{N_D}$ phase coincides with a break-up of the nematic ordered aggregates, with conservation of the nematic order. This is analogous to the well-established $\mathrm{N_{Col}}$ phase that forms a nematic phase from uniaxial assemblies[15] including the occurrence of $\mathrm{N_{Col}}$ to $\mathrm{N_D}$ transitions in some materials, see Chapter 3. X-ray diffraction is a very useful technique to differentiate between the various nematic phases, since microscopy experiments will yield the same optical textures.

Upon cooling, a transition into another mesophase was observed, assigned to a Col_h phase. It is stressed that it is difficult to make an unambiguous statement of the type of columnar mesophase, because XRD measurements only show two reflections and the OPM experiments showed a highly viscous texture that developed very slowly. To confirm the Col_h phase, XRD patterns must be recorded parallel to the columns of a macroscopically aligned sample. However, as yet we have not succeeded in preparing such samples.

Complex D5 with A2: The disordered columnar phases. At high temperatures, the complex **D5**:**A2** shows a N_D phase, that is easily identified by its diffuse diffraction pattern and confirmed by the clear *schlieren* texture, observed in OPM experiments. Upon cooling from the N_D phase, a transition into an intermediately viscous mesophase is observed. This mesophase shows the typical features of a columnar phase, i.e. the characteristic optical texture (Figure 5.4c) and a 1.2 $kJ \cdot mol^{-1}$ latent heat upon formation of the phase. However, XRD experiments yielded different results (Figure 5.8c). The radially integrated pattern (Figure 5.9) is still very diffuse. Remarkably, the intercolumnar reflection (d_{200}), that is usually well developed in a columnar phase, is identical to the reflection observed for the N_D phase at 160°C. The [001] reflection shows only a minor increase of the intracolumnar order. These results strongly oppose any suggestion of long-range positional order in the mesophase while that is indicated beyond any doubt by the optical texture. Note that the low correlation lengths are in marked contrast to those of CT complexes reported in the literature, where columnar phases with correlation lengths as high as 200 Å have been reported.[16] An imaginable phase assignment[17a] could be a Col_{hd} phase: hexagonal since only one reflection is observed in the small angle area and disordered because of the profound low order in the intracolumnar direction.

The monotropic columnar phase at lower temperatures shows a similar behavior. The mosaic-like optical texture is characteristic of a columnar phase. Moreover, an increased viscosity was observed, compared to the columnar phase at higher temperatures. In contrast, the XRD diffractogram only shows diffuse reflections. With respect to the enantiotropic columnar phase, the intracolumnar reflection slightly increased again, indicating better-defined intracolumnar packing. However, the intercolumnar reflection remained identical to those of the nematic and the other columnar phases (see Figure 5.8).

In this case, the interpretation of the XRD results is even harder. The unchanged reflection in the small angle region indicates preservation of a hexagonal arrangement.[17b] By taking the small sharpening of the intracolumnar reflection into account, the assignment leads to a Col_{ho} phase for the second columnar phase. However, the assignment to a Col_{ho} and the subsequent transition to a Col_{hd} phase is in contradiction with the Landau-Peierls instability criterion, that predicts that one-dimensional true long-range order, and hence, a transition from the Col_{hd} to the Col_{ho} phase is prohibited.[18]

We can make an alternative interpretation of our experimental results by imagining a columnar phase without two-dimensional positional order, that we call an 'amorphous columnar phase (Col_A).' The textures, shown by the optical microcopy experiments originate from the characteristic deformations that are allowed for a specific phase. For columnar phases splay and twist deformations are not allowed giving rise to the characteristic “columnar” textures, this of course is similar to the explanation of focal conic textures of the SmA phase where twist and bend is forbidden (see book of De Gennes & Prost). The absence of two-dimensional intercolumnar order would result in only an average column distance in the XRD patterns, like observed in the $\mathrm{Col_l}$ and the $\mathrm{Col_2}$ phase. Obviously, no higher order reflections are expected. By considering the small difference in the intracolumnar order, the phases can be interpreted as $\mathrm{Col_{Ad}}$ (disordered) and $\mathrm{Col_{Ao}}$ (ordered), respectively. We have to stress that a transition between the $\mathrm{Col_{Ad}}$ and $\mathrm{Col_{Ao}}$ phase is formally still forbidden by the Landau-Peierls instability criterion. Moreover, we would have expected a higher intracolumnar order for $\mathrm{Col_A}$ phases, because short-column $\mathrm{Col_A}$ phases would essentially be the same as $\mathrm{N_{Col}}$ phases and therefore should exhibit characteristic nematic textures.

5.3.4 Additional studies of the nematic-nematic phase transition in D5:P(A1a)

Because this is one of the few examples of a nematic-nematic phase transition in thermotropic materials, we decided to investigate the nature of the transition by additional techniques.

Birefringence studies. The relative optical retardation ($\Delta\Gamma/\Gamma$) was measured in a polarizing microscope using a variable compensator. The optical retardation is linearly related to the bi-refringence: $\Gamma \propto d\Delta n$, where d is the (constant) sample thickness. The results were plotted and fitted to an extended Maier-Saupe curve,[19] showing the temperature dependence of the order parameter $\langle P_2\rangle$, using equations 5.4.

$$\Gamma \propto c_1\langle P_2\rangle \tag{5.4a}$$

$$\langle P_2\rangle = 0.1 + 0.9\left\{1 - 0.99\left(\frac{T}{T_\mathrm{N}}\right)^{c_2}\right\}^{\frac{1}{4}} \tag{5.4b}$$

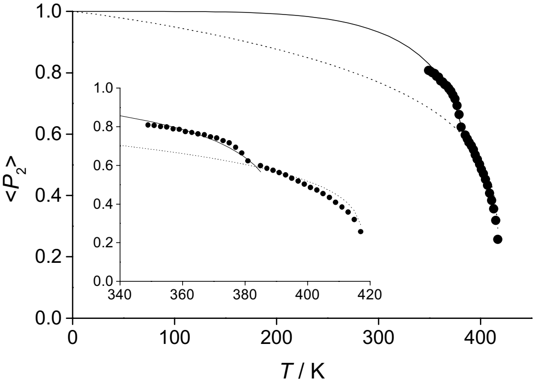

Figure 5.10. Temperature dependence of the order parameter: (•) experimental data; (—) fit of the $\mathrm{N_L}$ phase using equation (5.2) and (·····) fit of the $\mathrm{N_D}$ phase using equation (5.2). The inset shows a magnification.

Nematic phases can be described satisfactory with an (extended) Maier-Saupe curve. Therefore, equation 5.4 could be used to fit both the N_L phase and the N_D phase. The fitting parameter T_N represents the transition temperature of the N_L to N_D transition or the N_D to I transition, respectively.[20a] Constants c_1 and c_2 are fitting parameters as well. Note that c_1 is used to fix the y-axis at $\langle P_2 \rangle = 1$ for $T = 0$ K, which is required by the definition of $\langle P_2 \rangle$. Constant c_2 equals 1 for the common Maier-Saupe model, but larger values have been found for polymer materials (here, in the N_D phase $c_2 = 1$ and in the N_L phase: $c_2 = 2$).[20b] The thermal dependence of the order parameter $\langle P_2 \rangle$ is shown in Figure 5.10.

The model fits the experimental data rather well. At the nematic-nematic phase transition, a strong inflection point is observed. However, for a first order phase transition, a discontinuity of the order parameter at the phase transition is expected, which was not found.

Pitch measurements. By addition of small amount of a chiral mesogen to a nematogen, cholesteric phases (N_D*) can be induced without changing the phase behavior considerably. From the characteristic fingerprint texture, the pitch of the phase can be determined.

To complex **D5**:**P(A1a)** was added 3%-wt D-β-Cellobiose octadodecanoate,[21] a chiral dopant. OPM experiments revealed a clear fingerprint texture, shown in Figure 5.3d. To investigate the nematic-nematic phase transition any further, the pitch was measured as a function of temperature, expecting to find a discontinuity in the temperature dependence of the pitch length at the N_D to N_L phase transition, similar to what was observed for the birefringence analysis. However, the differences in the temperature range of the N_L and the N_D phase were too small to draw any useful conclusions. The pitch length at $T = 130$°C was determined: $p =$ 520 nm. The helical twisting power β is defined by $\beta = 10^{-4} p \cdot c \cdot r$, where c is the dopant concentration [%-wt] and r is the enantiomeric purity. For the complex **D5**:**P(A1a)** doped with D-β-Cellobiose octadodecanoate a helical twisting power of 15 nm was calculated.

5.4 Conclusions

We have prepared a series of CT complexes of the nematogenic donor **D5** and the non-liquid crystalline acceptors **A1**-**A3** (low molar mass), **(A1)$_2$** (dimer) and **P(A1a)** (polymer). A wide range of mesophases were observed for the CT complexes, from a destabilized N_D phase for the **D5**:**A1** complex to a well-ordered Col_{ho} phase of the **D5**:**A3** complex. Application of the same acceptor moiety in the form of a 'monomer', dimer or polymer has a large impact on the phase behavior. All three CT complexes show a N_D phase at high temperatures, however, where **D5**:**A1** crystallizes **D5**:**(A1)$_2$** and **D**:**P(A1a)** showed transitions to higher ordered columnar phases. In addition, the macromolecular complex showed the recently identified N_L phase. A remarkable behavior was observed for complex **D5**:**A2** that clearly showed two columnar phases during OPM experiments, whereas XRD experiments showed only diffuse reflections.

It is established that X-ray diffraction is a very useful tool to investigate the order in liquid crystalline phases. However, one has to be conscious of the fact that X-rays mainly probes the *local* environment of an average mesogen or supramolecular assembly of mesogens. From the results based on XRD experiments, conclusion can only be drawn, on length scales that are of the same order of the measured spacings. Commonly, this is the case and XRD provides an excellent tool to establish the order in mesophases. However, for more complex systems, like presented in this contribution, misinterpretations can be easily made. For example, the N_L phase of **D5**:**P(A1)** has a XRD pattern of a common columnar phase, but shows all the other features of a nematic phase. The other way around, the Col_1 and Col_2 phase of complex **D5**:**A2** in show a XRD pattern, typical for a nematic phase, but both show the optical characteristics of a columnar phase. The latter result seems to imply that it is possible to have columnar phases where the packing of the columns remains rather disordered. These materials could therefore, be considered as possible 'amorphous columnar phases (Col_A phases),' which can be subdivided into Col_{Ao} and Col_{Ad} phases, dependent on the intracolumnar order. In conclusion, it clearly will be difficult to distinguish the Col_A phase from the well-established N_{Col} phase, except by optical microscopy experiments and investigations of the local dynamics, e.g. by dielectric relaxation spectroscopy.

References and notes

(1) The thermal results of CT complex of **D2Prop** and **P(D2a)** with acceptors **A1**-**A3** and the corresponding intramolecular CT complexes are shown in the Table 5.5. Note that for most materials, no XRD measurements were performed and therefore the kind of nematic mesophase could not be specified.

Table 5.5. Thermal results of the equimolar CT complexes of **D2Prop** and **P(D2a)**. [a] Intramolecular CT complexes **D2A1** (low molar mass complex, left column) and **P(D2A1)** (macromolecular complex, right).

Complex	**D2Prop**	**P(D2a)**
A1	macroscopic phase separation	macroscopic phase separation
A2	K 106 (11) N_X 186 (0.8) I	G_N 78 N_{Col} 180 (5) N_D 215 (0.1) I
A3	K 148 (11) N_X 226 (0.5) I/d	G_N 94 N_X 222 I/d
Intramol. CT[a]	K 82 (9) N_X 129 (0.7) I	G_N 94 N_L 134 (5) N_D 155 (0.4) I

(2) Franse, M.W.C.P., *Unpublished results.*

(3) (a) Equation (5.1b) is valid in the wavelength region, where only the DA complex is absorbing. In eq. 5.2, D is the optical absorption density (= $\log(I_0/I)$) at this wavelength. Any component contributes to D by the Lambert-Beer's Law: $D = \sum D_i = \sum(l\varepsilon_i^{opt}C_i)$, where ε_i^{opt} is the molar extinction coefficient of the i^{th} component, C_i is the concentration of component i and l is the optical path length. (b) Benesi, H.A.; Hildebrand, J.H. *J. Am. Chem. Soc.* **1949**, *71*, 2703. (c) Gur'yanova, E.N.; Gol'dshtein, I.P.; Romm, I.P. *The donor-acceptor bond*; Keter Publishing House: Jerusalem, 1975, Chapter 2, pp 29-79. (d) In the Arrhenius equation R equals the gas constant and $K_{C,0}$ the complexation constant at infinite temperatures.

(4) (a) Kouwer, P.H.J.; Mijs, W.J.; Jager, W.F.; Picken, S.J. *Macromolecules* **2000**, *33*, 4336-4342. (b) Kouwer, P.H.J.; Gast, J.; Jager, W.F.; Mijs, W.J.; Picken, S.J. *Mol. Cryst. Liq. Cryst.* **2001**, *364*, 225-234 (c) Kouwer, P.H.J.; Mijs, W.J.; Jager, W.F.; Picken, S. J. *J. Am. Chem. Soc.* **2001**, *123*, 4645-4646.

(5) Janietz, D. *Chem. Commun.* **1996**, 713-714.

(6) From a fast OPM measurement on a (slowly degrading) polymer sample, a clearing temperature of the order of 230 °C could be determined.

(7) The broad melting temperatures of **A1** and **$(A1)_2$** are due to the presence of *E*/*Z*-isomers of **A1** and hence three isomers for **$(A1)_2$**, see also Chapter 2.2.3.

(8) (a) Kouwer, P.H.J.; Jager, W.F.; Mijs, W.J.; Picken, S.J. *Macromolecules* **2001**, *34*, 7582-7584. (b) Kouwer, P.H.J.; Van den Berg, O.; Jager, W.F.; Mijs, W.J.; Picken, S.J. *Macromolecules* **2002**, *35*, 2576-2582.

(9) Praefcke, K.; Singer, D.; Kohne, B.; Ebert, M.; Liebmann, A.; Wendorff, J.H. *Liq. Cryst.* **1991**, *10*, 147.

(10) Glüsen, B.; Kettner, A.; Wendorff, J.H. *Mol. Cryst. Liq. Cryst.* **1997**, *303*, 115-120.

(11) Kouwer, P.H.J., Unpublished results from DSC and OPM investigations in our own laboratories: the complex 2,3,6,7,10,11-hexakis(hexyloxy)triphenylene:**A2** shows the phase sequence: $\mathrm{Col_p}$ – $\mathrm{Col_{ho}}$ – I.

(12) Qualitatively discussed XRD results use the terms lateral for the [*h*00] or [0*k*0] direction and columnar for the [001] direction. Also when no columns are present, like in the nematic discotic ($\mathrm{N_D}$) phase.

(13) Usually, two spacing are not sufficient to calculate the parameters of an monoclinic unit cell (three variables: *a*, *b* and α). Estimation of the volume of the unit cell, assuming that it consists of one donor and one acceptor disk, offered us a third known quantity to calculate the lattice parameters *a*, *b* and α . For example, a unit cell consisting of 1 **D1** and ½ **$(A1)_2$** has a unit cell mass of $M = M_{\mathbf{D1}} + ½M_{\mathbf{(A1)2}}$ = 1428 g·mol^{-1} and a unit cell volume of $V = M/(\rho N_\mathrm{A})$ = 2.1 nm^3. Fitting the spacings with a monoclinic cell with a fixed volume gives in the presented results.

(14) (a) Some more remarks on the nematic texture as observed for the $\mathrm{N_L}$ phase: Long range smectic or columnar order is not compatible with a schlieren texture due to the incompressibility of the lamellae or 2D stacks. Defects in these materials results in focal conical textures (for lamellae) and 'oak-leaf' or mosaic textures (for columns). A SC phase, also exhibiting a *schlieren* texture in a homeotropic alignment, can be excluded due to the presence of clear ±½ disclinations in our texture. (b) If we would have been looking at a phase with long-range positional order, like a columnar phase, it would certainly have led to the formation of an elastic network due to the presence of the polymer backbone, contrarily to our observations.

(15) (a) Ringsdorf, H.; Wüstefeld, R.; Zerta, E.; Ebert, M.; Wendorff, J.H. *Angew. Chem. Int. ed. Engl.* **1989**, *28*, 914-918. (b) Praefcke, K.; Singer, D.; Kohne, B.; Ebert, M.; Liebmann, A.; Wendorff, J.H. *Liq. Cryst.* **1991**, *10*, 147-159. (c) The $\mathrm{N_{Col}}$ phase is characterized by an increase of the correlation length of only the intracolumnar reflection. See for example Figure 3.4 in Chapter 3.2.

(16) (a) Bengs, H.; Karthaus, O.; Ringsdorf, H.; Baehr, C.; Ebert, M.; Wendorff, J.H. *Liq. Cryst.* **1991**, *10*, 161-168. (b) Ebert, M.; Frick, G.; Baehr, C.; Wendorff, J.H.; Wüstefeld, R.; Ringsdorf, H. *Liq. Cryst.* **1992**, *11*, 293-309. (c) Möller, M.; Tsukruk, V.; Wendorff, J.; Bengs, H.; Ringsdorf, H. *Liq. Cryst.* **1992**, *12*, 17-36.

(17) (a) Contact samples of the complex **D5**:**A2** with discotic liquid crystals with a well-known mesophase are difficult to prepare. The electron acceptor **A2** also complexes the other mesogen and hence gives rise of a range of different mesophases, dependent on the exact local composition. Despite the effort, no conclusions could be drawn from these experiments. (b) A change in symmetry of the columnar organization (like the formation of a $\mathrm{Col_r}$ or $\mathrm{Col_{ob}}$ phase) would have resulted in, at least, an observable change in the small angle region of the XRD pattern. Tilting of the disks in the columns would have resulted in a rectangular or oblique columnar arrangement and in an increase in the d_{001} spacing.

(18) Fontes, E.; Heiney, P.A.; de Jeu, W.H. *Phys. Rev. Lett.* **1988**, *61*, 1202-1205.

(19) (a) Maier, W.; Saupe, A.*Z. Naturforsch.* **1958**, *13a*, 564. (b) Maier, W.; Saupe, A.*Z. Naturforsch.* **1959**, *14a*, 882. (c) Maier, W.; Saupe, A.*Z. Naturforsch.* **1960**, *15a*, 287.

(20) Obviously, for the $\mathrm{N_D}$ phase T_N should coincide with the clearing temperature: $T_\mathrm{N} = T_\mathrm{i}$ = 419 K. (b) The mean-field potential U of the extended Maier-Saupe theory, is defined as: $U = \varepsilon(T)\langle P_2\rangle P_2(\cos\theta)$, where $\varepsilon(T) \propto T^{1-c_2}$. A value of $c_2 \neq 1$ corresponds to an extra temperature dependence of the strength of the mean-field potential.

(21) D-β-Cellobiose octadodecanoate was a kind gift of Akzo Nobel. Estimated enentiomeric purity: 98%.

6 More specific interactions in discotic liquid crystals

Parts of this chapter have been submitted for publication to the *J. Am. Chem. Soc.*

Abstract

A series of novel mesogens have been prepared by a five-fold Sonogashira reaction of terminal acetylenes with a functionalized pentabromophenol. The corresponding side chain polymers were prepared by a polymer analogous substitution reaction. The mesogens differ in the nature of the substituents, linking five hexyl tails to the aromatic core, i.e. CH_2, O, S, SO_2 and CONH groups. A wide range of mesophases and corresponding transition temperatures has been detected, ranging from low melting nematic phases to highly stable columnar phases. The widely variable phase behavior is described in terms of specific intermolecular interactions.

Addition of planar electron deficient molecules resulted in the formation of charge transfer complexes. Stabilization and destabilization of the mesophases is explained by considering the complexation strength of the complex as well as steric factors.

6.1 Introduction

Supramolecular chemistry – “the chemistry beyond the molecule” – has a large number of non-covalent interactions at its disposal.[1] These secondary interactions include forces like (*i*) electrostatic interactions (ion-dipole, dipole-dipole), (*ii*) hydrogen bonding, (*iii*) π-π stacking, (*iv*) Van der Waals forces (dispersion and induction forces) and (*v*) hydrofobic or, more general, solvofobic effects. A combination of these non-covalent interactions is used in nature to build complex structures that can show multiple levels of organization. The interest in the self-organization and self-assembly in synthetic systems has grown considerably. This is displayed in numerous literature contributions, discussing the effects of the wide range of secondary interactions available.[2] Liquid crystals are self-assembling by nature. The interactions mentioned above, can improve or, oppositely, diminish the extent of organization (i.e. the extent of order) in the liquid crystalline phases. This makes liquid crystals ideal models to study the effects of various interactions on the molecular organization.

Specific interactions can be introduced conveniently via the substituent that links the flexible tail to the aromatic core. Although this linking group rarely bears specific functions (such as stabilizing columnar interactions, in order to obtain prototypes of molecular wires[3]), some investigations on its role on the phase behavior have been performed.

Substituents effects have been studied in triphenylenes (see Figure 6.1). The hexa ether[4a] (Figure 6.1a) exhibits a common columnar phase, while the corresponding hexathio derivative[4b,c] (Figure 6.1b) shows the same phase (with a slightly lower clearing temperature) and an additional soft-crystalline columnar phase, the so-called H phase[5] at low temperatures. For the sulfone derivative (Figure 6.1c) loss of all the liquid crystalline properties was observed.[4b] The strong aggregation of sulfone groups was demonstrated by the homologous series of hexakis(alkylsulfonyl)benzenes (Figure 6.1e), displaying columnar mesophases despite their small aromatic core. This in contrast to their nonoxidized thioether derivatives (Figure 6.1d) that show ordinary isotropic melting behavior.[6] In the literature only a few examples of disk-shaped materials are mentioned in which hydrogen bonds play an important role, some depicted in Figure 6.1f-h. Note that in 6.1f[7] the H-bonds are directed parallel to the plane of the disk whereas in 6.1g[8] and 6.1h[3] the H-bonds are expected to be directed perpendicular along the normal. For the latter a much stronger aggregation effect by the H-bonds is anticipated.

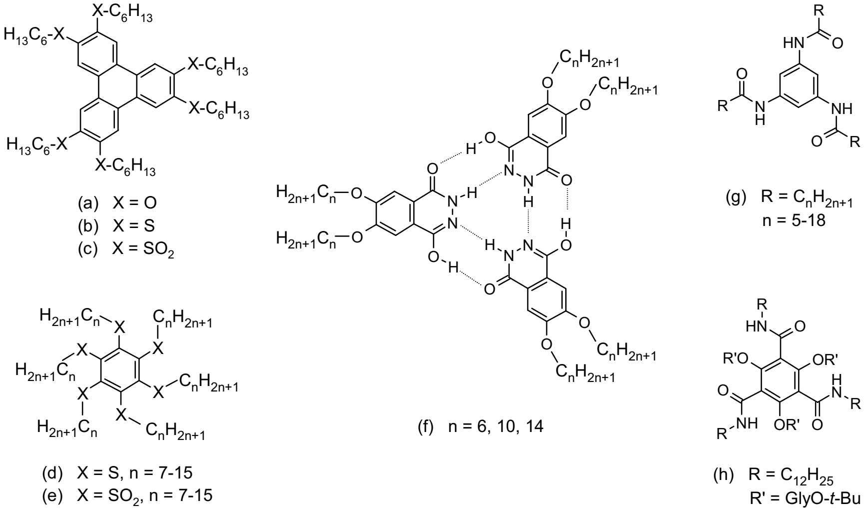
(a) X = O
(b) X = S
(c) X = SO_2

(f) n = 6, 10, 14

(g) R = C_nH_{2n+1}
n = 5-18

(d) X = S, n = 7-15
(e) X = SO_2, n = 7-15

(h) R = $C_{12}H_{25}$
R' = GlyO-*t*-Bu

Figure 6.1. Structure of (a-c) substituted triphenylenes, (d,e) substituted benzenes and (f-h) examples of discotic liquid crystals with hydrogen bonds involved.

Other ways to manipulate the phase behavior in disk-shaped materials have been reported,[9] including the use of metals in for example porphyrins and phtalocyanines,[10] the application of charge transfer interactions by application of an electron acceptor and attachment of the mesogens to a polymer backbone (the last two discussed in the previous chapters).

In this chapter, we present the phase behavior of a series of novel mesogens based on the pentakis(phenylethynyl)phenoxy core with various groups linking the tails to the aromatic core, including methylene (**D4**), ether (**D6**), thioether (**D7**), sulfone (**D8**) and amide(**D9**) (see Figure 6.2). The strong effect of the linking groups on the phase behavior of the mesogens is described in terms of various specific interactions between the mesogens. In addition, we modified the phase behavior in ways that we have done before; first of all, chemically by attaching the mesogens to a polymer backbone, and secondly, by doping with electron acceptors, giving rise to charge transfer complexes and even more specific interactions.

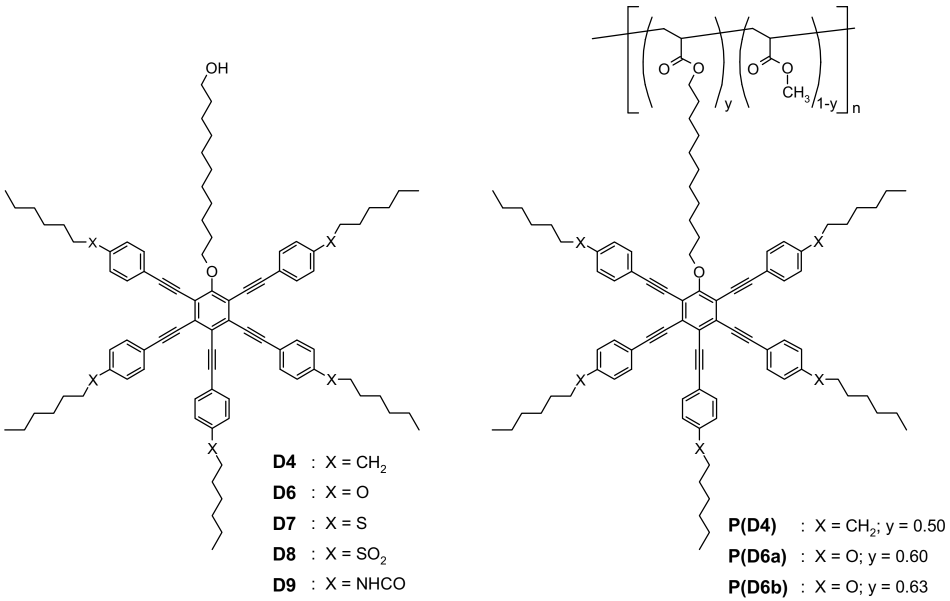

Figure 6.2. Low molar mass mesogens **D4**, **D6**-**D9** and comb-shaped polymers **P(D4)** and **P(D6)**.

6.2 Thermal analysis of the mesogens

The thermal properties of the mesogens and polymers were investigated with optical polarizing microscopy (OPM) and differential scanning calorimetry (DSC). The results are summarized in Table 6.1. Compound **D4** showed a monotropic nematic phase at low temperatures, easily recognized by the typical *schlieren* texture and low viscosity. In the corresponding polymer **P(D4)**, the mesophase disappeared completely and the material turned out to be an amorphous polymer with a low glass transition temperature. Compound **D6** exhibited a nematic phase over a temperature range of 45 °C. Thin samples of **D6** between two *unprepared* microscope slides quickly aligned homeotropically in the N_D phase. Figure 6.4a is taken 30 seconds after heating the sample at 80 °C. Further annealing (~5 minutes at 80 °C) resulted in almost complete homeotropic alignment. The latent heat at the nematic to isotropic transition is very small, as observed earlier for similar materials.[10] Polymers **P(D6)** also showed N_D phases with clearing temperatures and latent heat values of the order of those of the mesogen **D6**. Due to the presence of the polymer backbone, crystallization was suppressed and the polymers vitrified around room temperature, resulting in the formation of a nematic glass at low temperatures. Although room temperature nematic phases for rod-shaped liquid crystals (optically positive) are not uncommon, nematic phases occurring at such low temperatures are very rare for disk-shaped mesogens (optically negative).[11] Chemically linking mesogens to a polymer[12] or possibly well-defined flexible cores[13] proves to be an effective tool to reach low temperature nematic discotic phases. It is anticipated that the use of a more flexible backbone (like polyether or polysiloxane) could lower the glass transition temperature even more and, hence, real room temperature optically negative nematic phases can be envisaged.

Table 6.1. Thermal behavior of the mesogens, measured with OPM and DSC. Transition temperatures are shown in [°C] and latent heat values (between the brackets) in [kJ·mol^{-1}]. ^{a} Monotropic phase transition.

Material	Thermal behavior				
D4	**K**	[39 (34)	**N_D** 52 (1.2)]^a	57 (36)	**I**
D6	**K**	71 (33)	**N_D**	118 (0.15)	**I**
D7	**K**	56 (65)	**Col_{hd}**	167 (0.21)	**I**
D8	**Col_p**	115	**Col_{hd}**	>260	**d**
D9	**K**			215 (16)	**I/d**
P(D4)	**G_I**	-15			**I**
P(D6a)	**G_N**	25	**N_D**	107 (0.15)	**I**
P(D6b)	**G_N**	24	**N_D**	113 (0.18)	**I**

As expected, the mesogens attached to the polymer backbone did not show the fast alignment between the microscope slides. Even extensive annealing did not result in a significant growth of the domain sizes (see Figure 6.4b).

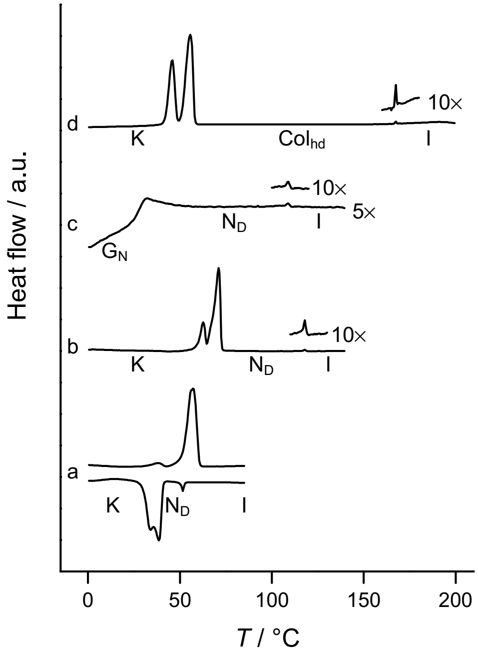

Figure 6.3. Normalized DSC thermograms of (a) **D4** (monotropic N_D phase); (b) **D6**; (c) **P(D6b)** (magnification 5×) and (d) **D7**. For **D6**, **P(D6b)** and **D7**, the small transitions to the isotropic liquid have been magnified (10×).

Mesogen **D7** shows a fan-shaped optical texture (see Figure 6.4c), characteristic for a columnar mesophase. DSC experiments first show two large transitions, the first is attributed to a crystal-crystal transition and the second to a transition to a columnar phase. At high temperatures, a small transition to the isotropic phase is observed.

The phase behavior of **D8** was hard to determine, since decomposition at very high temperatures (> 250 °C) precedes isotropization.[14] In a fast cooling experiment from a freshly molten sample, the mesophase of was identified by the observation of growing hexagons from the isotropic phase and the six 'oak-leaf' textures, both characteristic for a Col$_h$ mesophase. Compound **D8** did not show any melting or crystallization phenomena, but rather a second order transition at lower temperatures, attributed to the formation of a columnar plastic (Col$_p$) phase.[15] The penta-amide **D9** cleared at about 215 °C with some decomposition, but neither microscopy experiments nor DSC analysis could distinguish between a highly ordered columnar and an ill-defined crystalline phase at lower temperatures.

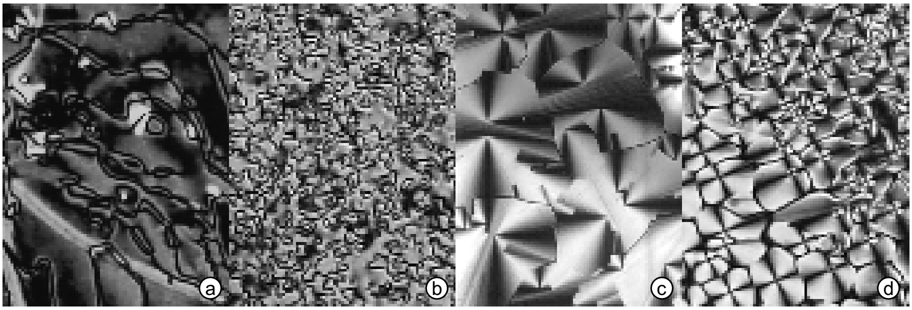

Figure 6.4. Optical textures of (a) low birefringent homeotropic N$_D$ phase of **D6** at 80 °C (annealing 30 s at 80°C from the at the first heating ramp); (b) N$_D$ phase of **P(D6b)** at 100 °C (annealing 30 min at 100 °C upon cooling from the isotropic phase); (c) Col$_{hd}$ phase of **D7** at 100 °C (upon cooling from the isotropic phase); (d) Col$_{hd}$ phase of **D8** at 255 °C (freshly formed columnar phase from the isotropic phase). All pictures were taken with crossed polarizers, magnification 40× (a-c), 85× (d).

X-Ray diffraction. To gain more insight into the (local) molecular order in the mesophases, the materials were subjected to powder X-ray diffraction (XRD) measurements. Radial scans of the patterns are displayed in Figure 6.5. Compound **D6** showed the typical pattern of the low ordered N$_D$ phase. Two diffuse weakly aligned reflections are observed, attributed to the lateral [100] and planar [001] disk-disk distances as well as a broad non-oriented halo at 4.5-5 Å, which is attributed to (non-oriented) alkyl chains. Polymer **P(D6)b** showed a pattern, very close to that of the monomer, apart from some extra broadening of the reflections, resulting in complete coincidence of the alkyl and [001] reflections. The nonaligned columnar phase of **D7** showed a much sharper lateral, intercolumnar [100] reflection, indicating a well-defined two-dimensional columnar organization. The intracolumnar [001] reflection is still very diffuse, which indicates a much less defined organization within the columns, typical for columnar disordered (Col$_{xd}$) phases. The XRD pattern of **D8** showed a narrowing of the intercolumnar reflections as well as some higher order reflections in the small angle region, the [110] and [210] reflections. The intracolumnar reflection shifted to higher diffraction angles (i.e. shorter distances) and sharpened a bit, compared to **D7**. Despite the increase in the intra-columnar interactions indicated by the observed shift and narrowing, the reflection is still characteristic for disorder within the columns, i.e. a columnar disordered phase. XRD experiments of **D9** below 215 °C (not shown) revealed a typical pattern of a crystalline phase, i.e. multiple sharp reflections in the small angle region.

The spacings *d*, corresponding to the maximum of the diffraction angles θ were calculated using the Bragg law: $2d\sin\theta = n\lambda$, where n is an integer and λ is the used wavelength: λ = 1.54 Å. The results are summarized in Table 6.2.

Table 6.2. X-ray diffraction results. Note that **D6** and **P(D6b)** do not posses any long-range positional order in the nematic phases and hence Miller indices do not apply. The indicated Miller indices [100] and [001] correspond to the lateral and planar disk-disk distances, respectively.

Material	*T* [°C]	Phase	Miller Indices	*d* [Å]
D6	90	N_D	100	20.8
			alkyl	5.2
			001	4.4
P(D6b)	50	N_D	100	20.5
			alkyl+001	4.5-5.0
D7	100	Col_{hd}	100	23.3
			alkyl	4.8
			001	3.9
D8	140	Col_{hd}	100	24.3
			110	14.3
			210	9.10
			alkyl	5.0
			001	3.70

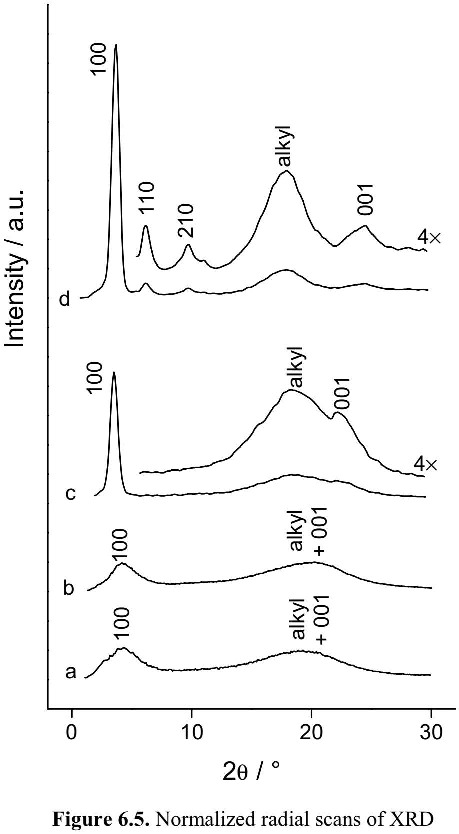

Figure 6.5. Normalized radial scans of XRD patterns of (a) **D6** at 90 °C (b) **P(D6b)** at 50 °C (c) **D7** at 100 °C, (wide-angle area 4×) and (d) **D8** at 140 °C (wide-angle area 4×).

6.3 Intermolecular interactions

The large differences in the phase behavior of the mesogens can be ascribed to differences in molecular structure. We will discuss the observed phase behavior in terms of intermolecular interactions, starting with the low ordered alkyl substituted mesogens and ending with the highly ordered sulfone and amide substituted molecules.

In Chapter 3.3, we reported the phase behavior of methyl-substituted mesogens (**D2**), its corresponding side-chain polyacrylates and a series of copolyacrylates with different pendent alkyl groups. A master phase diagram was established which showed a clear relation between the N_{Col}–N_D–I and the N_{Col}–I transitions and the weight fraction [M] of rigid mesogen.[12a] The transition temperatures were described by simple exponential fits and were valid for all copolymers, irrespective of the length and the degree of substitution of the dangling alkyl groups along the polymer backbone.[16]

In **D4**, the well-known pentyl substituted **D3** and their corresponding side-chain polymers, the rigid mesogen fraction is reduced by the laterally attached tails. When their N_D to I transition temperatures are added to the master phase diagram, Figure 6.6 is obtained.

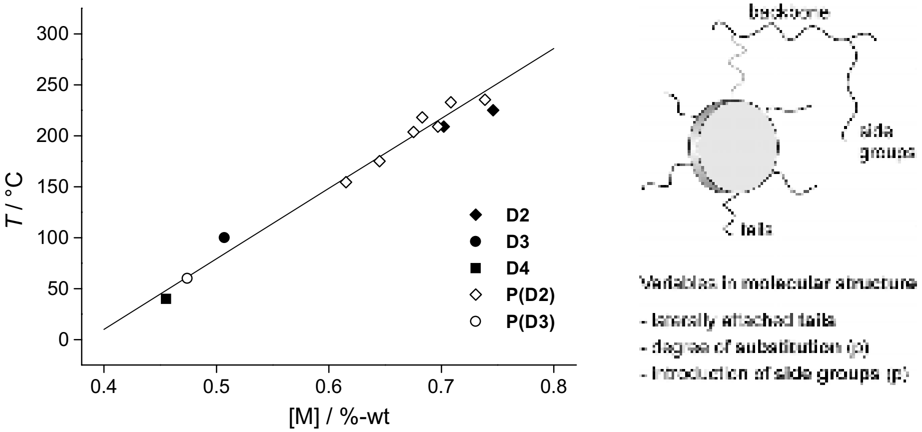

Figure 6.6. Clearing temperature T_{NI} as a function of the rigid mesogen fraction [M] for various alkyl substituted mesogens. In the schematic picture (right) all the variables in the molecular structure for this series of materials are illustrated. The materials differ in size of the laterally attached tails, the presence of a polymer backbone or not and the polymers show also differences in the degree of substitution and the presence (and concentration) of any side groups attached to the backbone. The solid line[16b] represents the power-law equation: $T_{NI} = 695 \cdot [M]^{0.98}$.

The clearing temperatures of all alkyl-substituted mesogens (**D2**-**D4** and their corresponding side chain polymers) all coincide the drawn curve. This means that the transition temperatures for these series of mesogens can be tuned conveniently, either by attaching long tails to the mesogens or by copolymerization of a mesogen with different alkylacrylates. In other words, regardless of the length and the position (attached to the mesogen or to the polymer backbone) of any alkyl group, the N_D to isotropic transition temperature can simply be predicted, just by calculating its fraction of rigid mesogens [M]. It is remarkable to see that this relation holds for such a variety of materials and over a wide temperature range.

As a rule of the thumb, for disk- and rod-shaped mesogens, the alkoxy-substituted mesogens show an increase in both the clearing temperature and the melting temperature, compared to their alkyl substituted counterparts. The introduction of oxygen in the linking group results in an increased electron density of the aromatic core. The corresponding enhancement of the attractive π–π interactions results in a higher clearing temperature of **D6** compared to **D4**. Replacement of oxygen by sulfur in the substituents of discotic liquid crystals usually results in similar phase behavior with a slight decrease in the transition temperatures,[10] as was observed for the triphenylenes in Figure 6.1. However, when comparing **D7** with **D6**, we found a columnar mesophase, instead of the N_D phase, and a higher clearing temperature. The formation of this columnar phase could be attributed to packing effects, due to the larger dimensions of the sulfur atom compared to oxygen and maybe reinforced π interactions involving the sulfur *d*-orbital. It is clear that the effects of subtle changes in the molecular geometry on mesophase formation can be significant. Interestingly, the latent heat at the Col_{hd} to I transition of **D7** is very small, at least a factor 10 than would be expected.[17] At a phase transition the total amount of free energy is constant: $\Delta G = \Delta H - T\Delta S = 0$, so when ΔH is small, either the order in the columnar phase is extraordinary low, or, more likely, in the isotropic phase the extent of local organization is still substantial! Unfortunately, reliable XRD measurements in the isotropic phase could not be obtained, because of severe thermal degradation.

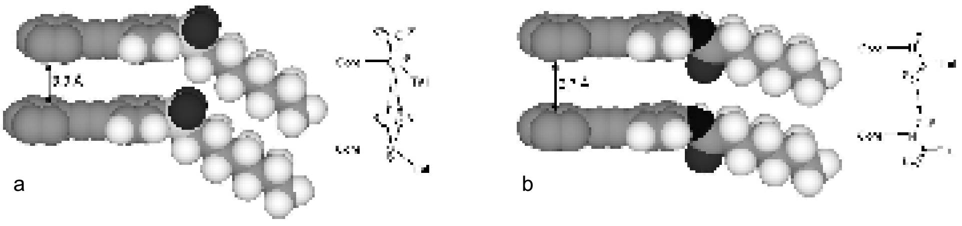

Figure 6.7. Schematic representation of the attractive forces due to: (a) dipole-dipole interactions in **D8** and (b) hydrogen bonding in **D9**. Note that non-hydrogen substituted benzene at the left-hand side represents the central benzene group of the core and that for the sake of clarity only one of the five substituted phenyl-ethynyl groups is exposed. Recent calculations have elucidated that a 45° out of plane twist of the amide groups is sufficient to efficiently stabilize a 3.8 Å distance between the aromatic cores.[3] The pictures are obtained, using CS Chem3D Ultra®, supplied by CambridgeSoft.com.

Sulfone and amide functional groups are rarely applied in liquid crystals, since they display a tendency to form highly ordered (crystalline) phases. The high clearing temperatures of **D8** and **D9**, strongly indicate that the sulfone and amide groups, contribute to the intermolecular non-covalent interactions between the mesogens. It is anticipated that these interactions are directed in the *intra*columnar direction, since the functional groups are confined in between the core and the tails. This is schematically illustrated in Figure 6.7, that shows the central aromatic core (on the left side), substituted with one of the five phenylethynyl groups and the appropriate tail. When two neighboring disks are in the correct position and conformation (multiple) attractive interactions can occur: dipole-dipole interactions for **D8** and hydrogen bonds for **D9**. The intracolumnar interactions promote a columnar organization with a well-developed two dimensionally ordered columnar structure, that is easily recognized by the sharp intercolumnar reflection [100] and the higher order reflections observed in the XRD pattern of **D8** (as well as in the XRD pattern of the crystalline phase of **D9**).

Despite the present intracolumnar attractive forces, a substantial amount of *disorder* is found in the XRD experiments (indicated by the diffuse [001] reflections), which, in our opinion, can be attributed to two major causes. (*i*) A 'random' organization of the linking groups. E.g., if the dipole moment of sulfone groups of neighboring mesogens (in the column) point up or down irregularly, it will give rise to a defect structure, causing disruption of the intracolumnar order. Alternatively, sulfone groups with dipoles pointing in the same direction (i.e. up or down with respect to the disk-plane) in a large stack of sulfone groups, contribute to a high intracolumnar organization. (*ii*) The presence of the flexible spacer, anchored at the central phenyl group in the core, prevents effective packing of the mesogens and, hence, further diminishes the intramolecular order in the material.

The multiple dipolar interactions in **D8** resulted in the formation of a columnar mesophase that was stable until degradation at high temperatures. The aggregation process in the multi-hydrogen bonded structure in **D9** even yields a crystalline phase.[18] A clear illustration of the extent of aggregation in **D9** is that upon dissolving small amounts of **D9** in chloroform, viscous gels are obtained. Addition of 10% of methanol breaks-up the hydrogen bonds and obtain low viscous solutions, although the width of the NMR signals still indicates substantial interactions.

6.4 Charge transfer complexes.

Doping **D4**, **D6** and **D7** with electron acceptors **A2** and **A3** gave rise to the formation of strongly colored CT complexes. The results are summarized in Table 6.3. In complexes of **D4** or **D3** with **A2** or **A3** enantiotropic columnar hexagonal (Col_h) phases were induced. Complexes with the more electron deficient **A3** showed higher clearing temperatures. The formation of the CT complex also suppresses crystallization; instead a transition to the crystal-like columnar plastic (Col_p) phase is observed at much lower temperatures, which resulted in a wide temperature range of the columnar mesophase. It should be mentioned that the most stable complexes (maximum of the clearing temperature in the phase diagram) are found for complexes with an excess of acceptor. This is in contrast to what was observed before, since earlier we always found optimum complexing conditions at equimolar ratios.[19]

Table 6.3. Thermal behavior of the charge transfer complexes of mesogens **D3**, **D4**, **D6** and **D7** with **A2** and **A3**, measured with OPM and DSC. Transition temperatures are shown in [°C] and latent heat values (between the brackets) in [J·g^{-1}].

Mesogen	Acceptor	Phase behavior at equimolar concentrations						
D3	**A2**[a,c]	Col$_p$	15	Col$_h$	110 (3.2)			I
	A3	Col$_p$	16	Col$_h$	173 (3.4)			I
D4	**A2**[b]	Col$_p$	15	Col$_h$	72 (1.3)			I
	A3	K/Col	28 (3.0)	Col$_h$	95 (0.3)			I
D6	**A2**	K	64 (21)			N$_D$	94 (0.4)	I
	A3	Col$_p$	50	Col$_h$	91 (8.0)	N$_D$	128 (0.4)	I
D7	**A2**	Col$_p$	4	Col$_h$			83 (0.6)	I

[a] Most stable CT complexes of **D3**:**A2** were observed at an **A2** fraction of 0.6: Col$_p$ 15 Col$_h$ 126 (5.0) I. [b] Most stable CT of **D4**:**A2** complexes were observed at an **A2** fraction. of 0.65: Col$_p$ 15 Col$_h$ 93 (3.1) I. [c] The thermal results of complex **D3**:**A2** have been published before.[20]

CT complexes of **D6** and **D7** with **A2** had lower clearing temperature than the pure mesogens. Complexes of **D6** with various amounts of **A2** were prepared and investigated and a schematic phase diagram was constructed[21] (see Figure 6.9). An increasing content of **A2** caused decreases in both the melting and the clearing temperature, compared to pure **D6**. Alternatively, the corresponding change in entropy at the N$_D$ to I transition increased. Hence, while the complexes show an increase in the intermolecular interactions (increase in ΔH at the clearing temperature), other effects destabilizing the mesophase are dominating.

Application of the stronger acceptor **A3** to **D6** resulted in stabilization of the nematic mesophase. In equimolar complexes, the nematic discotic phase cleared at 128 °C (with ΔS = 0.72 J·mol^{-1}K^{-1}). In addition a columnar phase was observed.

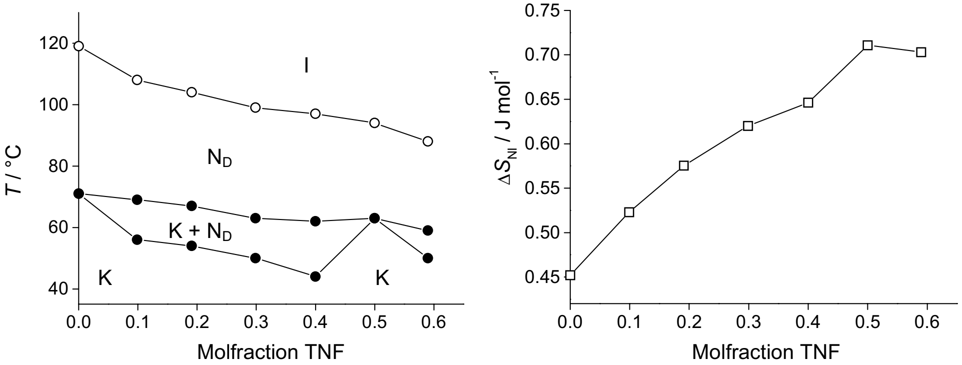

Figure 6.9. (a) Schematic phase diagram of **D6** and **A2**. (b) Change in entropy at the nematic – isotropic phase transition, calculated using: $\Delta G = \Delta H - T\Delta S = 0$.

CT complexes of **D7** with **A2** showed a similar behavior. At equimolar concentrations a strong decrease in the clearing temperature to 83 °C was observed (with an increase in the latent heat at the transition). Crystallization was also suppressed and a glass transition was found below room temperature, resulting in an overall shift of the temperature window of the columnar phase from 56-167 °C to 4-83 °C.

It was expected that the (weakly) electron deficient **D8** would show the formation of stable charge transfer complexes with **D6** and **D7**, since the molecules are similar in the molecular structure and in dimensions. However, no CT interactions were observed for mixtures of **D8** with either **D6** or **D7**.[22] While **D6**:**D8** macroscopically demixed, mixtures of **D7** with **D8** showed a linear mixing behavior with clearing temperatures in between those of the two constituents.[22] Nevertheless, as was expected from the electron deficient nature of **D8**, it does not form CT complexes with the electron acceptors **A2** and **A3**.

In our experience, several factors determine the degree of stabilization of mesophases via charge transfer complexation. The first important parameter is the strength of the donor-acceptor complex (ΔH_{DA}). However, this has to be compared to the sum of donor-donor and acceptor-acceptor interactions that are broken because of the complex formation. This can be summarized as an effective complexation enthalpy: $\Delta H_{\mathrm{eff}} = \Delta H_{\mathrm{AD}} - ½(\Delta H_{\mathrm{DD}} + \Delta H_{\mathrm{AA}})$. It is stressed that in this expression all relevant contributions must be taken into account, including CT energies, Van der Waals and quadrupolar forces. Another important factor to be considered in this process comprises steric effects. For our complexes two important steric contributions can be distinguished: (*i*) the long spacer that is anchored at the center of the core; and (*ii*) the misfit in dimensions of the donor and the acceptor. Both effects give rise to spatial distortion in a columnar organization. For example, complexing a large donor with a small acceptor in an alternating columnar arrangement of the donor and acceptor molecules would result in a high amount of free volume in a local stack, which will cause a strong destabilization of the mesophase. The steric effects can foremost be considered as entropic effects.

Usually, investigations of series of CT complexes yield the complementary effect of both the enthalpic and the entropic effects. In some cases, however, the effects are separated. For example, the enthalpic effects were studied in a series of CT complexes of donors with a range of acceptors that were similar in size but had different electron affinities.[24] Furthermore, steric effects were studied in a series of materials with increasing steric repulsion by the spacer as well as in a series of materials with varying size of the donor and acceptor, investigating the role of their dimensional misfit.[25]

Taking the enthalpic and entropic contributions into account, we can qualitatively explain the thermal results of the CT complexes: The enthalpic effects are responsible for the observed stabilization of the mesophase. Alternatively, the CT complexes discussed here, experience a destabilizing effect on the mesophase formation originating from steric effects. Balancing the effects results in an overall stabilization or destabilization. For example, in **D6**:**A2** the steric destabilizing forces dominate, whereas in the complex with **A3** (a stronger acceptor of a similar size as **A2**) stabilization is observed. Clearly, in CT complexes of the alkyl substituted mesogens, the stabilizing enthalpic forces play a dominant role, much more important than in the complexes of **D6** and **D7**. This can be well understood when it is realized that the important parameter is the *gain* in enthalpy, represented by ΔH_{eff}, which is expected to be much higher for the weakly interacting alkyl substituted mesogens then for their alkoxy or thioalkyl substituted analogues. Similarly, the dipole-dipole interactions of **D8** are so strong (large ΔH_{AA}) that no complex is formed with **D6** and the mixture macroscopically phase separates.

6.5 Conclusions

A series of discotic liquid crystals, with varying substituents that link the flexible spacer to the aromatic core, has been studied. The nature of this linking group gives rise to a number of intermolecular interactions, which supplementing the interactions already present in (discotic) liquid crystals.

In alkyl and alkoxy substituents, π-π interactions and solvofobic effects play an important role in the mesophase formation. The series of alkyl-substituted mesogens (**D2**-**D4**) show a particularly interesting result, since their clearing temperature is solely determined by the fraction rigid mesogen. In addition, attachment of the mesogen to a polyacrylate backbone suppresses the crystallization process, resulting in room temperature N_D mesophases.

For thiohexyl (**D7**), hexylsulfonyl (**D8**) and hexylamido (**D9**) substituted mesogens, additional interactions have a major influence on the phase behavior. Packing effects, dipole-dipole interactions and H-bonds, respectively, stabilize the formation of columnar phases. Ultimately, for the penta-amide (**D9**) the strong interactions result in the disappearance of the mesophase and a crystalline phase was found instead.

The use of charge transfer complexing agents offers an easy and versatile tool to manipulate the liquid crystalline properties. Often CT interactions give rise to stabilization of the mesophase (due to enthalpic effects), but in some cases, presented here, the steric effects (entropic) dominated, which resulted in an overall destabilization of the observed mesophases. It is apparent that ultimate CT stabilization can be achieved by increasing the effective donor-acceptor interactions *or* by diminishing the steric factors, as discussed above.

References and notes

(1) Lehn, J. M. *Supramolecular Chemistry*; VCH: Weinheim, New York, 1995.

(2) For example, read: (a) Lawrence, D. S.; Jiang, T.; Levett, M. *Chem. Rev.* **1995**, *95*, 2229-2260. (b) Philip, D.; Stoddart, J. F. *Angew. Chem. Int. ed. Engl.* **1996**, *35*, 1154-1196.

(3) Bushey, M. L.; Hwang, A.; Stephens, P. W.; Nuckolls, C. *J. Am. Chem. Soc.* **2001**, *123*, 8157-8158.

(4) (a) Destrade, C.; Mondon, M. C.; Malthête, J. *J. Phys. Paris C3* **1979**, *40*, 17-21. (b) Kohne, B.; Poules, W.; Praefcke, K. *Chem. Z.* **1987**, *108*, 408. (c) Praefcke, K.; Kohne, B.; Poules, W.; Poetsch, E. In *Ger. Pat. DE 3346980A1*; Merck GmbH: Germany, 1983.

(5) (a) Gramsbergen, E. F.; Hoving, H. J.; de Jeu, W. H.; Praefcke, K.; Kohne, B. *Liq. Cryst.* **1986**, *1*, 397-400. (b) Fontes, E.; Heiney, P. A.; de Jeu, W. H. *Phys. Rev. Lett.* **1988**, *61*, 1202-1205.

(6) Praefcke, K.; Poules, W.; Schleube, B.; Poupko, R.; Luz, Z. *Z. Naturforsch.* **1984**, *39*, 950.

(7) Suárez, M.; Lehn, J. M.; Zimmerman, S. C.; Skoulios, A.; Heinrich, B. *J. Am. Chem. Soc.* **1998**, *120*, 9526-9532.

(8) Matsunaga, Y.; Miyajima, N.; Nakayasu, Y.; Sakai, S.; Yonenaga, M. *Bull. Chem. Soc. Jpn.* **1988**, *61*, 207.

(9) For example read: (a) Ringsdorf, H.; Wüstefeld, R. *Phil. Trans. R. Soc. Lond.* **1990**, *A 330*, 95-108. (b) Janietz, D. *J. Mater. Chem.* **1998**, *8*, 265-274.

(10) Cammidge, A. N.; Bushby, R. J. In *Handbook of Liquid Crystals*; Demus, D., Goodby, J. W., Gray, G. W., Spiess, H. W., Vill, V., Eds.; Wiley VCH: New York, 1998; Vol. 2B, pp. 693-748.

(11) (a) Most rod-shaped mesogens show a positive birefringence ($\Delta n = n_e - n_o > 0$). For disk-shaped liquid crystals, the birefringence is usually negative, making discotics very suitable for application as compensation layers in display technology. (b) Only recently, the first example of a room temperature nematic phase obtained from disk-shaped liquid crystals was reported. it was observed in a discotic liquid crystal based on a hexakis(phenylethynyl)benzene core and substituted with a *rac*-4-methylnonyl tails, resulting in a distribution of stereo isomers: Kumar, S.; Varhney, S. K. Angew. *Chem. Int. Ed. Engl.* **2000**, *39*, 3140-3142.

(12) (a) Kouwer, P.H.J.; Gast, J.; Jager, W.F.; Mijs, W.J.; Picken, S.J. *Mol. Cryst. Liq. Cryst.* **2001**, *364*, 225-234; see also Chapter 3.2 and 3.3. (b) Kouwer, P.H.J.; Van den Berg, O.; Jager, W.F.; Mijs, W.J.; Picken, S.J. *Macromolecules*, **2002**, *35*, 2576-2582; see also Chapter 4.2.

(13) Elsässer, R.; Mehl, G. H.; Goodby, J. W.; Veith, M. *Angew. Chem. Int. ed. Engl.* **2001**, *40*, 2688-2690 and references therein.

(14) By fast heating in an OPM experiment a clearing temperature of ~280 °C could be estimated.

(15) Glüsen, B.; Kettner, A.; Wendorff, J. H. *Mol. Cryst. Liq. Cryst.* **1997**, *303*, 115-120.

(16) (a) Kouwer, P. H. J.; Mijs, W. J.; Jager, W. F.; Picken, S. J. *J. Am. Chem. Soc.* **2001**, *123*, 4645-4646. (b) The drawn curve was taken from ref.16a and was calculated from fitting the series of alkyl substituted polymers to a power-law (see also Chapter 3.5).

(17) In Chapter 4 we describe some very disordered columnar materials, as determined with XRD, and even they exhibited quite ‘normal’ latent heat values.

(18) Some experiments have been performed to decrease the number of H-bonds, e.g. by preparing the meta-amide substituted derivative of **D9**. It was anticipated that the number of hydrogen bonds strongly reduced by assuming a random orientation of the amide group. Indeed, the obtained material showed a stable columnar mesophase, but unfortunately, we were not able to purify the material to the high level that is required for a good analysis of the liquid crystalline properties.

(19) See Chapters 4 and 5.

(20) Janietz, D.; Praefcke, K.; Singer, D. *Liq. Cryst.* **1993**, *13*, 247-253.

(21) Addition of **A2** also results in a broad biphasic area in the phase diagram. Strikingly, only at an exact equimolar ratio, the biphasic area has disappeared. Complexes with an **A2** mol fraction higher than 0.6 were unstable and show macroscopic phase separation.

(22) The formation of charge transfer complexes between materials based on the pentakis(phenylethnyl)phenoxy core and **A2** derivatives is easily recognized by the formation of a clear charge transfer band in the absorption spectrum of the complex. The complexes are usually orange (weak complex) to dark red (strong complex) compared to (pale) yellow constituents.

(23) This is a proof that the mesophase observed in **6S-D** and **$6SO_2$-D** is identical, i.e. the Col_{hd} phase.

(24) (a) Wüstefeld, R. PhD Thesis: Johannes Gutenberg Universität, Mainz, Germany 1990. (b) Ebert, M. PhD Thesis: Technische Hochschule Darmstadt, Darmstadt, Germany, 1990.

(25) (a) Praefcke, K.; Singer, D.; Langner, M.; Kohne, B.; Ebert, M.; Liebmann, A.; Wendorff, J. H. *Mol. Cryst. Liq. Cryst.* **1992**, *215*, 121-126. (b) Bengs, H.; Karthaus, O.; Ringsdorf, H.; Baehr, C.; Ebert, M.; Wendorff, J. H. *Liq. Cryst.* **1991**, *10*, 161-168.

General Considerations

The previous chapters discussed the properties of specific mesogens, the corresponding polymers and their charge transfer complexes. There are some important issues that have not been raised, since they have a more general character. This final chapter will consider some of theses topics, including the versatility of the polymer synthesis and the multiple nematic phases that we have found in our systems.

Polymer synthesis

Multiple attempts to prepare the discotic polyacrylates from the corresponding monomers under free radical conditions failed. In all cases starting materials and low molar mass oligomers were recovered after all the initiator was consumed. Probable reasons are the interference of the five triple bonds present in one monomer and the high degree of dilution used during the polymerization reactions, necessary to keep the mesogens dissolved.

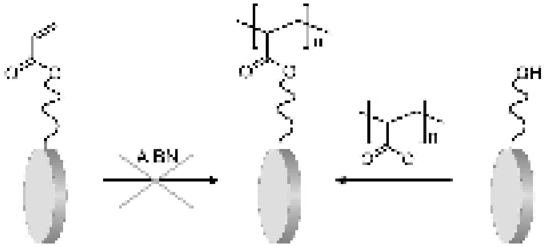

Figure 1. Schematic presentation of the polymer synthesis: the approach of polymerization of the acrylic functional mesogen under free-radical conditions or a polymer analogous reaction with poly(acryloyl chloride).

The problems occurring with the polymerization of complex molecules are widely recognized. Therefore, polymer analogous reactions are applied more and more frequently. In general, these reactions constitute substitution reactions between a functional molecule and a preformed polymer backbone, e.g. primary alcohols or amines substituted on poly(acryloyl chloride) or poly(methacryloyl chloride),[1a] or derivatives of carboxylic acids on poly(hydroxypropylmethylsiloxane).[1b] The main advantage of this method is its general applicability. The disadvantage, however, is that a virtually inaccessible full conversion must be reached to obtain a homopolymer. If this is not the case, (statistical) copolymers are obtained. In addition the non-reacted groups may have a negative effect on the final polymer properties.

We have successfully applied a polymer analogous substitution reaction of both donors and acceptors to the reactive poly(acryloyl chloride). By using an excess of alcohol, the degree of substitution can be as high as 95%. It is important to realize that the remaining acyl groups have been converted to methyl esters to prevent the formation of anhydrides (crosslinking) or carboxylic acids, both having a strong effect on the thermal properties of the polymer. Application of the polymer analogous reaction offers more advantages. The use of the same batch of reactive polymer for investigation of polymers with different substituents ensures the constant chain length of the various samples. Moreover, by using a mixture of mesogens or by adding them subsequently, copolymers can be obtained. This opens a versatile route to obtain a series of copolymers where the mesophase behavior can be readily tuned.

Associated nematic phases

The nematic phase is characterized by long-range orientational order between the mesogens. The disk- or rod-shaped mesogens lack any long-range positional order. However, locally, the mesogens may be well ordered, forming aggregates that effectively act as the principal unit of the nematic phase. Good examples of such aggregated nematic phases are the well-established N_{Col} phase,[2a,b] nematic phases of worm-like micelles,[2c] chromonic liquid crystals[2d] and reentrant N_D phases observed in certain truxene derivatives.[2e]

In Chapters 4 and 5, we reported another example of an associated nematic phase, referred to as the nematic lateral (N_L) phase. Both the N_{Col} and the N_L phase are often observed in materials in which the preferred columnar organization (often using improved intracolumnar interactions) is avoided due to spatial restrictions. These restrictions can be introduced in low molar mass materials (only N_{Col} phases observed) as well as in macromolecular materials (both N_{Col} and N_L phases observed). Examples include (*i*) the introduction of asymmetry in the substitution of the core,[3] (*ii*) using an insufficient spacer length between the mesogens to adept to the columnar structure[4] or (*iii*) the introduction of spatial packing problems when the mesogens lack flexible tails surrounding the core, and where the backbone causes distortion of long-range positional order.[5]

In the associated nematic phases, the principal unit is an aggregate of molecules rather than a single mesogen as in the N_D phase, see Figure 2. The aggregation in the N_{Col} phase is uniaxial (in the columnar direction) and in the N_L phase (locally) in all three directions. The transition from the N_L or the N_{Col} to the N_D phase corresponds to a break-up of the local assemblies while the nematic organization is conserved.

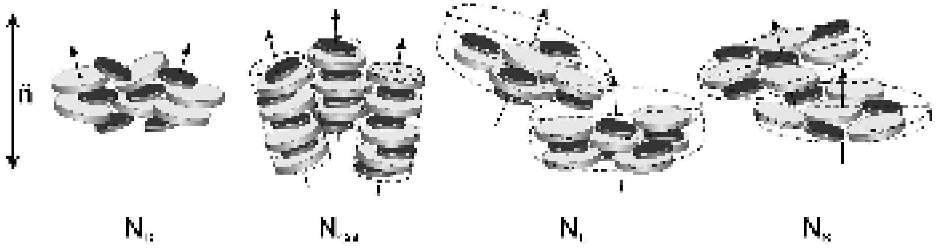

Figure 2. Schematic illustration of the various nematic phases, drawn for charge transfer complexes with equimolar rations. The donors (⬭) are represented larger than the acceptors (⬬) as is the case in our systems.

Based on symmetry reasons, we might consider another (associated) nematic phase that consist of two-dimensional assemblies, i.e. aggregation in the plane of the disk. The mesogens will form thin and flat super-disks that will organize in a nematic phase, referred to as e.g. the nematic sheet (N_S) phase, see Figure 1. A transition from this N_S phase to the N_D phase corresponds to a break-up of the sheets with conservation of the nematic order.

It is noted that the three cases the N_{Col}, N_L and the proposed N_S phase are extreme cases of self-associating materials, with the association in the columnar direction, in three directions and in the planar direction, respectively. It is emphasized that usually intermediate cases are/will be observed.

Distinguishing between nematic phases

The various nematic phases are hard to distinguish. Since the symmetry in all nematic phases is identical, optical polarizing microscopy experiments will yield the same characteristic *schlieren* textures for all the nematic phases. X-ray diffraction can be used to measure the local order between the mesogens and the technique is therefore exceedingly suitable to differentiate between the nematic phases. By measuring the correlation length ξ of a particular spacing, the extent of local order can be established and hence, ξ can be used to determine the type of associated nematic phase, see Table 1. Dividing the ξ by the actual spacing d results in a dimensionless quantity that allows comparison between different materials. Typically, the N_{Col} phase shows a high value for the intracolumnar relative correlation length only, whereas the N_L phase shows high values in both the inter- and intracolumnar direction. The Ns phase, discussed above is expected to show a high relative correlation length of the corresponding intercolumnar reflection.

Table 1. XRD characteristics of the various nematic phases: Typical values of the relative correlation lengths (ξ/d) in the in the *intra*columnar (||) and the *inter*columnar ($\perp$) direction. [a] Both ξ and d are calculated from the [100] and the [001] reflection, however, for CT complexes, the [200] and [002] reflections were used, since the unit-cell consists of two donors and acceptors.

Relative correlation length	Miller Indices[a]	N_D	N_{Col}	N_L
$(\xi/d)_{alkyl}$	alkyl	2.3	2.3	2.3
$(\xi/d)_\perp$	*h*00	2.0	2.8	**8.5**
$(\xi/d)_\parallel$	00*l*	4.2	**8.5**	**8.5**

The use of polymers in the field of discotic liquid crystals has resulted in new insight and also new opportunities in the application of discotic liquid crystals. Attachment of the mesogens as pendant groups along a polymer backbone strongly suppresses crystallization. This results in an extension of the temperature window of the mesophases, the formation of additional mesophases, as well as the formation of near room temperature mesophases, including the rather uncommon N_D phase, usually only observed at high temperatures. With the application of low T_g polymers or multipodes[6] real room temperature N_D mesophases are within arm's reach.

Outlook

The various intermolecular interactions have a large effect on the phase behavior. A considered use of intermolecular forces, such as hydrogen bonding, dipole-dipole interactions and charge transfer interactions, but also steric, and ion-dipole interactions, can result in an improved insight in phase formation and self-organization mechanisms at several length scales.
The charge transfer interactions investigated here proved to be an effective tool to manipulate (or induce) liquid crystalline properties. By using mixtures, a large number of complexes (and corresponding properties) have been obtained with only a limited number of materials. For example, charge transfer complexes of **D5** with various acceptors show a wide range of mesophases: Complexes of the macromolecular acceptor **P(A1a)** show the assembled N_L phase next to the traditional N_D phase. Alternatively, complexes with the stronger acceptor **A2** show two highly disordered columnar phases apart from the N_D phase. The phases in the CT complexes often are not easily characterized. XRD measurements showed higher local order in the N_L phase of **D5**:**P(A1a)** than in the two columnar phases of **D5**:**A2**! These complex phases are just in the initial stage of characterization and some are not fully understood. More detailed investigation on these materials is necessary to reveal their intricate order and to understand their phase behavior.
Apart from electro-optic applications such as displays and photovoltaic cells, detailed understanding is clearly necessary in relation new fields like smart materials and materials mimicking biological systems.

References and notes

(1) (a) Strohriegl, P. *Makromol. Chem.* **1993**, *194*, 363-387. (b) Bengs, H.; Ringsdorf, H. *Makromol. Chem.* **1992**, *193*, 2659-2668.

(2) (a) Ringsdorf, H.; Wüstefeld, R.; Zerta, E.; Ebert, M.; Wendorff, J.H. *Angew. Chem. Int. ed. Engl.* **1989**, *28*, 914-918. (b) Praefcke, K.; Singer, D.; Kohne, B.; Ebert, M.; Liebmann, A.; Wendorff, J.H. *Liq. Cryst.* **1991**, *10*, 147-159. (c) Lawson, K. D.; Flautt, T. J. *J. Am. Chem. Soc.* **1967**, *89*, 5489; (d) Lydon, J. In *Handbook of Liquid Crystals*; Demus, D., Goodby, J. W., Gray, G. W., Spiess, H. W., Vill, V., Eds.; Wiley VCH: New York, 1998; Vol. 2B, pp 981-1007. (e) Warmerdam, T. W.; Nolte, R. J. M.; Drenth, W.; Miltenburg, J. C. van; Frenkel, D.; Zijlstra, R. J. J. *Liq. Crys.* **1988**, *3*, 1087-1104.

(3) Praefcke, K.; Singer, D.; Eckert, A. *Liq. Cryst.* **1994**, *16*, 53.

(4) Bengs, H.; Karthaus, O.; Ringsdorf, H.; Baehr, C.; Ebert, M.; Wendorff, J.H. *Liq. Cryst.* **1991**, *10*, 161-168.

(5) (a) Kouwer, P.H.J.; Gast, J.; Jager, W.F.; Mijs, W.J.; Picken, S.J. *Mol. Cryst. Liq. Cryst.* **2001**, *364*, 225-234. (b) Kouwer, P.H.J.; Jager, W.F.; Mijs, W.J.; Picken, S.J. *Macromolecules* **2001**, *34*, 7582-7584.

(6) Elsässer, R.; Mehl, G.H.; Goodby, J.W.; Veith, M. *Angew. Chem. Int. ed. Engl.* **2001**, *40*, 2688-2690.

Summary

Recently, disk-shaped liquid crystals have gained substantial attention due to their possible applications in for example display technology and photovoltaic cells. However, before they can be applied, an improved understanding of and control over their liquid crystalline properties is essential. This thesis describes the synthesis, characterization and liquid crystalline properties of a series of novel disk-shaped mesogens. To obtain a wide range of properties, various techniques to manipulate the phase behavior were applied: firstly attaching the mesogens to a polymer backbone, and secondly doping the mesogens, resulting in the formation of charge transfer (CT) complexes.

In Chapter 2, we describe the synthesis of the investigated materials. The mesogens are based on a pentakis(phenylethynyl)phenoxy core, substituted with an undecanol spacer. Various substituents are located at the *para*-position of the lateral phenyl groups, including alkyl, alkoxy, thioalkyl, alkylsulfonyl and alkylamido groups. The applied acceptors are based on 2,4,7-trinitro-9-fluorenone. Both the donors and the acceptors have been attached to a polyacrylate backbone by means of a polymer analogous substitution reaction. The advantage of this approach over conventional polymerization of the mesogens is that in this way macromolecules of a sufficient chain length can be prepared, despite the presence of groups preventing efficient polymerization (e.g. nitro or acetylene groups). In addition, it is a simple route to prepare series of copolymers incorporating a variety of pendant groups.

The liquid crystalline properties of the mesogens, the corresponding polymers and their charge transfer complexes are discussed in Chapters 3-6. These properties are investigated with various techniques, such as differential scanning calorimetry, optical polarizing microscopy, X-ray diffraction and dielectric relaxation spectroscopy. Chapter 3 describes the study of methyl-substituted mesogens and their related polyacrylates. The polymer backbone of the macromolecular mesogens effectively suppresses the formation of high order in the materials. Therefore, in these polymers a nematic columnar phase (N_{Col}) was observed at low temperatures, besides the nematic discotic (N_D) phase. This to our knowledge is the first example of a thermotropic polymer material showing a nematic to nematic phase transition. A series of copolymers with alkylacrylates was prepared to investigate the role of the mesogen concentration on the phase behavior. All copolymers fitted in a single universal phase diagram after calculating the weight fraction of rigid mesogen. Subsequently, the phase diagram was described with an extended McMillan theory, which seems to be a useful first step towards theoretical description of these complex systems.

Chapters 4 and 5 discuss the study of a series of CT complexes of the non-substituted and the methoxy-substituted mesogens, respectively. The CT complexes of the mesogens without substituents showed a rich phase behavior, in contrast to the pure materials that were crystalline or amorphous solids. It is demonstrated that the liquid crystalline properties of the complexes can be manipulated by altering the strength of the complex or, alternatively, by steric factors. Dielectric relaxation studies show that the dynamics in the various mesophases is strongly related to the extent of order in these phases.

In some of the complexes a phase with apparent nematic characteristics was observed, while the corresponding X-ray diffractograms showed a high local order. Detailed investigations of these phases resulted in the identification as the new nematic lateral (N_L) phase. In the N_L phase, the discotic mesogens are associated into larger disk-shaped assemblies. A subsequent nematic organization of the super structures yields the N_L phase. One of the complexes discussed in Chapter 5 even showed a transition from the N_L to the N_D phase, which gave us the opportunity to investigate the N_L phase comprehensively. A classification for the various nematic phases has been proposed, which is based on x-ray diffraction results. Remarkably, another complex showed the typical texture of a columnar phase, while x-ray diffraction analysis showed very low local order. This illustrates that the mesophases formed by these charge transfer complexes are complex systems that need to be studied with care.

The mesogens, discussed in Chapter 6, all experience various specific interactions, such as dipole-dipole interactions and hydrogen bonding. These interactions originate from the substituents linking the tails to the mesogens. It is shown that the interactions have a major influence on the phase behavior of the mesogens. Besides, a qualitative model is proposed that explains the liquid crystalline properties of CT complexes in enthalpic and entropic terms.

Samenvatting

Schijfvormige vloeibare kristallen staan recent in de belangstelling door hun mogelijke toepassingen bijvoorbeeld in scherm technologie en in zonnecellen. Echter, om ze toe te kunnen passen is meer kennis van en controle over hun vloeibaar kristallijne eigenschappen nodig. Dit proefschrift beschrijft de synthese, karakterisatie en de vloeibaar kristallijne eigenschappen van een serie nieuwe schijfvormige mesogenen. Daarnaast worden vloeibaar kristallijne eigenschappen van de mesogenen op verschillende wijzen gemanipuleerd: door de mesogenen te bevestigen aan een polymere hoofdketen en door middel van *doping* van de mesogenen dat tot de vorming van *charge transfer* (CT) complexen leidt.

In hoofdstuk 2 beschrijven we de synthese van de onderzochte materialen. De mesogenen zijn gebaseerd op een pentakis(fenylethynyl)fenoxy kern, gesubstitueerd met een undecanol *spacer*. Op de *para*-positie van de laterale fenylgroepen zijn verschillende substituenten aangebracht, zoals alkyl, alkoxy, thioalkyl, alkylsulfonyl en alkylamido groepen. De gebruikte acceptoren zijn gebaseerd op 2,4,7-trinitro-9-fluorenon. Zowel de donoren als de acceptoren zijn als zijgroepen aan een polymeer bevesigd, via een polymeer analoge substitutie reactie aan poly(acryloyl chloride). Het voordeel van deze methode ten opzichte van conventionele polymerisatie van de mesogenen is dat op deze manier macromoleculen van een redelijke lengte verkregen kunnen worden, ondanks de aanwezigheid van groepen die de polymerisatie hinderen (zoals nitro en acetyleen groepen). Een extra voordeel is dat het een eenvoudige route biedt om copolymeren te vervaardigen, waarin verschilende moleculen aan dezelfde *backbone* gesubstitueerd kunnen worden.

De vloeibaar kristallijne eigenschappen van de mesogenen, de corresponderende polymeren en hun CT complexen worden in de hoofdstukken 3-6 besproken. Deze eigenschappen zijn onderzocht met technieken als *differential scanning calorimetry*, optische polarisatie microscopie, röntgen diffractie en dielectrische relaxatie spectroscopie. Hoofdstuk 3 beschrijft de studie van de methyl-gesubstitueerde mesogenen en een serie polyacrylaten daarvan. De hoofdketen van de polymere mesogenen zorgt ervoor dat de materialen zich niet eevoudig kunnen ordenen. Daardoor hebben de polymeren behalve de nematisch discotische (N_D) fase ook een nematisch kolomnaire (N_{Col}) fase bij lagere temperaturen. Dit is het eerste voorbeeld van thermotrope polymere materialen die een overgang van een nematische fase naar een andere nematische fase vertonen. Een serie copolymeren met alkylacrylaten is gesynthetiseerd om de rol van de mesogeen concentratie op het fasegedrag te bestuderen. Een universeel fasediagram van de verschillende copolymeren werd geconstrueerd en de faseovergangstemperaturen kunnen worden beschreven als een functie van de rigide mesogeenfractie in de polymeren. Het fasediagram bleek uitstekend te beschrijven met de McMillan theory uitgebreid voor kolomnaire fasen, wat een goede aanzet te zijn voor een volledigere theoretische beschrijving van deze complexe systemen.

Hoofdstukken 4 en 5 beschouwen de studie naar een serie CT complexen van de respectievelijk niet gesubstitueerde en methoxy-gesubstitueerde mesogenen. De CT complexen van de mesogenen zonder substituenten laten een uitgebreid fasegedrag zien, dit in tegenstelling pure materialen, die kristallijn dan wel amorf zijn. Er wordt aangetoond dat de vloeibaar kristallijne eigenschappen van de complexen gemanipuleerd kunnen worden door verandering van de sterkte van het complex of alternatief, met behulp van sterische interacties. Dielectrische relaxatie studies laten zien aan dat de dynamica in de verschillende mesofasen sterk gecorreleerd is aan de orde in die betreffende fase.

In een aantal complexen werd een fase met duidelijke nematische karakteristieken gevonden, terwijl het bijbehorende röntgen-diagram een hoge orde liet zien. Verder gedetailleerd onderzoek naar deze fase leverde de karakterisatie als de nieuwe nematisch laterale (N_L) fase op. In de N_L fase zijn de schijfvormige moleculen geassocieerd tot grotere schijfvormige structuren. Een nematische ordening van deze aggregaten levert de N_L fase op. Bij één van de complexen uit hoofdstuk 5 werd zelfs een overgang van de N_L naar de N_D fase waargenomen, wat de gelegenheid gaf de N_L fase uitgebreid te onderzoeken. Vervolgens is een classificatie voor de verschillende nematische fasen voorgesteld, die gebaseerd is op röntgen diffractie resultaten. Opvallend genoeg werd bij een ander complex een typisch columnaire textuur waargenomen, terwijl de bijbehorende röntgen analyse erg lage orde liet zien. Dit geeft aan dat de mesofase die gevormd worden via CT complexatie ingewikkende systemen zijn, die met zorg bestudeerd dienen te worden.

In hoofdstuk 6 staan de specifieke interacties tussen de mesogen centraal, zoals bijvoorbeeld dipool-dipool interacties en waterstof bruggen. De interacties komen voort uit de groepen die gebruikt zijn om de staarten aan de mesogenen te bevestigen. Er wordt aangetoond dat de interacties een bijzonder grote invloed hebben op het fasegedrag van de mesogenen. Daarnaast is een kwaltitatief model voorgesteld dat vloeibaar kristallijne eigenschappen van CT complexen verklaard op basis van enthalpische en entropische overwegingen.

Curriculum vitae

Op 29 november 1972 ben ik geboren in Nijmegen. De middelbare school heb ik doorlopen aan het Christelijk Lyceum te Apeldoorn. Het VWO diploma behaalde ik in juni 1991. Daarna begon ik aan de studie Scheikunde aan de Rijksuniversiteit Groningen, waar ik mijn propaedeuse behaalde in juli 1992 en mijn doctoraal examen in augustus 1996 aflegde. Mijn hoofdrichting was polymeerchemie en het afstudeerwerk werd uitgevoerd binnen de groep van prof. dr. G.G. Hadziioannou.

Na een korte aanstelling bij ATO-DLO te Wageningen ben ik in juli 1997 begonnen aan een promotieonderzoek aan de faculteit Technische Natuurwetenschappen van de Technische Universiteit Delft. Het project is begeleid door prof. dr. W.J. Mijs, dr. W.F. Jager en prof. dr. S.J. Picken. De resultaten van het onderzoek zijn gepresenteerd op verschillende internationale congressen, in wetenschappelijke tijdschriften en in dit proefschrift. Tijdens mijn promotieonderzoek ben ik geregistreerd als register polymeerkundige.

Per 1 november 2001 werk ik als Ramsay Fellow aan de Universiteit van Hull (Verenigd Koninkrijk) in de groep van dr. G.H. Mehl en prof. dr. J.W. Goodby.

List of publications

Bolink, H.J.; Krasnikov, V.V.; Kouwer, P.H.J.; Hadziioannou, G. “A Novel Polyaryl Ether Based Photorefractive Composite,” *Chem. Mater.* **1998**, *10*, 3951-3957.

Kouwer, P.H.J.; Mijs, W.J.; Jager, W.F.; Picken, S.J. “Synthesis and Characterization of a Novel Liquid Crystalline Polymer Showing a Nematic Columnar to Nematic Discotic Phase Transition,” *Macromolecules* **2000**, *33*, 4336-4342.

Kouwer, P.H.J.; Gast, J.; Jager, W.F.; Mijs, W.J.; Picken, S.J. “A Series of Novel Liquid Crystalline Polymers Showing a Nematic Discotic and/or Nematic Columnar Phase,” *Mol. Cryst. Liq. Cryst.* **2001**, *364*, 225-234

Kouwer, P.H.J.; Mijs, W.J.; Jager, W.F.; Picken, S.J. “Modeling of N_D and N_{Col} Phase Transitions in Discotic Side Chain Polymers by the Extended McMillan Theory,” *J. Am. Chem. Soc.* **2001**, *123*, 4645-4646.

Kouwer, P.H.J.; Jager, W.F.; Mijs, W.J.; Picken, S.J. “Nematic-Nematic Phase Transitions in Discotic Liquid Crystals,” *Polym. Mater. Sci. Engin.* **2001**, *85*, 303-304; *Abstr. Pap. Am. Chem. Soc.* **2001**, *222*, 185.

Kouwer, P.H.J.; Jager, W.F.; Van den Berg, O.; Mijs, W.J.; Picken, S.J. “Inducing Novel Mesophases by Attaching Discotic Mesogens to a Side-Chain Polymer,” *Polym. Mater. Sci. Engin.* **2001**, *85*, 546-547; *Abstr. Pap. Am. Chem. Soc.* **2001**, *222*, 326.

Kouwer, P.H.J.; Jager, W.F.; Mijs, W.J.; Picken, S.J. “Modeling of N_{Col} to N_D Phase Transitions by the Extended McMillan Theory,” *Polym. Mater. Sci. Engin.* **2001**, *85*, 395-396; *Abstr. Pap. Am. Chem. Soc.* **2001**, *222*, 236.

Kouwer, P.H.J.; Jager, W.F.; Mijs, W.J.; Picken, S.J. “The Nematic Lateral Phase: A Novel Phase in Discotic Supramolecular Assemblies,” *Macromolecules,* **2001**, *34*, 7582-7584.

Kouwer, P.H.J. “Nieuwe nematische fase in schijfjes,” *Chem. 2 Weekblad* **2001**, *97 (1 december)*, 7 (in Dutch).

Kouwer, P.H.J.; Van den Berg, O.; Jager, W.F.; Mijs, W.J.; Picken, S.J. “Induced Liquid Crystalline Diversity in Molecular and Polymeric Charge Transfer Complexes of Discotic Mesogens,” *Macromolecules* **2002**, *35*, 2576-2582.

Kouwer, P.H.J.; Jager, W.F.; Mijs, W.J.; Picken, S.J. “Charge Transfer Complexes of Discotic Liquid Crystals: A Flexible Route to a Wide Variety of Mesophases,” *Macromolecules, in press*.

Kouwer, P.H.J.; Jager, W.F.; Mijs, W.J.; Picken, S.J. “Specific Interactions in Discotic Liquid Crystals,” *Submitted to J. Am. Chem. Soc.*

Dankwoord

Als eerste wil ik mijn begeleiders Wim Mijs, Wolter Jager en Stephen Picken bedanken voor de gelegenheid die ze mij geboden hebben en het vertrouwen dat ze in mij gesteld hebben. Met hun uitstekende begeleiding ben ik in staat geweest uit te groeien tot de wetenschapper die ik nu ben. Ik heb veel geleerd van de vele discussies over vloeibare kristallen die vaak overliepen in discussies over wetenschap in het algemeen.

Daarnaast wil ik iedereen bedanken die direct aan mijn onderzoek meegewerkt hebben: Otto van den Berg voor de synthese van verschillende acceptoren en verder Vera Iakovidou, René Westbroek, Jeroen Gast, Niina Hokkanen, Patricia van Rooyen, Marjolein de Jong en Vanina Kleiman. In het bijzonder bedank ik Enno Klop van Akzo Nobel Chemicals Research in Arnhem, van wie ik gebruik mocht maken van de röntgen diffractie faciliteiten. Daarnaast heeft Enno een grote bijdrage geleverd door de discussie aan te gaan over de verschillende röntgen diffractogrammen. Michael Wübbenhorst wil ik bedanken voor het uitwerken en de interpretatie van de diëlectrische metingen en de daarbij horende resultaten.

Er zijn veel mensen binnen de vakgroep die bijgedragen hebben aan de goede tijd die ik in Delft genoten heb. In het bijzonder de mede-AIO’s met wie ik een kamer heb gedeeld: Harry Veenstra en Marcel Franse. Met beiden was het een feest te discusieren over zowel de wetenschap als de maatschappij. Daarnaast Ben Norder, Gerard de Vos, Piet Droppert en Nico van der Knaap voor hun technische assistentie en Tonny Verheul-Mentink en Fem Brenk voor de administriële ondersteuning. Maar eigenlijk het meest iedereen van de vakgroep voor de prettige, informele werksfeer.

Op deze plaats wil ik ook graag mijn ouders bedanken. Zij hebben mij steeds gestimuleerd om me verder (wetenschappelijk) te ontwikkellen. Ook al heeft dat er toe geleid dat ik nu uit Nederland vertrokken ben.

Tenslotte bedank ik Suzan. Voor het vertrouwen en voor het geduld dat ik van haar gevraagd heb. Voor het luisteren. Voor de steun en de liefde. Eigenlijk voor alles.